ISAS - INTERNATIONAL SCHOOL FOR ADVANCED STUDIES

A study of the mechanisms regulating network rhythmicity in the neonatal rat spinal cord

Thesis submitted for the degree of

"Doctor Philosophiae" – Biophysics Sector

Candidate
DVM Aldo Rozzo

Supervisors
Prof. Andrea Nistri
Dr. Enrico Tongiorgi

SISSA - SCUOLA INTERNAZIONALE SUPERIORE DI STUDI AVANZATI
TRIESTE
Via Beirut 2-4

TRIESTE

to Tiziana

Index

NOTE

Part of the data reported in the present thesis have been presented or published (or submitted for publication) in the articles listed below. In all cases the candidate personally performed all the electrophysiological and biochemical experimental work and data analysis. He directly collaborated to molecular biology experiments and to modelling.

Rozzo A., Ballerini L. and Nistri A. (1999) Antagonism by (1,2,5,6-tetrahydropyridine-4-yl) methylphosphinic acid of synaptic transmission in the neonatal rat spinal cord in vitro: an electrophysiological study. *Neurosci.* **90**, 1085-1092

Rozzo A., Ballerini L. and Nistri A. (2000) Role of the sodium pump in nonlinear summation of afferent inputs or spontaneous rhythmic bursts in the rat spinal cord. *Soc. Neurosci. Abst.* **26**, 157

Rozzo A., Armellin M., Franzot J., Chiaruttini C., Nistri A. and Tongiorgi E. (2001) Expression and dendritic mRNA localisation of $GABA_C$ receptor ρ1 and ρ2 subunits in developing rat brain and spinal cord. *Submitted.*

Abbreviation:

3'UTR	= 3' untranslated regions
ACSF	= artificial cerebrospinal fluid
CNS	= Central Nervous System
cpm	= counts per min
CV	= coefficient of variation
DR	= spinal cord dorsal root
E	= embryonic day
L	= lumbar root
MDDL	= maximal distance of dendritic labelling
Na^+/K^+ ATPase	= electrogenic sodium pump
p	= the probability that two groups are not significantly different, or that correlation coefficient is zero
P	= postnatal day
PBS	= phosphate buffer saline
PFA	= paraformaldehyde
r	= correlation coefficient
RT-PCR	= reverse transcriptase-polymerase chain reaction
SD	= standard deviation
VR	= spinal cord ventral root
xTh	= times threshold (electrical pulse intensity)

Abstract

Our focus was to study the processes involved in the generation of rhythmic oscillations by a functional network made up by excitatory connections only. For this purpose we used the spontaneous rhythm generated by the *in vitro* neonatal rat spinal cord preparation when fast, chloride-mediated inhibition via $GABA_A$ and glycine receptors was blocked. We then addressed the issue of the role played by two distinct membrane mechanisms responsible for ionic movements across neuronal membranes, namely $GABA_C$ channels and the Na^+/K^+ ATPase pump. The spontaneous pattern, termed disinhibited rhythm, was stable, robust, regular and organized with intraburst oscillations.

Using electrophysiological, *in situ* hybridisation and immunocytochemical techniques we evaluated the presence and the role of the third component of fast synaptic inhibition (chloride mediated like $GABA_A$ and glycine ones), namely the $GABA_C$ conductance. We observed that in the rat spinal cord $GABA_C$ receptor mRNA and expression was developmentally regulated. Electrophysiological results confirmed differential postnatal distribution of $GABA_C$ receptors which, however, played a minor role in rhythmogenic network activity. In fact, $GABA_C$ channel activity only modulated the disinhibited rhythm, confirming that this bursting activity was generated by a purely excitatory network.

Applying a biochemical assay and electrophysiological techniques, we characterized the role of the Na^+/K^+ electrogenic pump in the generation and/or maintenance of rhythmic activity. After the demonstration of complete block of the sodium pump by our experimental protocol (4 μM strophanthidin), we studied the effect of blocking this pump on spontaneous and electrically evoked events in the spinal cord network. During a high frequency stimulus train in control solution, the pump activity normally prevented linear summation of responses and

sped up network recovery. Long term strophanthidin application during disinhibited rhythm disrupted bursting which was later replaced by much longer and irregular bursts. This new activity, namely strophanthidin bursting, was very robust and organized with intraburst oscillations. Pharmacological experiments indicated that strophanthidin bursting was a network phenomenon driven by recurrent glutamatergic excitation mediated by non-NMDA and NMDA receptors. It was not possible to accelerate this pattern with conventional excitatory agents like serotonin, NMDA or high K^+. Experiments based on bursts evoked by single and repeated electrical stimulation during disinhibited or strophanthidin bursting, suggested that while the former was limited by the Na^+ pump activity, the latter was constrained by development of synaptic fatigue. These proposals were applied to a mathematical model developed in collaboration with Dr S. Bianchini (Istituto per le Applicazioni del Calcolo "M. Picone", Rome) who was able to provide realistic simulations of spontaneous discharges generated by the excitatory spinal cord network in the presence or in the absence of Na^+/K^+ pump activity.

Introduction

Spontaneous activity: role and function in the developing nervous system:

During Central Nervous System (CNS) development, the period in the embryonic and early postnatal life in which neuronal structures reach mature architecture and function, spontaneous electrical activity is present in many regions even in the absence of afferent stimuli. This activity falls into two main patterns: steady tonic firing and rhythmic bursting, both with specific characteristics (frequency, duration, distribution, etc.) in various regions (Feller, 1999). What is the role of this spontaneous activity?

One view regarding neuronal development is that electrical activity would be unimportant for establishing the main aspects of gross morphology and topology of the CNS (for example how neurons develop distinct phenotypes, migrate to a characteristic position and establish an initial set of connections; Crair, 1999). According to this hypothesis, the presence of electrical neuronal activity is traditionally thought to be essential only for the fine development of a mature system of neuronal connections: thus, activity drives the refinement of the initially crude connectivity (Crair, 1999). This view needs, however, revision. Recently, neuronal activity has been shown to influence circuit development at very early stages: in fact, chemical and electrical activity can profoundly modulate a variety of intracellular processes including cell phenotype differentiation, activation of enzymes and gene expression. There are many demonstrations that immature circuits generate activity patterns that can potentially drive developmental processes (for review see: Feller, 1999).

Neuronal activity during circuit development may be instructive or permissive (Crair, 1999); permissive means necessary to enable other primary developmental cues, instructive means

that it directly moulds neuronal connections (Crair, 1999). The precise role of spontaneous activity is frequently uncertain; a way to distinguish between these two roles is to change the pattern (or information content) of neuronal activity or to interfere with spontaneous activity without a complete block that demonstrates only the overall activity relevance. For example, pharmacological block of retinal waves prevents the formation of the mature visual cortex because eye-specific laminae fail to form (Penn *et al.,* 1998). This result shows that development needs an electrical activity, but the approach does not discriminate between instructive or permissive a role. Is any patterned activity crucial for the complete development of the visual cortex? Superimposing, over spontaneous activity, optic nerve stimulation changes the normal development of the visual cortex, reducing orientation selectivity and responsiveness of visual cortical neurons (Weliky and Katz, 1997). Thus, interfering with spontaneous electrical activity, without blocking it, suggests that the spontaneous pattern is essential ("instructive") for network development.

Spontaneous rhythmic activity

One of the most diffuse and relevant characteristics of spontaneous activity is rhythmicity: a spontaneous rhythm consists of bursts of action potentials correlated across tens to hundreds of cells, that occur with a certain periodicity. Similar properties shared among different areas of the CNS arise from two general organizing principles: 1) highly interconnected excitatory synapses may be responsible for generating rhythmic activity, and 2) homeostatic mechanisms may act to regulate the overall level of network activity (Feller, 1999).

Spontaneous rhythmic activity has been shown to be present during development of many areas of the CNS and, in several cases, network driven rhythmicity generates this. In Fig. 1 (from Feller, 1999) three examples of spontaneous rhythmic activity are shown; such rhythms are expressed only in a time window during development. In this figure the retina (A) was from a postnatal day 2 (P2) ferret, the spinal cord (B) from an embryonic day 24 (E24) chick and the hippocampus (C) from a P1 rat. D shows a rhythm induced by removal of extracellular magnesium from a different preparation, namely cultured dissociated cortical neurons.

Common features of all these examples are that these behaviors are extremely conserved in evolution, since they are observed in a large variety of vertebrate species (from chick to rat, from tadpole to cat), possessing comparable periodicity.

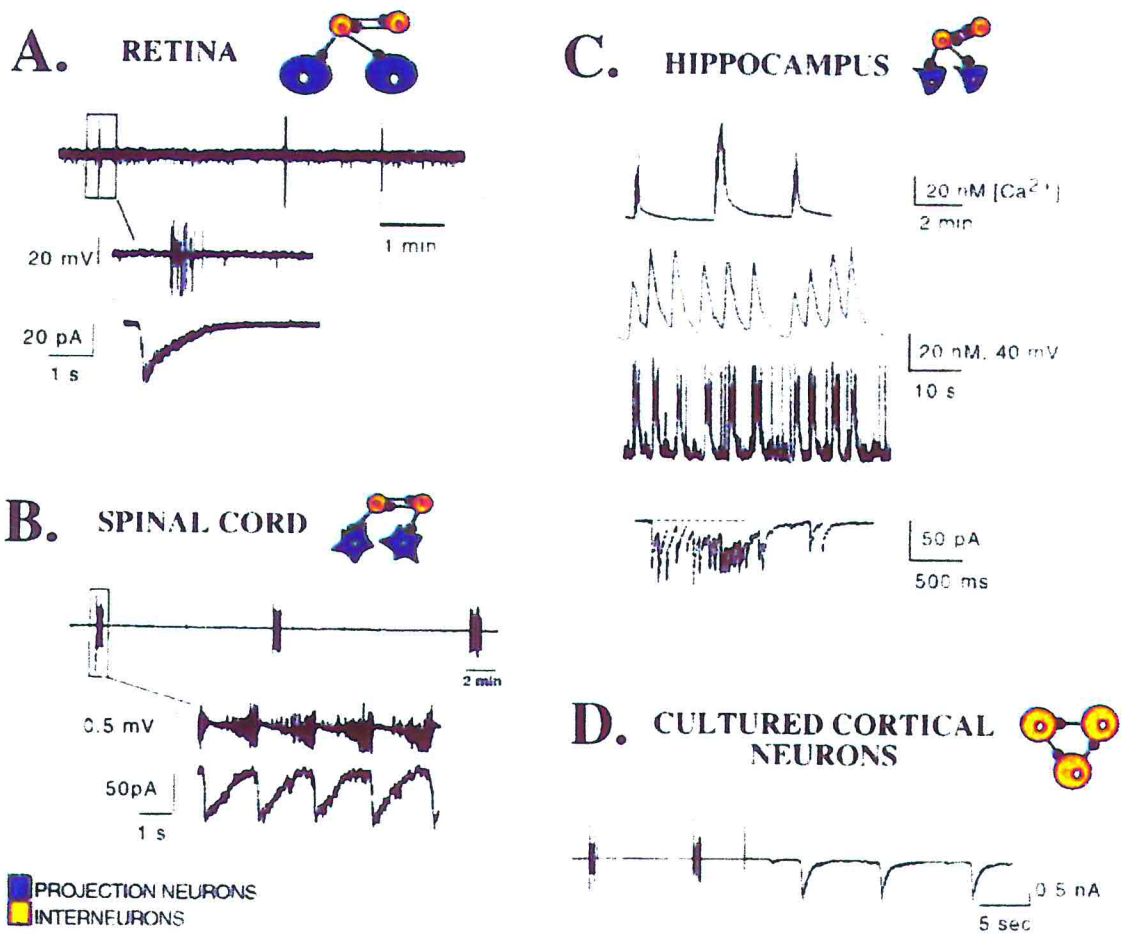

Fig. 1 Spontaneous rhythmic activity in developing circuits is generated by synaptically coupled circuits with similar architectures. (from Feller, 1999)

A) Top and middle: extracellular recording from P2 ferret retinal ganglion cell. Bottom: whole-cell voltage clamp recording from the same cell shows that burst and action potentials are generated by compound postsynaptic currents. Scheme: rhythmic activity in the developing retina is generated by a network containing cholinergic and GABAergic amacrine cells (yellow) and retinal ganglion cells (blue).
B) Top and middle: extracellular recording from E24 chick spinal motor neuron. Bottom: whole cell voltage clamp recording from an unidentified neuron in the ventral horn. Scheme: rhythmic activity in the developing spinal cord is generated by a network of recurrently connected interneurons (yellow) and motor neurons (blue).
C) Top: calcium imaging fluorescence trace from a pyramidal cell in CA1 of a P1 rat hippocampus. Middle two traces simultaneous calcium imaging and current clamp recording, showing the intraburst structure. Bottom: whole-cell voltage clamp recording from a pyramidal cell. Scheme: rhythmic activity is generated by GABAergic interneurons (yellow) and can be recorded in pyramidal cells (blue).
D) Extracellular recording from cultured neocortical neuron in magnesium-free medium, followed by whole-cell voltage clamp recording. Scheme: rhythmic activity is generated by a homogeneous population of cells with recurrent excitatory connections.

These rhythms are conserved also during development within the same species, although with different contribution by transmitters. For example, in the ferret retina the main excitatory mediator is acetylcholine before P10, and it becomes glutamate after P18 (Feller *et al.,* 1996; Penn *et al.,* 1998; Wong, 1999). In the chick retina the evolution is similar but the variation happens around E11 (Catsicas *et al.,* 1998; Wong *et al.,* 1998). In the chick spinal cord the activity driving excitatory transmitter shifts from acetylcholine (E5) to glutamate (E10) during circuit maturation (Chub and O'Donovan, 1998; Milner and Landmesser, 1999).

Also the rat CNS shows highly conserved rhythmicity during embryonic and early neonatal life. In the rat spinal cord rhythmic bursts occur synchronously before E18.5 (Nishimaru and Kudo, 2000). Nevertheless, with the emerging contribution of new channels (glycine receptors), the generation of different ionic gradients for Cl^-, and the onset of new interconnections, the rhythm evolves to gain alternation between different roots (Nishimaru and Kudo, 2000). The postnatal rat spinal cord, extensively studied *in vitro*, expresses alternating rhythmic bursts in the left-right and putative extensor-flexor ventral roots (VRs; for recent reviews, see: Cazalets *et al.,* 1998; Kiehn and Kjaerulff, 1998; Nishimaru and Kudo, 2000).
Finally, the robustness of circuit activity is also demonstrated by its capacity to compensate for perturbations. For example, chick spinal circuits can produce appropriate rhythmic activity via more than one mechanism: at E5 GABA alone can drive the rhythm, at E11 GABA and glycine can potentially drive this activity, if acetylcholine and glutamate receptors are blocked (Chub and O'Donovan, 1998). Similarly, in the neonatal rat spinal cord, block of fast chloride mediated inhibition (GABA and glycine receptors) does not prevent rhythmicity but only alternation, inducing a stable, periodic activity, termed disinhibited rhythm (Bracci *et al.,* 1996a).

These data suggest that firing properties of spinal networks may be regulated by homeostatic mechanisms, to preserve a certain rhythm. Thus, it is suggested that rhythmic spontaneous activity should have a crucial functional role for the development of several CNS structures.

Randomised neuronal networks

The simplest network where spontaneous rhythmic activity is observed is made up by dissociated cultured neurons. Robinson and co-workers (Fig. 1D) observed, 5 days after

culturing rat cortical neurons, an extensive network of processes. In Mg^{2+} free solution these neurons entered a stable firing mode consisting of regular bursts of action potentials at 5-20 s intervals. In 1 mM Mg^{2+} (a more physiological condition) rhythmic activity disappeared and only isolated spontaneous action potentials were detected in some neurons. In this preparation pacemaker potentials were never found and the rhythm appeared to be generated via synaptic glutamate receptors (TTX, APV and CNQX abolished the rhythm). The cell that initiated each burst changed randomly and, once started, bursting activity spread (within 50 ms) to all monitored cells (Robinson *et al.,* 1993).

Latham and co-workers (2000b) obtained similar results from mouse cultured ventral horn neurons. To understand the source of spontaneous bursts generated by the network in the absence of stimuli, they investigated spontaneous activity in pharmacologically isolated cells. Blocking all synaptic activity (presynaptically applying tetanus toxin and/or postsynaptically coapplying APV, CNQX, mecamylamine, atropine, bicuculline and strychnine), they identified a subset of endogenously active cells. From a model of intrinsic dynamics of a large neuronal network (Latham *et al.,* 2000a) and from experimental evidence (Latham *et al.,* 2000b), they established that firing patterns were critically controlled by one parameter: the fraction of endogenously active cells. In a bursting random neuronal network this number is within a permissive range; if the fraction of active cells exceeds or goes below this range, tonic firing replaces rhythmic bursting (Latham *et al.,* 2000b).

Streit's group, using randomised network (cultures of 2-8 weeks from the whole spinal cord of rats E14), grown on multielectrode arrays (Streit *et al.,* 2001), extended the previous data and compared them with responses of spinal cord slice cultures. Rhythmic activity generated by developing rat spinal cord had the following characteristics:

- absence of pacemaker neurons,
- role of spontaneously active cells in the bursting initiation,
- main control of rhythmicity due to the fraction of these active cells,
- primary role of glutamatergic, $GABA_A$ and glycinergic pathways.

In conclusion they argued against one specific network architecture as the basis for rhythmogenesis.

An elementary form of rhythmicity may be an intrinsic property of neurons in culture, resulting from the interplay of spontaneous neuronal activity and recurrent excitation within the neuronal network. Endogenously active cells may start bursts but the mechanisms that guide shape and duration of a burst are unclear.

Rhythmic activity in spinal cord

The spinal cord provides a considerable experimental advantage, namely a defined network output to skeletal muscles. In particular, as lumbar (L) motoneurons innervate all hind limb muscles (Sweet *et al.,* 1986), their activity can be recorded directly from motoneurons (intracellular recordings), from VRs (extracellular recordings) or from muscles involved in locomotion (electromyographic recordings; Nishimaru and Kudo, 2000).

The spontaneous rhythmicity of the in vitro spinal cord has another relevant feature: both the structures that generate the rhythm and the targets of the rhythm are bilateral. The spontaneous activity recorded from different motoneuronal pools, known to innervate different muscles (Swett *et al.,* 1986), may be synchronous or out of phase (Nishimaru and Kudo, 2000). In the lumbar region signal alternation may be observed in left and right, rostral (L2-L3) and caudal (L5-L6) VRs and motoneurons, or left and right extensor and flexor muscles. This feature is correlated with the physiological behaviour of locomotion as lumbar areas of the spinal cord innervate the hind limbs. In rat spinal cord the left-right alternation appears after E18.5, while the rostro-caudal (L2-L5) one after E20.5 (Nishimaru and Kudo, 2000).

Rhythms in rat spinal cord

Usually in all networks that conserve at least in part the original cyto-architecture (en bloc spinal cord, hippocampal slice, organotypic spinal cord culture; Feller, 1999; Bracci *et al.,* 1996a, Tscherter *et al.,* 2001), just boosting ongoing activity by inducing a network depolarisation or by decreasing inhibition, generates spontaneous rhythmicity.

Spontaneous motor activities, under normal conditions, are infrequently expressed in the isolated spinal cord preparation. However, spinal rhythms can be evoked either by electrical or by chemical stimulation; in neonatal rat spinal cord there are rhythms induced by high K^+, NMDA, 5-HT, dopamine, strychnine coapplied with bicuculline, low Mg^{2+} and many other substances (for recent reviews, see: Cazalets *et al.,* 1998; Kiehn and Kjaerulff, 1998; Nishimaru and Kudo, 2000).

Excitatory amino acids and monoaminergic systems appear to be the most potent pharmacological activators and regulators of long-lasting episodes of rhythmic motor bursting characterised by alternation between left-right and extensor-flexor output, namely fictive locomotion (Cazalets *et al.,* 1998; Kiehn and Kjaerulff, 1998). The complete block of fast synaptic Cl^- mediated inhibition leads to a different rhythm, synchronous in all segments and

on both side of the spinal cord, the so called disinhibited rhythm (Bracci *et al.,* 1996a). Both patterns are produced by the neonatal rat spinal cord.

Each one of the wide range of rhythmic motor activities in which vertebrates engage (swimming or walking) is thought to be generated by the neuronal networks collectively known as the Central Pattern Generator (CPG) located in the spinal cord itself (Grillner, 1975). Both fictive locomotion and disinhibited rhythm recorded from the neonatal rat spinal cord are apparently generated by the same network, namely the ventral horn of the lumbar spinal cord (Bracci *et al.,* 1996a; Kjaerulff and Kiehn, 1996) and both rhythms require glutamatergic activity (Bracci *et al.,* 1996a; Beato *et al.,* 1997). There is also strong interaction between these two types of rhythmic activity (Beato and Nistri, 1999). Moreover, similar activity waves and common start areas were detected by multisite recording from organotypic co-cultures (Tscherter *et al.,* 2001).

Disinhibited rhythm in the neonatal rat spinal cord

Coapplication of the $GABA_A$ antagonist bicuculline (20 μM) and the glycine blocker strychnine (1 μM) to the neonatal rat spinal cord (P0-12) invariably induces, in a few minutes, a very regular and robust rhythm recorded from both motoneurons and VRs (Bracci *et al.,* 1996a,b; Ballerini *et al.,* 1997; Bracci *et al.,* 1997).

After abolishing fast Cl^- mediated inhibition, a virtually pure excitatory network is able to generate regular rhythmic bursts (frequency between 2 and 3 per min, duration between 3 and 7 seconds in different preparations) that lasts as long as the drug application is maintained (Bracci *et al.,* 1996a,b).

An event is constituted by a rapid depolarisation (rise time = 96 ±15 ms, peak amplitude 52 ± 9 mV), followed by a plateau phase (lasting 0.3-1 seconds) after which large rhythmic oscillations develops. Intraburst oscillations frequency is between 8 and 2 Hz (see Fig. 2; from Bracci *et al.,* 1996b). Action potentials are always present during the early plateau phase of each event, and on the rising phase and at the top of each intraburst oscillation. Between bursts the baseline is typically free from spontaneous synaptic events. Because extracellular recording shows a very similar profile (Fig. 2, 21 and 22; Bracci *et al.,* 1996b), the long term recording stability of this methods justifies its use for our experiments.

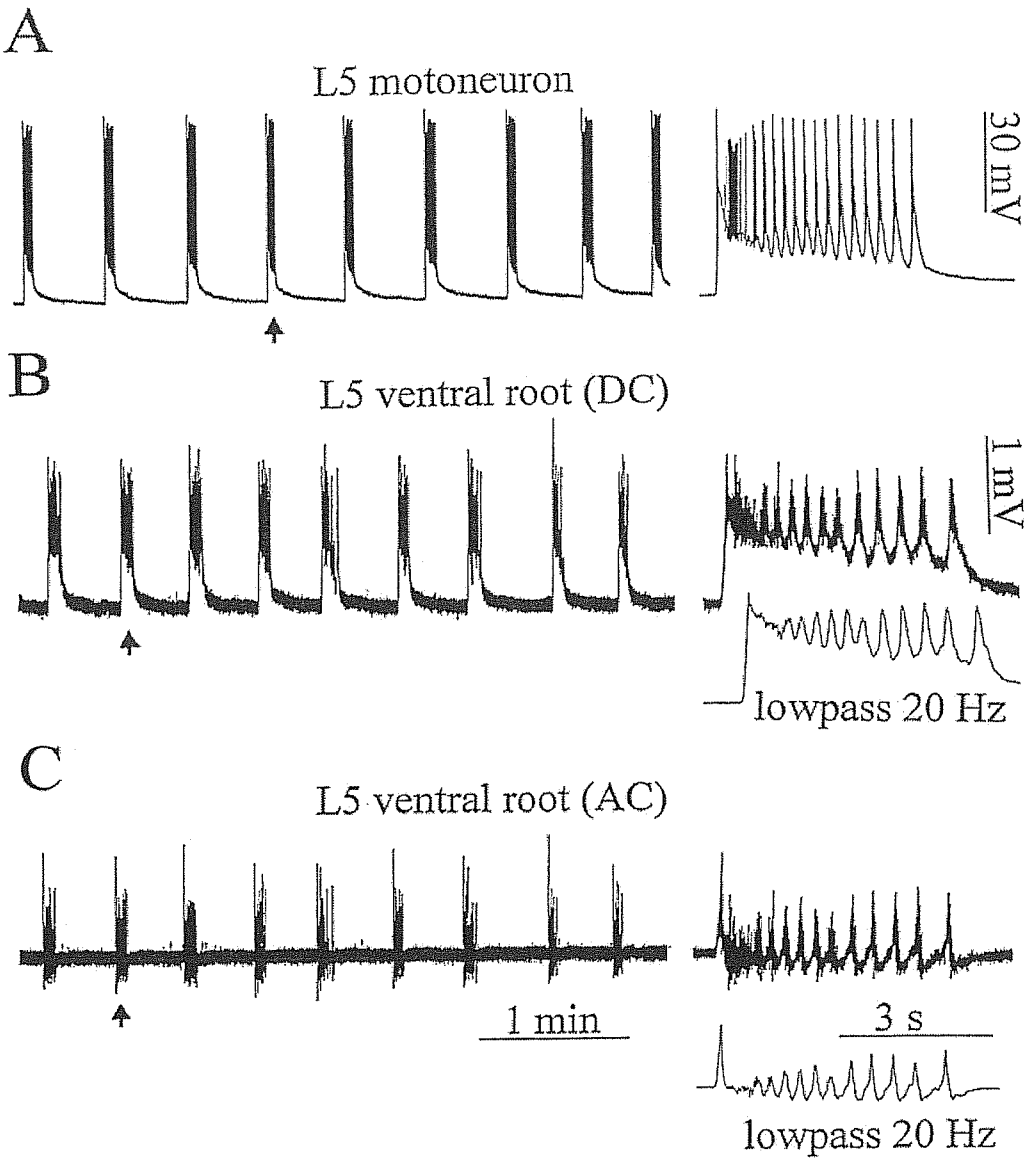

Fig. 2 Comparison of intracellular and extracellular recordings of bursting activity induced by strychnine and bicuculline in neonatal rat spinal cord (from Bracci *et al.,* 1996b).

A) Intracellular traces from L5 motoneuron (resting membrane potential -75 mV) displaying regular rhythmic bursting characterized by rapid depolarization with superimposed trains of action potentials. A single event (indicated by the arrow) is shown on the right with a faster timebase to resolve intraburst oscillatory activity.

B) DC-coupled extracellular recording of similar bursting (different preparation from A) from L5 ventral root. Note the similar bursting pattern and structure as observed with the intracellular electrode. Traces on the right represent faster timebase records [with wideband (top) or lowpass (bottom) filter] of the same individual burst indicated by the arrow.

C) AC-coupled extracellular recording of the same activity depicted in B Right traces show the same single event (faster timebase) with wideband (top) or lowpass (bottom) filter. Note that extracellular recording (either DC- or AC-coupled) from ventral root provides a reliable method to observe bursting activity.

Motoneurons are widely believed to represent mainly the network output without playing a direct role in the generation of spinal cord disinhibited rhythmicity (Bracci *et al.,* 1996a; Tscherter *et al.,* 2001). The primary excitatory transmitter driving this activity in the disinhibited interneuron network is glutamate. NMDA antagonists (APV and CPP) reversibly block or slow down disinhibited bursting, whether the non-NMDA blocker CNQX completely abolishes any spontaneous activity. Tetrodotoxin (TTX) or Cd^{2+} also abolishes this rhythm (Bracci *et al.,* 1996a).

Excitatory agents, such as 5-HT and NMDA, are known to accelerate the event frequency (inducing also a decrease in burst duration) in a dose dependent fashion (Bracci *et al.,* 1996a,b).

Surgical ablation of spinal cord tissue has been used to localize the rhythmogenic network. Transverse cuts showed the rhythm persistence in the L5 motoneuron pool after ablation rostral to L3 and caudal to L6. Dorsal horn ablation was not able to modify the rhythmicity but it decreased burst duration while preserving intraburst oscillations. An isolated ventral quadrant displayed bursting with decreased cycle period and duration, and devoid of intraburst oscillations (Bracci *et al.,* 1996b).

Afferent inputs were also able to modulate the disinhibited rhythm. Stimuli (0.1 ms, 1-4 times threshold) applied to dorsal roots (DR) or to ventro-lateral descending fibers could evoke a burst absolutely similar to a spontaneous one. Trains of pulses, between 0.5 and 0.05 Hz, were able to entrain bursts on a 1:1 basis and to reduce burst duration. At higher frequency, entrainement was always lost and the spontaneous rhythm returned even if electrical stimuli still elicited ventral root reflexes (Bracci *et al.,* 1997).

In conclusion a purely excitatory network (part of the CPG) is able to generate very regular spontaneously rhythmic activity and with very precise and highly complex burst structure, never observed in any randomized network. There is some evidence about a stochastic origin of bursts, due to spontaneously active neurons, but much less is known about the determinants of burst shape. Still unanswered questions are:

- mechanism for the end of a burst,
- the source of the intraburst oscillations,
- the role of additional GABA receptor classes ($GABA_C$),
- the precise role of the Na^+/K^+ ATPase in rhythmicity.

$GABA_C$ receptors; a recently characterized protein mediating Cl^- inhibition

Is the spontaneous disinhibited rhythm generated by a lumbar spinal network effectively devoid of any fast chloride mediated inhibition?

Bracci and co-workers (1996b) demonstrated the absence of a role for $GABA_B$ receptors (that regulate K^+ and Ca^{2+} channels through GTP-binding proteins and intracellular messenger pathways) in this spinal cord rhythmicity. However, a new class of GABA receptors was recently identified and characterised: the $GABA_C$ receptors directly gate Cl^- channels (similarly to $GABA_A$) insensitive to bicuculline ($GABA_A$ blocker; Polenzani *et al.,* 1991), and also to baclofen ($GABA_B$ agonist; Polenzani *et al.,* 1991).

Tentatively designed by Johnston and colleagues (Drew *et al.,* 1984) as $GABA_C$ for bicuculline insensitive GABA responses, this nomenclature is not yet official, but it is widely accepted and strongly supported by pharmacological, structural, functional and genetic evidence (Barnard *et al.,* 1998; for a review see Bormann, 2000).

Fig. 3 shows the membrane topology of the $GABA_C$ receptor and compares the two GABA receptors ($GABA_A$ and $GABA_C$) associated with Cl^- channels (from Bormann, 2000). In summary, the $GABA_C$ receptor fundamental characteristics, that discriminate it from $GABA_A$ receptors, are:

- pharmacology: high affinity for GABA, insensitivity to bicuculline and to barbiturates, affinity for (1,2,5,6-tetrahydropyridine-4-yl) methylphosphinic acid (TPMPA, Murata *et al.,* 1996; Ragozzino *et al.,* 1996), which acts as a potent and highly selective antagonist (see later). Other pharmacological differences are shown in Table 2;
- function: high sensitivity to the physiological agonist (about ten fold more than $GABA_A$) supposed to be due to five ligand binding sites on this receptor class (only two in $GABA_A$); very slow time constant of both activation and inactivation, and weak desensitization;
- structure: functional channels can assemble as homo-oligomers (ρ1 subunits; ρ2 subunits are extremely less efficient in forming homo-oligomeric receptors, Chebib *et al.,* 1998) or pseudo-homo-oligomers (ρ1, ρ2 and ρ3 subunits) in the rat (Zhang *et al.,* 1995; Ogurusu *et al.,* 1995, Ogurusu *et al.,* 1999). To date three different ρ-subunits have been cloned from human retina (three from rat, two from mouse and chick, and five from white perch) and detected with immunohistochemistry, RT-PCR and *in situ* ibridization in many tissues of several vertebrate species, sharing high homology between the isoforms, and only 30-38% aminoacid sequence identity with $GABA_A$ receptors and with no evidence of coassembling with α, β, or γ subunits of the $GABA_A$ receptor;

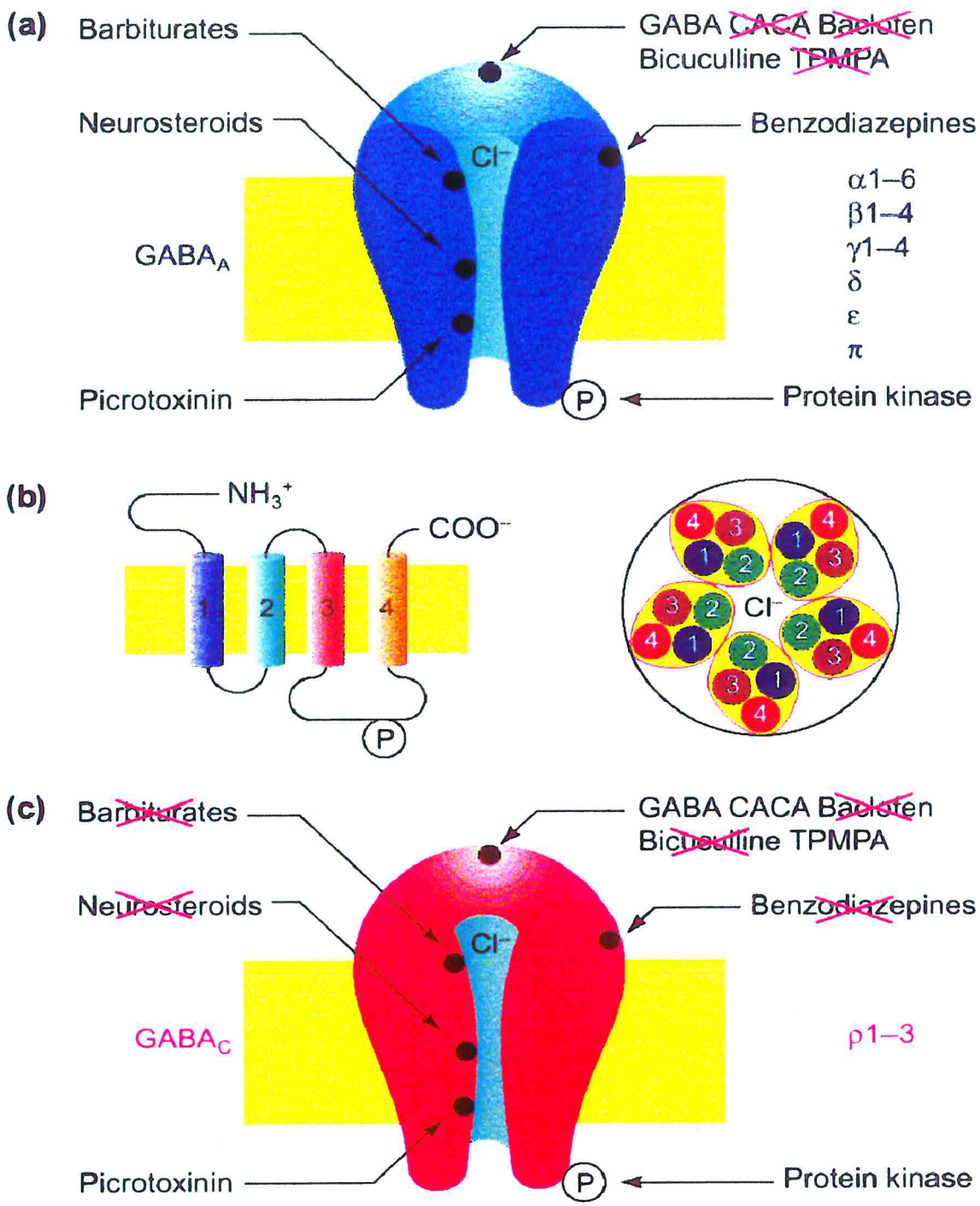

Fig. 3 Multiplicity of ionotropic GABA receptors (from Bormann, 2000).

(a) shows the $GABA_A$ receptor with the Cl^- pore, the binding sites for modulators and blockers and the intracellular phosphorylation site; on right side the subunits that build the vertebrate receptor. **(b)** presents the four transmembrane domains of each subunit (TM1-TM4, left) and the pentameric structure of the channel (right). **(c):** the membrane topology of $GABA_C$ receptors is assumed to be very similar to the one of $GABA_A$ receptors. However, $GABA_C$ receptors are composed exclusively by ρ (ρ1- 3; right) subunits and show different pharmacology. Red crosses indicate inactive drugs.

- genes: the genes for ρ1 and ρ2 subunits are clustered and have a chromosomal localisation distinct from those for $GABA_A$ subunits; they are localised on chromosome 6 in human and on 4 in mouse.

Table 1 Functional comparison of $GABA_C$ and $GABA_A$ ionotropic receptors (from Bormann, 2000).

property	**$GABA_C$ receptor (ρ1, ρ2 and ρ1ρ2)**	**$GABA_A$ receptor**
GABA EC_{50}	1-4 μM	5-100 μM
Hill slope	3-5	2
activation/inactivation	slow	fast
desensitisation	weak	strong
conductance	7 pS	27-30 pS
open time	150-200 ms	25-30 ms
selectivity	anions (Cl^-)	anions (Cl^-)
pore size	5.1 Å	5.6 Å

$GABA_C$ expression

Studies of ρ subunit expression in the rat brain and retina have indicated that the ρ2 subunit is the most widely distributed one, that ρ1 appears to be restricted to certain areas, and that ρ3 is strongly expressed in the embryonic brain and largely decreases after birth (Enz *et al.*, 1995; Ogurusu *et al.*, 1997; Ogurusu *et al.*,1999; Wegelius *et al.*, 1998; Boue-Grabot *et al.*, 1998). Although most studies have dealt with ρ1 and ρ2 subunits because of their postnatal predominance, the ρ1 and ρ2 precise cellular localisation remains controversial in certain areas or even absent for some regions (Wegelius *et al.*, 1998; Ogurusu *et al.*, 1999).

In the spinal cord of the adult rat, electrophysiological studies have provided evidence for the presence of $GABA_C$ receptors (Johnston, 1976), a result supported by the presence of ρ1 transcripts in the adult spinal cord (Enz *et al.*, 1995). However, there is no description, as yet, of the topographical and cellular distribution of $GABA_C$ subunits in the spinal cord.

$GABA_C$ selective antagonist: TPMPA

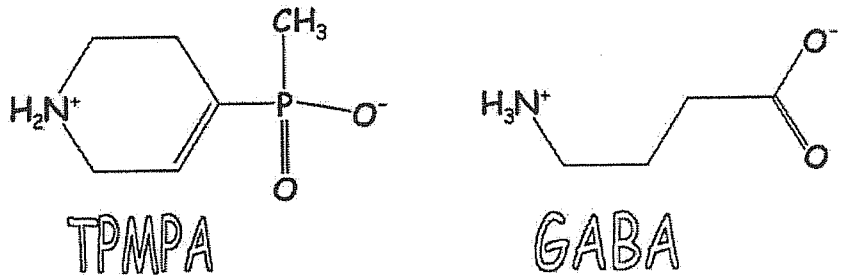

The availability of a highly selective agonist or antagonist is very useful to study the role of receptors; GABA is a highly flexible compound that can attain many low energy conformation states, which are conducive for binding to all GABA receptors classes.

To design a molecule very selective for $GABA_C$ receptors, Miledi's group (Murata *et al.*, 1996; Ragozzino *et al.*, 1996) considered two GABA analogues: the flexible 3-aminopropyl(methyl)phosphinic acid (3-APMPA or CGP35024, inactive on $GABA_A$ receptors, agonist for $GABA_B$ receptors and antagonist for $GABA_C$ receptors) and the semi-rigid isoguvacine (agonist for $GABA_A$, inactive at $GABA_B$ and partial agonist for $GABA_C$). They then synthesized the methylphosphinic acid analog of isoguvacine: (1,2,5,6-tetrahydropyridine-4-yl) methylphosphinic acid (TPMPA).

TPMPA is a conformationally restricted analogue of GABA and displays a weak antagonism for $GABA_A$ receptors and also a very weak agonism for $GABA_B$ receptors (see Table 2), but it is a highly competitive antagonist on $GABA_C$ receptors. The commercial supply of this antagonist, highly soluble in water, provided the first tool to study the role of the $GABA_C$ channels in neuronal networks. Table 2 reports the effects of the natural agonist and its analogues on known GABA receptor classes.

Table 2 Effects of agonists and antagonists at GABA receptors (from Bormann, 2000; Chebib *et al.*, 1998).

		GABA	TPMPA	3-APMPA[a]	isoguvacine
$GABA_C$ ρ1[b]	K_d	1.01 ±0.06 μM	potent antagonist	potent antagonist	137 ±6 μM
	K_b		2.0 ±0.4	0.75 ±0.07 μM	partial agonist
	EC_{50}				99 μM
$GABA_C$ ρ2[b] (not natural)	K_d	0.52 ±0.10 μM	potent antagonist		110 ±12 μM
	K_b		15.6 ±1.6 μM	3.5 ±0.3 μM	partial agonist
$GABA_A$	K_b		320 μM	Inactive	agonist
	EC_{50}	5-100 μM	weak antagonist		310 μM
$GABA_B$	K_b		weak agonist	potent agonist	inactive
	EC_{50}		~500 μM	~0.2 μM	

[a] or CGP35024 is 3-aminopropyl(methyl)phosphinic acid. [b] human **ρ** cDNA expressed in *Xenopus* oocites forming homo-oligomers. K_d is the dissociation constant for the agonist; K_b is the binding constant for the antagonist; EC_{50} is the concentration estimated to produce 50% maximum effect.

In conclusion, it seems interesting to study the presence and distribution of $GABA_C$ receptors in the neonatal rat spinal cord using specific probes and antibodies, and to assess their functional role by applying TPMPA.

Na^+/K^+ pump activity

Previous work showed a critical role for Na^+/K^+ ATPase in the spinal cord disinhibited rhythm (Ballerini *et al.,* 1997). In fact, blocking the sodium pump was a very effective protocol to disrupt regular rhythmicity within a few min. Spontaneous bursts were replaced by irregular, fast discharges indicating that network interneurons remained spontaneously active but were unable to synchronize their firing to generate bursts. This observation was obtained with pharmacological blockers of the electrogenic sodium pump. However, it left unanswered a number of questions:

1) was the pump activity fully or partially inhibited?
2) Was the pump inhibition at steady state by the time bursting disappeared?
3) Was the spinal network able to eventually compensate for this effect and to regenerate rhythmicity?

These issue required further studies. Nevertheless, same general aspect of sodium pump activity should be first considered.

P-type pumps

The Na^+/K^+ ATPase is a member of the P-type pumps family, integral membrane proteins able to pump cations (H^+, Na^+, K^+, Ca^{2+}, Mg^{2+}, Cd^{2+} and Cu^{2+}) through a lipid membrane against chemical and/or electrical gradient, by formation of a phosphoenzyme intermediate (P-type) of the catalytic subunit (Solioz and Vulpe, 1996).

This enzyme family, in combination with selectively permeable lipid membranes, helps to establish a distinct intracellular environment and, in eukaryotic cells, also a subcellular compartmentalization of certain ions (for example: sarcoplasmatic Ca^{2+}ATPase, gastric H^+/K^+ ATPase). These intracellular compartments avoid excessive variation in intracellular space (for example: due to a sustained depolarization) and can couple secondary transporters with active pumps (es. Na^+/Ca^{2+} exchanger with Na^+/K^+ pump via Na^+ electrochemical gradient) in a highly efficient way (Fujioka *et al.,* 1998).

A series of protein conformational changes have been postulated to explain coupling of the energy release by hydrolyzing ATP to ion movement; this proposed mechanism could explain ion specificity and stoichiometry of the ion transport process experimentally demonstrated (Glynn, 1993).

Up to now more than one hundred molecules are reported as capable of pumping cations, are widely express in organisms (from prokaryotics to humans), are purified and sequenced to

demonstrate high homology in different species but also high ion selectivity (Solioz and Vulpe, 1996).

Na^+/K^+ pump biochemistry

In animal cells, the major ion-motive pump is the Na^+/K^+ ATPase; the ubiquitous distribution of this transmembrane enzyme ensures the primary control of cell volume, via osmotic gradient, and maintains the differential Na^+ and K^+ distribution across the cell membrane. Because of its high requirement for ATP (about 40% of brain metabolism is devoted to supply its activity; Johnson *et al.,* 1992), anoxia rapidly blocks this powerful machinery which becomes a critical factor for cell survival.

One fundamental characteristic is its stoichiometry: in mammals it extrudes intracellular sodium ions pumping into the cell potassium ions with a 3/2 ratio for every ATP molecule consumed. This ratio suggested another name for this pump, commonly used in neuroscience: electrogenic sodium pump, or simply electrogenic pump. It is considered to be the origin of the cell regenerative excitability. The relevance of the Na^+ and K^+ gradient to tissue excitation via ions flux through the membranes is well known; the first idea of an active pump to maintain such a gradient originated from the observation that heart cells maintain life long rhythmicity (Overton, 1902), preserving their ionic gradients despite generating membrane currents.

Mammalian Na^+/K^+ ATPase is composed of two monomers: the catalytic α-subunit (111 kDa, 3 isoforms in rat) and the glycoprotein β-subunit (55 kDa, 2 isoforms in rat) in a 1:1 ratio. Fig. 4 shows a cartoon of the proposed structure of the Ca^{2+} ATPase α-subunit (allegedly highly similar to the yet unknown Na^+/K^+ ATPase structure); ten transmembrane α-helices are supposed to transport alternatively 3 Na^+ or 2 K^+ ions across the membrane. The pump activity (α1 subunit) is reported in Table 3. The α-chain carries all the known functional properties of the enzyme (catalitic activity, ions and inhibitor-modulator binding sites) and the 3 isoforms are distinguished by their affinity for the inhibitor ouabain (low in α1 subunit, high in α2 and α3) and for ions. Also the expression in tissues differs, preferentially α1 subunit in kidney, α2 and α3 in neurons. The expression is not exclusive and changes during development (Sweadner, 1989).

The β-chain is an adhesion molecule, necessary for pump activity; the β1 isoform is ubiquitous, the β2 is expressed in glia only (Horisberger *et al.,* 1991).

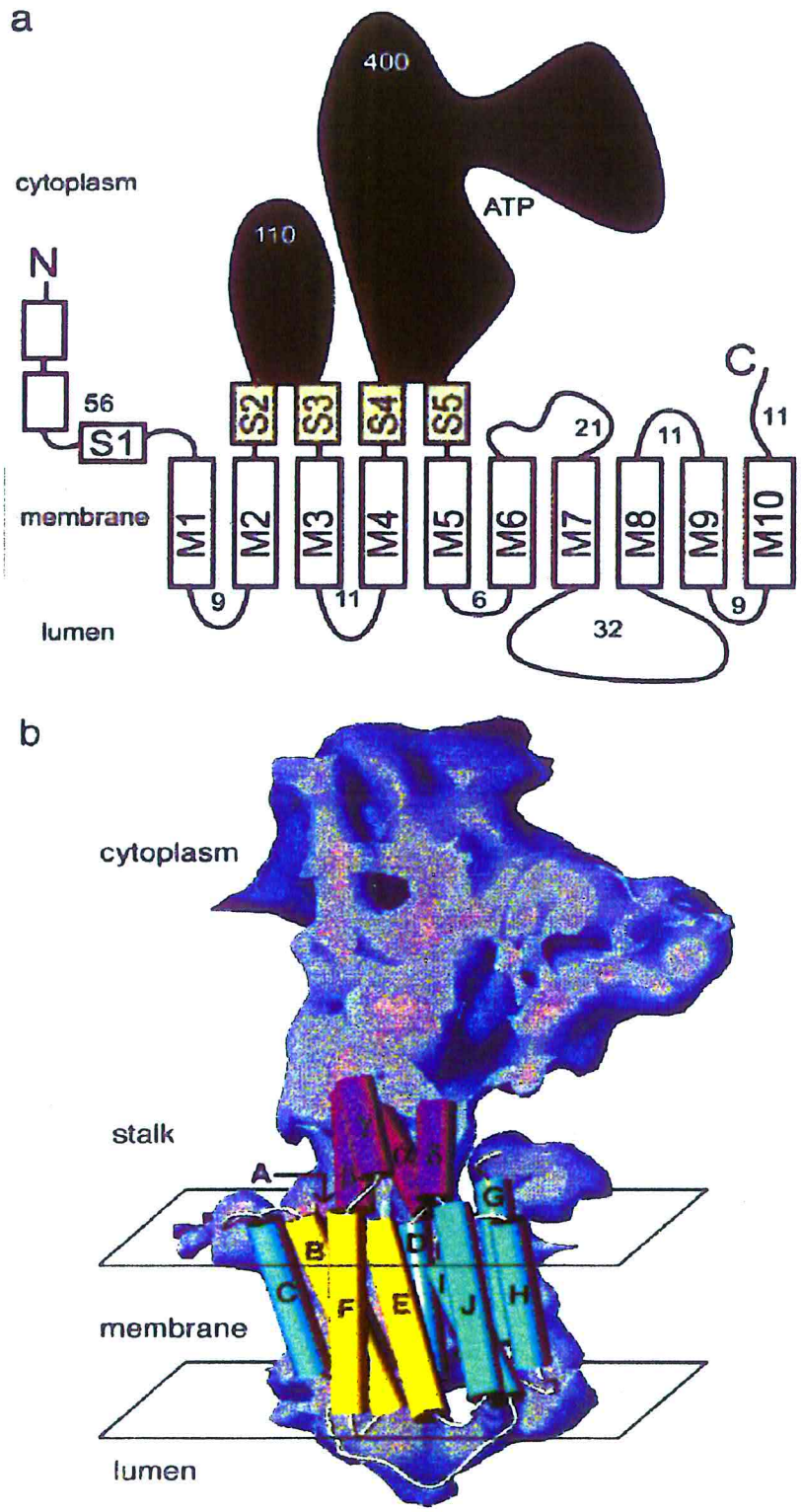

Fig. 4 Structure of a Ca^{++} ATPase at 8-Å resolution (from Zhang *et al.*, 1998).

a, rectangles correspond to predicted α-helices and numbers indicate the number of residues in intervening loops. The two long black loops compose the cytoplasmic domains, which were not considered in the subsequent fitting. **b:** result of fitting transmembrane and stalk helices to the density map.

Table 3 α1 rat subunit: affinity to natural substrate and activity in physiological condition (Toudstrup-Jensen *et al.*, 2001).

rat kidney (α1) sodium pump	$K_{0.5}$ (mM)			turnover rate[a] (min^{-1})
	ATP	Na^+	K^+	
	0.435 ± 0.019	9.85 ±0.14	0.615 ±0.011	8474 ±165

[a] calculated at 37 °C in the presence of 130 mM NaCl, 20 mM KCl, and 3 mM ATP. $K_{0.5}$ is the ligand concentration giving half-maximum activation or inhibition.

Na^+/K^+ pump physiology

The main role of the Na^+/K^+ ATPase is to maintain high $[K^+]_{in}$ and low $[Na^+]_{in}$. The pump is sensitive especially to $[Na^+]_{in}$. Na^+ homeostasis is ensured by the capacity of the pump (despite its high basal level) to increase significantly its transport rate in response to increasing intracellular Na^+ concentration and it does not saturate until $[Na^+]_{in}$ is 50-100 mM (Shen and Johnson, 1998). Alternative regulatory mechanisms induced during a persistent increase in $[Na^+]_{in}$ may be an accelerated membrane insertion of pre-existing pump molecules and/or their assembly from α- and β-subunits. The pump site density may increase in a couple of min by a 3-fold factor, suggesting the presence of a pre-existing pool of pump molecules for rapid recruitment (Senatorov *et al.*, 2000). If $[Na^+]_{in}$ is maintained elevated for tens of min, the rate of transcription of the α-subunit mRNA may be increased and the rate of degradation of β-subunit mRNA may be decreased in response to elevation in $[Ca^{2+}]_{in}$ (via Na^+/Ca^{2+} exchanger). Na^+ can also directly modify gene expression inducing an increase in cytoplasmatic pump expression by 1-3-fold (Senatorov, *et al.*, 2000).

The pump activity may be finely tuned by ouabain-like factors, especially in kidney (low affinity isoform). Ouabain (or G-strophanthin) and strophanthidin are the most used, uncompetitive sodium pump blockers. They are glycosides extracted from *Strophanthus*, and are both highly

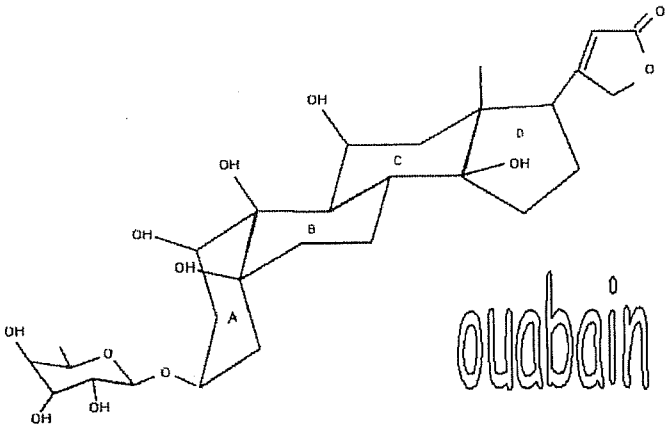

selective blockers that bind to specific site on cytoplasmic side (α subunit). The actions of strophanthidin can be reversed washing out the drug, whereas the actions of ouabain are usually irreversible and accompanied by a gradual increase in membrane conductance (Willis *et al.,* 1974). In the rat, the α1 sodium pump subunit displays an ouabain IC_{50} (inhibition constant for [γ^{32}P]ATP hydrolisis at 37° C by microsomal preparation) of 50 μM, the α2 and the α3 subunits an IC_{50} of approximately 0.02 μM (Tao *et al.,* 1996).

Na^+/K^+ pump spinal cord distribution

The data concerning the distribution of the Na^+/K^+ ATPase isoforms in the spinal cord are limited and to a certain extent controversial. In the rat brain the α3 and α2 isoforms appear to constitute about 100% of sodium pump expressed, the α1 is estimated 2 ±1% (standard error; Tao *et al.,* 1996). In the rat spinal cord only motoneurons were studied in detail with specific antibodies, revealing immunostaining for all five subunit isoforms (3 α and 2 β) with different distribution on different membrane areas and also in the cytoplasm (Dolapchieva, 1998). The α3 subunit mRNA was detected at high level in all neurons of the ventral horn, and the α1 subunit mRNA in a limited set of motoneurons only (Mata *et al.,* 1991), never in interneurons.

Na^+/K^+ pump and rhythms

Although the Na^+/K^+ ATPase is the main regulatory enzyme of intracellular monovalent cation concentration, in the absence of any excitatory signal its steady state activity is low and its contribution to the membrane potential is minimal in the large majority of cells (Willis *et al.,* 1974). To study electrogenic sodium pump activity, manifested as an hyperpolarizing current, the enzyme activity can be increased by intracellular $[Na^+]_{in}$ accumulation via tetanic stimulation (opening Na^+ channels), inhibited by temperature decrease or stimulated by direct injection of Na^+ into a single cell (Willis *et al.,* 1974). Increase in intracellular $[Na^+]$ results in a larger current (estimated between 200 and 800 pA in rat dopamine neurons by Shen and Johnson, 1998) that repolarises the cell to the resting potential while pumping out the excessive Na^+ content.

Up to now only three examples of the utilisation of the sodium pump current during rhythmic bursts have been observed (Shen and Johnson, 1998). In L3 *Aplysia* neurons (Willis *et al.,* 1974) and in midbrain dopamine neurons (Johnson *et al.,* 1992) burst firing probably is not a

network driven rhythmicity but is generated by pacemaker neurons that, in the presence of ouabain or strophanthidin, lost their rhythmogenic properties. In spinal cord disinhibited rhythm (Ballerini *et al.,* 1997) the pump contributes to network driven rhythmicity. In this preparation also sodium pump blockers can disrupt bursting rhythm.

Aims

The main aim of the present work was a detailed characterisation of disinhibited rhythmicity generated by the neonatal rat spinal cord; in particular we were interested to:

1) evaluate the presence and the role of a third component of fast synaptic inhibition (chloride mediated like $GABA_A$ and glycine ones), namely the $GABA_C$ conductance, using:

- electro-physiological studies applying a selective $GABA_C$ receptors blocker;
- *in situ* hybridisation with ρ1 and ρ2 probes;
- immunohistochemical techniques with specific polyclonal antibodies;

2) identify the role of the Na^+/K^+ electrogenic pump in the generation and/or maintenance of rhythmic activity. Thus we studied:

- the effectiveness of the strophanthidin induced block with $^{86}Rb^+$ biochemical assay;
- the effect of blocking this pump on the spontaneous and evoked electrical activity;
- if spontaneous activity can still be generated in the absence of Na^+/K^+ ATPase;
- the characteristics of late bursting unmasked by long term strophanthidin application on disinhibited rhythm;

3) set up a very simple mathematical model to describe rhythms generated by the purely excitatory spinal cord network (in the presence and in the absence of the Na^+/K^+ pump).

Methods

Dissection

Spinal cords (from thoracic to sacral segments) were isolated from neonatal (zero to nine day old: P0-P9) rats (Wistar). After deep anesthesia induction with an intraperitoneal injection (0.2-0.4 ml) of urethane (10% w/v in water), the animal was decapitated and the ventral aspect of the vertebral column exposed through a ventral approach. The remaining part of the body (the back and the hindlimbs) was washed and cooled in chilled artificial cerebrospinal fluid (ACSF; see below for composition). Then it was fixed (ventral side up) with pins to the sylgard bottom of a Petri dish and immersed in the same cold solution, continuously bubbled with O_2 (95%) and CO_2 (5%).

The spinal cord was exposed by bilateral complete laminaectomy (rostro-caudal; Fig. 5) using micro-scissors (FST GmbH) under a stereomicroscope (Wild Heerbrugg). After cutting the exposed ventral side of the meninges, ventral and dorsal roots were cut as close as possible to ganglia. After removing the dorsal part of the meninges the spinal tissue isolation was complete (dissection time: ~15 min).

Electrophysiological experiments

The en bloc isolated spinal cord was pinned to the bottom of a recording chamber (volume ~1 ml) and continuously superfused with ACSF (at room temperature) by a peristaltic pump (Gilson; flow 7-8 ml/min). A flow spacer (between pump and chamber) ensured constant flow rate during drug application and reduced electrical noise.

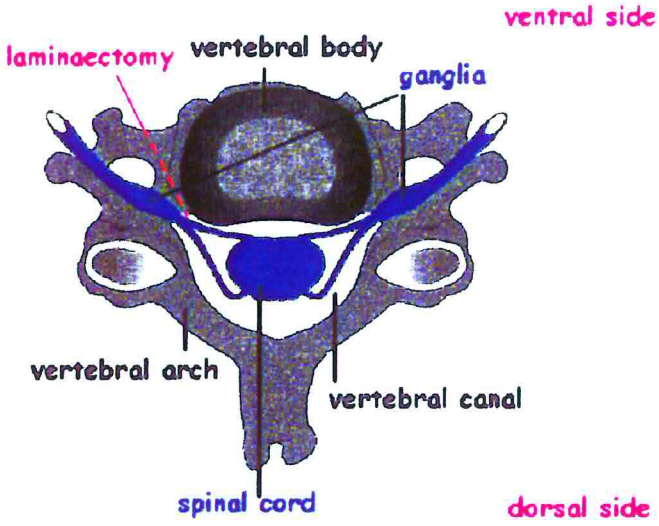

Fig. 5 View of a coronal section of the vertebral column (ventral side up). Blue is the nervous tissue, red the line of one laminaectomy used to expose the spinal cord.

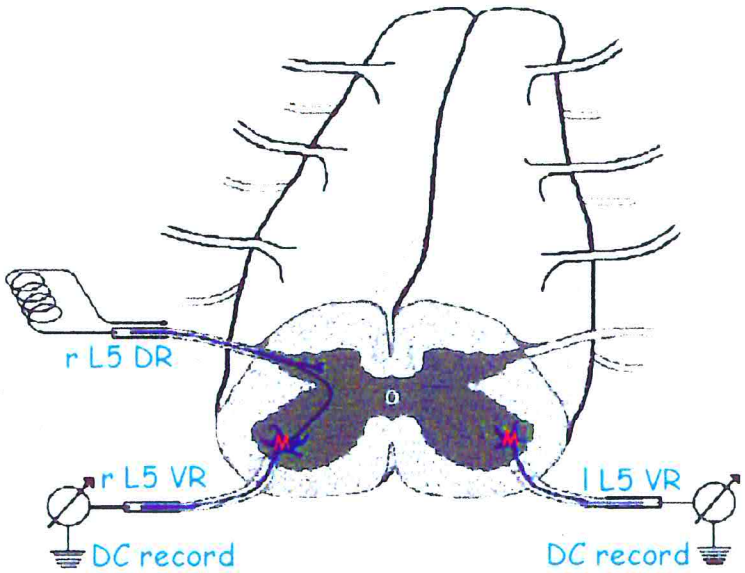

Fig. 6 A schematic view of a portion of spinal cord. Two suction electrodes for DC recording and a bipolar electrode for stimuli are shown.

ACSF (control solution) had the following composition (in mM): NaCl 113, KCl 4.5, $MgCl_2$ 1, NaH_2PO_4 1, $CaCl_2$ 2, glucose 11 and $NaHCO_3$ 25, gassed with 95% O_2 and 5% CO_2, pH = 7.4.

High potassium solutions were in the 5.5-9.5 mM K^+ range; since they altered osmolarity and chloride concentration by less than 3.5%, no ionic compensation was applied.

Experimental configuration: the spinal cord was pinned, in the recording chamber, lateral side up or ventral side up, for protocols with or without stimulation, respectively. Extracellular recordings from lumbar (L2-L6) VRs were performed via one or two suction electrodes (Fig. 6). The suction electrodes were made by heating and pulling (List-Medical) glass capillaries (outØ 2mm, inØ 1.5mm). After heating and polishing them with sandpaper (P1000) or carborundum stone, the tip internal diameter was between 0.1-0.3mm (to closely fit the roots). All electrodes were filled with normal ACSF. One silver/silver cloride wire (925‰ Ø 0.2 mm) or one silver chloride ($AgCl_2$) pellet (Clark Electromedical Instruments, Ø 1.0 mm) was inserted into the recording electrode and another pellet (ground) was placed into the bath. Stimuli were applied by a bipolar suction electrode (Fig. 6) to a single lumbar dorsal root (DR). Electrical pulses were delivered via a pair of silver or platinum wires (925‰, Ø 0.2 mm or 950 ‰, Ø 0.3 mm respectively), one inserted into the suction electrode while the other one was near the electrode tip to reduce stimulus artifacts.

Recording tecnique: VRs were completely drawn into the electrodes to establish a good seal between the electrode tip (outØ ≥0.3mm) and the cord surface. The offset of the trace was neutralized by current injection though an Axoclamp 2A (Axon Instruments, via the 1x headstage). A low-noise battery-powered DC-coupled differential amplifier (World Precision Instrument, DAM 50) amplified the signal 1000 times and filtered it with 0.1 Hz and 10KHz passbands. The records were displayed on line on a chart recorder (Gould RS3400), stored with a digital recording system (analog to digital converter by Instrutech Corporation, VR-10A, and a tape recorder; acquisition frequency 18KHz) and with a computer (analog to digital converter by DigiData 1200 Interface, Axon instruments; acquisition frequency 1 or 10KHz) for further analysis.

Under this condition, DC-coupled VR recordings contained firing activity by motor axons, plus membrane potential variations generated within the motoneuron population and electrotonically spread along the motor axons (Fig. 2; see also Bracci *et al.,* 1996b, for recording from a single motoneuron and one VR simultaneously).

Electrical stimuli: single or repetitive stimuli were applied to a single DR in order to evoke a reflex or a burst detected from the corresponding VR. Pulses were 0.1-1.0 ms long, with 0.5-20V intensity and were given at 0.008-2 Hz frequency. For each preparation stimulus intensity was expressed as times threshold (xTh), where Th was the lowest amplitude which could elicit a detectable postsynaptic response in a VR (see Fig. 34). The frequency was set with a Digitimer D100, the amplitude and duration with an isolated stimulator (Digitimer DS2 or Devices 2533).

Impulse conduction: the compound action potential in DR fibers was measured using cut DRs, applying stimuli to one root end and recording from the other one; the responses obtained from each root were compared in different conditions and were the average for 30 pulses (7-10xTh, 0.1ms, 1Hz). The difficulty to measure accurately such a short root length (2-3mm) did not permit calculation of conduction velocity.

Drugs

Substances were stored in small aliquots at –20°C, highly concentrated (usually 10^3 times larger than the final concentration), and dissolved in distilled water or dimethylsulphoxide (DMSO, C_2H_6SO, Sigma) prior to use. All drugs were bath applied via the superfusion solution.

The following drugs were used:

(1,2,5,6-tetrahydropyridin-4-yl)methylphosphinic acid (TPMPA, Tocris, water soluble)

5-hydroxytryptamine (5-HT or serotonin, Sigma, water soluble)

6-cyano-7-nitroquinoxaline-2,3-dione (CNQX, Tocris, DMSO soluble)

γ-aminobutyric acid (GABA, BDH, water soluble)

(-)baclofen (Sigma, water soluble)

bicuculline methiodide (Bic, Sigma, water soluble)

isoguvacine hydroclhoride (Iso, Tocris, water soluble)

N-methyl-D-aspartic acid (NMDA, Tocris, water soluble)

ouabain (Oua, Sigma, DMSO soluble)

pentobarbitone (sodium salt, BDH, water soluble)

strophanthidin (Stro, Sigma, DMSO soluble)

strychnine nitrate (Stry, Sigma, water soluble)

tetrodotoxin (TTX, Affinity, water soluble)

Data analysis

The following electrical responses were analyzed: evoked VR reflexes (via DR stimuli, Fig. 7), slow VR depolarizations induced by drugs (Fig. 9A), bursts appearing in the absence of fast, chloride mediated, synaptic inhibition (Fig. 12) and, in particular, after Na^+ pump inhibition by strophanthidin (Fig 8).

To compare single pulse VR reflexes (acquisition 10KHz, 20ms pre-pulse and first 180ms of response), the average of 3-10 (see each result) evoked responses were considered and the peak amplitude and/or the depolarization area was measured. Each pulse delivered to one DR (usually the corresponding ipsilateral), was 0.1 ms of duration, between 1 and 12 times threshold (12xTh).

To compare VR responses induced by train of stimuli (3 to 60 pulses, 0.33-1Hz, 1-10xTh and 0.1-1ms), cumulative depolarization amplitude, half decay time and cumulative depolarization velocity (early=from 3rd to 7th stimulus; late= last five stimuli) were measured (see Barbieri and Nistri, 2001). To compare responses of different cumulative depolarization amplitude, we normalized the peak of cumulative depolarization with respect to the control one and superimposed the two responses after scaling.

Disinhibited rhythm bursts were regular events (Bracci *et al.*, 1996a). In the presence of strophanthidin bursts became very variable. Thus, a burst was defined as a large, sustained depolarization starting suddenly from baseline, reaching a persistent plateau, typically comprising repeated oscillations, and decaying slowly back to the baseline. A burst was at least five times longer than a DR evoked reflex (measured from its onset to noise threshold).

Quantitative analysis of bursting activity required definition of several parameters (Fig. 8):

- interburst interval: the time between the onset of one burst and the onset of the subsequent one, its variability (expressed as CV) was an index of regularity;
- duration: the time during which the membrane potential remained above preset noise threshold (usually set at 25 time the standard deviation of base line noise; about 100-120 μV);
- pause: the time between the end of one burst and the onset of the subsequent one;
- time to plateau: the time between the onset of the burst and the plateau phase;
- recovery time: the time between the plateau phase of the burst and its end;
- amplitude: the depolarization between baseline and plateau;

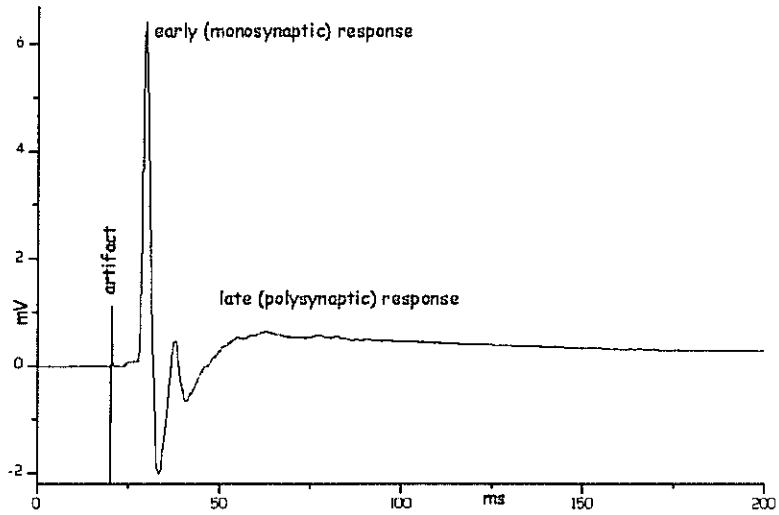

Fig. 7 Example of the average of ten consecutive evoked events by DR stimuli; note its component.

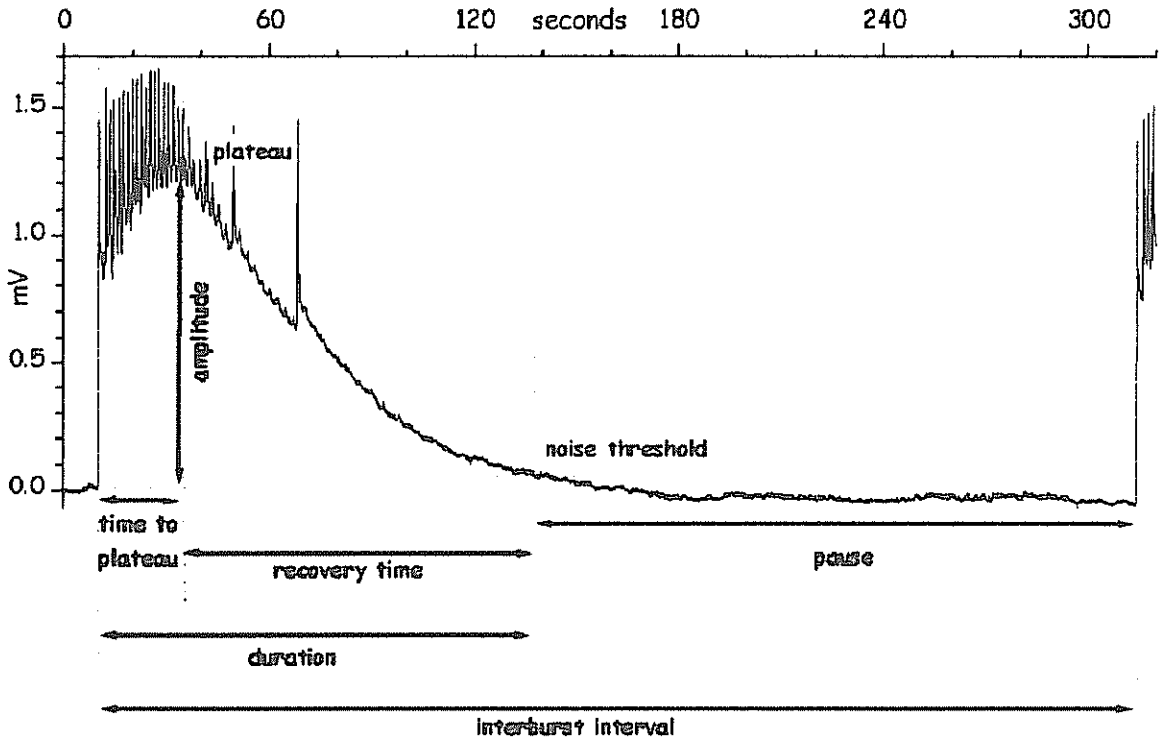

Fig. 8 The various components of a late spontaneous burst induced by strychnine, bicuculline and strophanthidin (1, 20 and 4 μM respectively).

Pooled data were expressed as means ± standard deviation (SD) or means and coefficient of variation (CV); statistical difference were evaluated using paired or unpaired t-test and one-way ANOVA (significance level used: $P<0.05$). The acquisition programs were Axoscope 7.0 and 8.0 (Axon Instruments), the analysis programs were Origin 6.0 (Microcal Software) and Excel 97 (Microsoft Corporation).

Biochemical assay

The en bloc isolated spinal cord (after complete removal of meninges) was included in agar (Sigma; 2.5% w/v in ACSF; fluid over 36° C, solid under 30°) and cut in ice cold solution with a Vibratome (series 1000). The acutely cut slices (350-400 μm thick) were allowed to recover for at least 1 hour before the experiment started.

To evaluate the Na^+/K^+ pump activity the slices were incubated in the presence of radioactive rubidium ($^{86}Rb^+$, Amersham Pharmacia Biotech). The pump does not discriminate between potassium and rubidium and thus transports the radioactive monovalent cation into the cell (Longo *et al.,* 1991; Bowen, 1992).

After preincubation in control solution (normal ACSF) or in the presence of different sodium pump blocker (strophanthidin 4 μM, ouabain 50-200μM) for different time (30-60 min), slices were incubated in the presence of $^{86}Rb^+$ at room temperature. At different times (1.5-11.5 min), in order to construct a plot of radioactivity versus incubation time, the slices were removed from the bath and washed three times in isotonic saline solution (NaCl 150 mM, ice cold), to remove $^{86}Rb^+$ from the extracellular space. The slices were then stored in small tubes (1.5 ml) and dissolved in NaOH (0.2-0.5 M, 500 μl) to test for radioactivity and protein concentration. The radioactivity was measured with a β counter (liquid scintillation analyzer: TRI-CARB 2100TR, Packard) referred to the amount of tissue proteins measured with a colorimetric assay (Bio Rad protein assay, based on the Bradford dye-binding procedure, Bradford, 1976) using a spectrophotometer (Spectracount, Packard,).

Heat inactivated (60 min at 55°C) spinal cord samples were used to evaluate unspecific $^{86}Rb^+$ binding. Slices preincubated in ACSF gave the total $^{86}Rb^+$ uptake (without any blocker) as control after subtracting unspecific binding. After 30 or 60 min of incubation in 4 μM strophanthidin solution (the concentration used for all electrophysiological experiments) activity was measured. Any residual $^{86}Rb^+$ signal left in the samples in the presence of saturating concentrations (50-200 μM) of the irreversible Na^+ pump inhibitor ouabain was used to measure $^{86}Rb^+$ accumulation into cells via pump independent transport.

Molecular biology experiments

Sequencing analysis: the cDNAs coding for the rat ρ1 and ρ2 subunit were kindly provided by Dr. S. Lipton (Burnham Institute, La Jolla, California, USA; see Zhang *et al.,* 1995). The 3' untranslated (UTR) region of the cDNA coding for the rat ρ2 subunit was sequenced with an automated DNA sequencer (LI-COR 4000L, LI-COR Inc) on both strands with a SequiTherm Excel II DNA sequencing kit (Epicentre Technologies Corporation) using Infra Red Dye 800-labelled primers (MWG Biotech).

Western blotting: adult rat brain, ovary, testis and retina proteins were resolved on a 8% SDS polyacrylamide gel and transferred to nitrocellulose (Shleicher and Schuell). Membranes were blocked in 5% non-fat dry milk in Tris-buffered saline (TBS)/0.05% Tween 20 (TBST). After incubation with the primary rho 63 polyclonal antibody against ρ1, ρ2 and ρ3 subunits kindly provided by Prof. H. Wässle (Max-Planck-Institute for Brain Research, Frankfurt, Germany; see Enz *et al.,* 1996) in blocking solution (1:250 dil.), overnight at 4°C, membranes were washed thrice with TBST, incubated with anti rabbit secondary antibody coupled with alkaline phosphatase (Vector Labs Inc) for two h at room temperature. After incubation, the membranes were washed twice with TBST and once with TBS. Proteins were visualized using p-nitro blue tetrazolium chloride (NBT; Sigma, 0.5 mg/ml) and 5-bromo-4-chloro-3-indoyl phosphate p-toluidine salt (BCIP; Sigma, 0.25 mg/ml) in developing buffer (0.1 M Tris, 0.5 mM $MgCl_2$, pH 9.5).

In situ hybridisation: rats, deeply anesthetised with an i.p. injection of chloral hydrate (10 % in saline, Sigma), were killed by transcardial perfusion with 4% paraformaldehyde (PFA; Rieder-de Haën) in phosphate buffer saline (PBS; pH 7.4), for *in situ* hybridisation.
In situ hybridisation was carried out on P1 (n=4 animals), P7 (n=5 animals), or adult (n=4 animals) as described by Tongiorgi *et al.* (1998). In brief, 40 μm sections were post-fixed in 4% PFA overnight at 4°C and permeabilised in Na-metaperiodate (2.3% in H_2O; Sigma), followed by 1% Na-borohydrate (Sigma) in 100 mM Tris/HCl (pH 7.5) and, finally, by 8 mg/ml Proteinase K (Roche Diagnostics) in PBS plus 0.1 % Tween 20. The sections were then pre-hybridised at 55°C in the hybridisation mix containing 300 mM NaCl and 50% formamide (Sigma) and hybridised overnight at 55°C in the hybridisation mix with the riboprobes (50 ng/ml). The ρ1 anti-sense digoxigenine-labelled riboprobes were made from 2 Kb long fragment obtained from the 3' UTR of ρ1 cDNA (sequence accession # NM 017291,

nucleotides 2836- 4183) and the ρ2 subunit 3' UTR sequence encompassing nucleotides 1621-3170 of the new sequence described in the present paper (see Fig. 13). The two riboprobes were hybridised in parallel on adjacent sections from the same animals to rule out artifactual changes affecting signal expression and to enable direct comparison between the two subunits. Washes were carried out up to 0.1% Na saline citrate (0.1 x SSC) plus 0.1% Tween 20 at 60°C. After overnight incubation with anti-digoxigenine, alkaline phosphatase-coupled Fab fragments (1:1000, Roche Diagnostics), the reaction was developed for 3 h at room temperature with 337 ng/ml 4-nitro blue tetrazolium and 175 ng/ml 5-bromo-4-chloro-3-indolyl-phosphate (Eurobio) in 100 mM Tris/HCl (pH 9.5), 50 mM $MgCl_2$, 100 mM NaCl, 1 mM levamisol (Sigma). For the competition experiments, the competitor anti-sense riboprobes were synthesised with unlabelled nucleotides and added (20 fold excess) to the hybridisation mix containing the labelled riboprobes. The maximal distance of dendritic labelling (MDDL) was measured on 50 dendrites from motoneurons (n=8 sections from 2 animals, 4 sections each) with the function "trace" of the program Image ProPlus (Media Cybernetics, Silver Spring) as described previously (Tongiorgi *et al.*, 1997).

Immunohistochemistry: brains and en bloc spinal cords (P1 n=4, P7 n=4, adult n=3) were fixed in paraformaldehyde (4% in phosphate buffer saline; incubation 5-10 min), cryoprotected in 20% sucrose in PBS overnight at 4° C and frozen in embedding medium (OCT). Sagittal 12 μm sections from the whole brain or 12 μm coronal sections from the lumbar segment of the spinal cord were cut with a cryostate (Leica) and allowed to dry overnight at room temperature. After hydration (10 min in PBS), the sections were incubated (1 h at room temperature) with anti-rho 63 polyclonal antibodies diluted 1:200 (in PBS, 5 % fetal calf serum; Gibco Lifetech). The slices were then incubated (30 min at room temperature) with a secondary anti-rabbit immunoglobulin G conjugated with horse radish peroxidase (1:200; DAKO). The reaction development (15-20 min at room temperature) used 3,3'-di-aminobenzidine tetra-hydrochloride (0.4 mg/ml; Sigma), 2 mg/ml D-glucose (Sigma), 0.02 mg/ml glucose oxidase (Sigma), 2 mg/ml nickel (II) ammonium sulphate (Carlo Erba) in PBS. In total, we analysed 18 sections of P1, 23 sections of P7 and 26 sections of adult spinal cord.

Results

Results I: $GABA_C$ receptor

The presence and the functional role of $GABA_C$ receptors in the spinal cord network, and the developmental regulation of its ρ1 and ρ2 subunits, were evaluated with three different approaches:

1) electrophysiological studies of the effects induced by (1,2,5,6-tetrahydropyridine-4-yl) methylphosphinic acid (TPMPA, Murata *et al.,* 1996; Ragozzino *et al.,* 1996), a specific blocker for all isoforms of $GABA_C$ receptors;

2) *in situ* hybridisation using ρ1 and ρ2 specific probes, taking the retina as standard reference region (Enz *et al.,* 1995);

3) immunohistochemical techniques using anti-rho 63 (Enz *et al.,* 1996), a polyclonal antibody against the three ρ subunits.

Effects of TPMPA on GABA mediated responses

This batch of experiments was carried out on spinal cord preparatioins from P3-P8 rats.

Fig. 9A shows records from a VR L5 during a train of electrical pulses (10xTh, 0.1ms, 1/30s) applied to the ipsilateral L5 dorsal root. Bath application of exogenous GABA (500 μM, 120s) is indicated by the filled horizontal bar. The short upward deflections throughout this

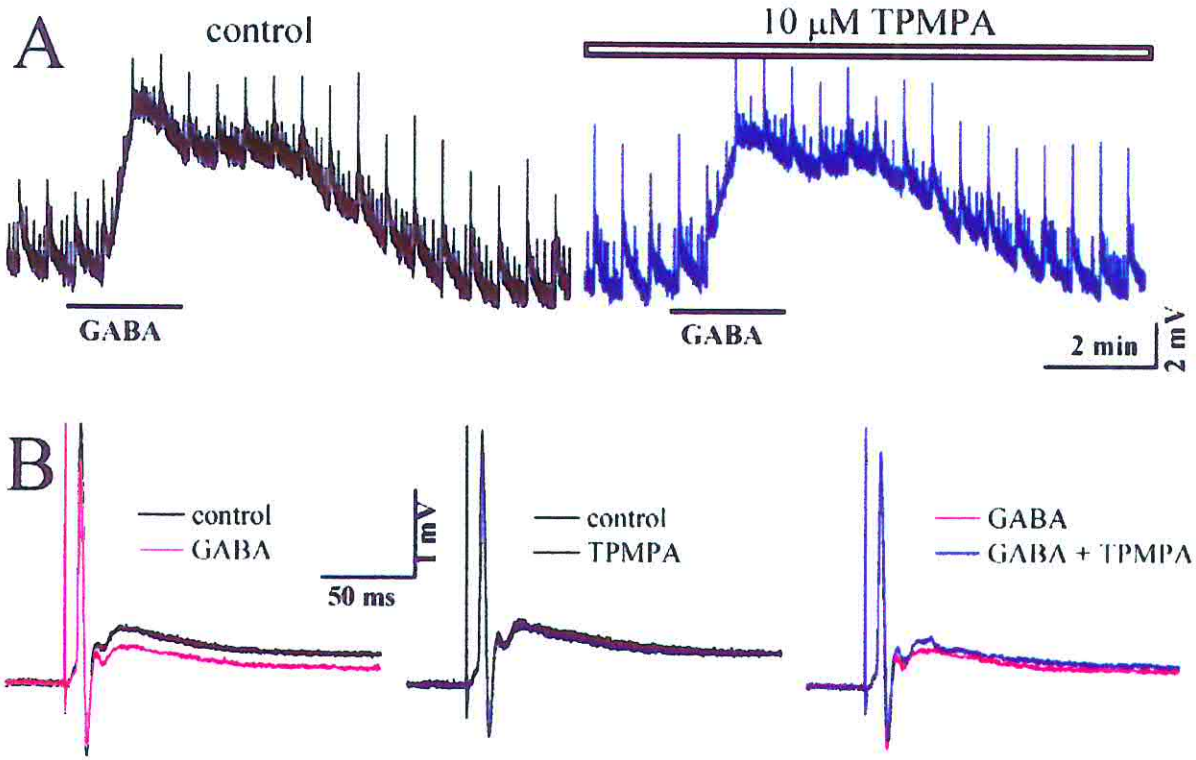

Fig. 9 Effect of TPMPA on changes in VR polarization level and spinal reflexes induced by exogenously applied GABA

Fig. 9 Effect of TPMPA on changes in VR polarization level and spinal reflexes induced by exogenously applied GABA.

A: slow time base VR responses indicating depolarization elicited by 0.5 mM GABA (applied as shown by the horizontal filled bar) which peaks and fades during 2 min application. The left panel shows effect in control solution while the right panel shows effect in the presence of TPMPA (horizontal open bar; exposure to TPMPA started 10 min before GABA). Note that the action of GABA is unaffected and that there is no change in baseline polarization level. **B**: changes in reflex responses induced by GABA (0.5 mM). Left, control trace (red line obtained by averaging 10 responses) and trace following GABA application (black line obtained by averaging three responses after the depolarization peak). Note that slow component of the reflex is depressed by GABA. Middle, control and TPMPA traces (thin and black records, respectively) are similar. Right, trace during GABA application in the presence of TPMPA (black line) shows only modest depression of slow reflex when compared with trace in GABA solution (red line). All records are from the same preparation.

trace represent polysynaptic reflexes; the slow DC changes in baseline is the motoneuron depolarization by exogenous GABA, comprising direct effects on motoneurons themselves plus indirect ones via the local network of interneurons (Evans, 1978; Long *et al.,* 1989). The action of GABA reached a peak and then faded during the continuous application of the amino acid through a combination of receptor desensitization and uptake (Hackman *et al.,* 1982). Recovery to baseline after wash took several min.

Whilst this concentration of GABA is lower than the half maximal dose for in vitro spinal cord preparations (Nistri and Constanti, 1979), it was used as the test dose since it has been routinely employed in previous studies of various CNS preparations (Evans, 1978; Kemp *et al.,* 1986; Long *et al.,* 1989) to minimize response fading.

In the spinal cord GABA produces motoneuronal depolarization and inhibits polysynaptic transmission elicited by dorsal root stimuli (for reviews see Nistri and Constanti, 1979; Sivilotti and Nistri, 1991). These effects of GABA are mainly mediated by activation of conventional receptor classes such as the $GABA_A$ and $GABA_B$ ones. Could pharmacological antagonism of $GABA_C$ receptors modify responses to GABA?

The effect of GABA was again tested (Fig. 9A right) after applying TPMPA (10 μM, 10 min preincubation) which *per se* did not alter baseline or reflex activity. This concentration of TPMPA was chosen on the basis of previous in vitro studies, which indicated it as capable of saturating $GABA_C$ receptors, and free from non-selective actions (Murata *et al.,* 1996; Ragozzino *et al.,* 1996; Chebib *et al.,* 1998). Under these conditions the GABA induced depolarization was essentially unaffected by TPMPA.

Fig. 9B displays, on a faster timebase, the reflex responses recorded at various times during application of GABA. Control and TPMPA are the average of ten consecutive responses, while GABA and GABA+TPMPA only of three responses at the peak of depolarization. In the left panel it is clear that at the peak of the GABA depolarization the slow component of the reflex was severely depressed (32.4% decrease) leaving the early (presumably monosynaptic) response slightly reduced in amplitude (14.3 % decrease). Subsequent application of TPMPA failed to affect any component of the reflex (middle panel) where the two traces (in the absence and in the presence of TPMPA alone) are superimposed. However, TPMPA impaired the depressant action of exogenous GABA on the slow component (right panel in which this effect is compared with the one by GABA alone). Such a partial block was reversible after 60 min washout (not shown).

Table 4 Sensitivity of GABA receptor agonist mediated responses to TPMPA

		% reduction in reflex area		
	μM	control solution	TPMPA (10 μM)	n
GABA	500	45 ± 10	28 ± 13 *	7
baclofen	2.0	69 ± 7	74 ± 11	3
baclofen	0.5	50 ± 18	58 ± 14	3
isoguvacine	50	57 ± 15	57 ± 17	7

* Significantly different from control data with $P < 0.0001$

Table 4 shows that, on average, the GABA induced depression of the slow component of the reflex was 45±10 % and became 28±13 % in the presence of TPMPA ($P<0.0001$; pooled results from 7 preparations by comparing data before and after adding TPMPA to each spinal cord). This antagonism was observed in 7/11 spinal cord preparations while in the remaining 4 of them there was no change: thus, in the majority of cases a small, albeit consistent, antagonism could be observed.

Fading and relatively slow recovery of responses to exogenous GABA made it impractical to construct dose-response curves but dictated the need to validate the reliability and reproducibility of responses to the test dose of GABA as depicted in Fig. 10A. In this example the first and second (20 min later) application of GABA induced an equivalent VR depolarization. Fig. 10B shows that the action of GABA on reflex activity was also highly reproducible as the first application evoked a reduction of the slow reflex (left) mimicked by analogous depression 20 min later (right). Pooled data from 4 spinal cord preparations indicated that the depression of spinal reflexes was virtually identical during the first and second application of GABA (54 ±13 and 53 ±12 %, respectively). These data show that our experimental approach was capable of detecting even small changes in responses and that the observed antagonism by TPMPA of the GABA mediated reflex depression was a genuine phenomenon.

Effects of TPMPA on $GABA_A$ and $GABA_B$ receptor mediated responses

It was important to further examine if TPMPA might have interacted non selectively with

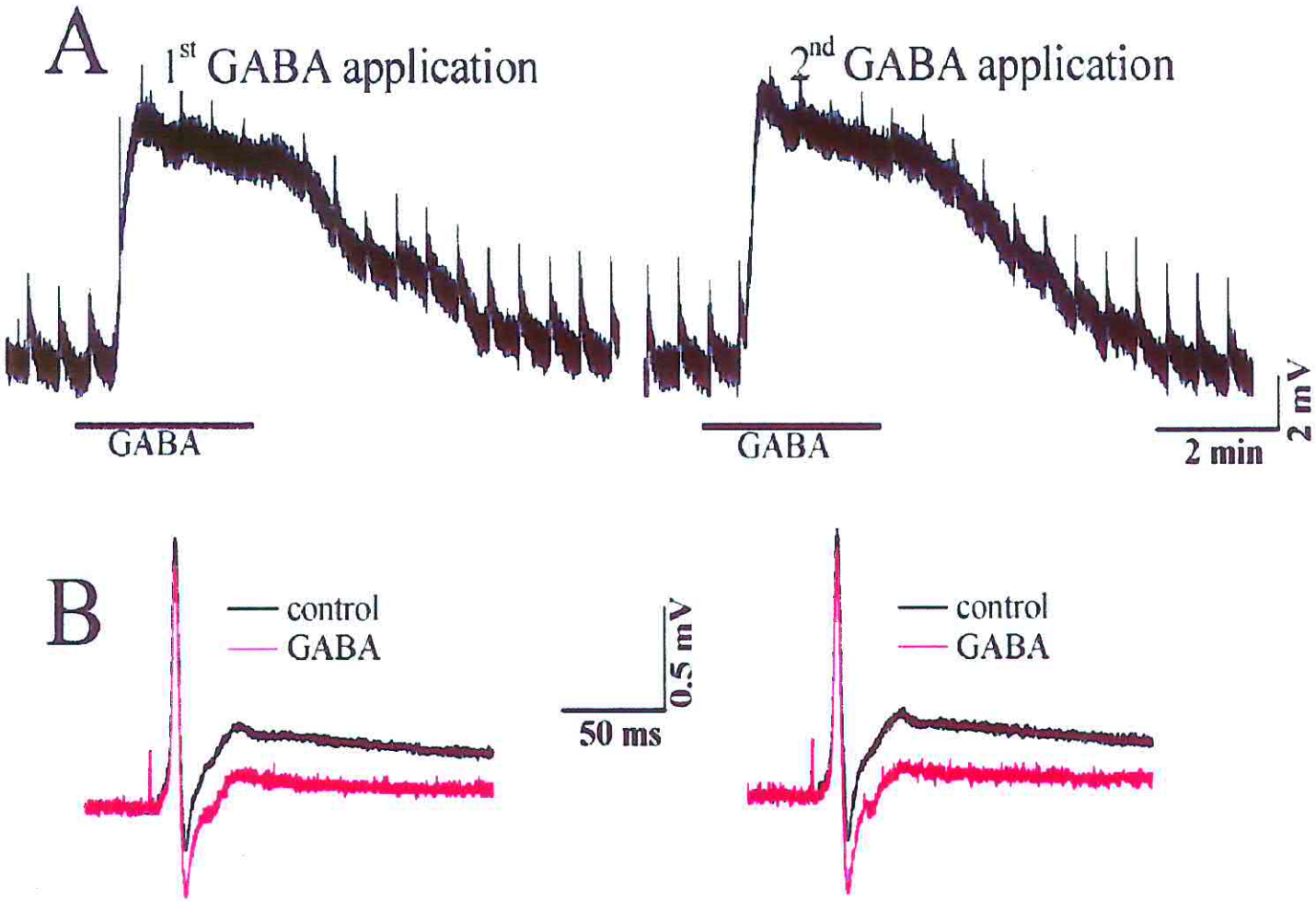

Fig. 10 Close reproducibility of GABA responses

Fig. 10 Close reproducibility of GABA responses. **A**: slow time base records of VR depolarizations induced by 0.5 mM GABA in control solution. The two applications spaced by 20 min interval gave analogous effects. **B**: reflex responses are similarly depressed during the two successive applications of GABA shown in A.

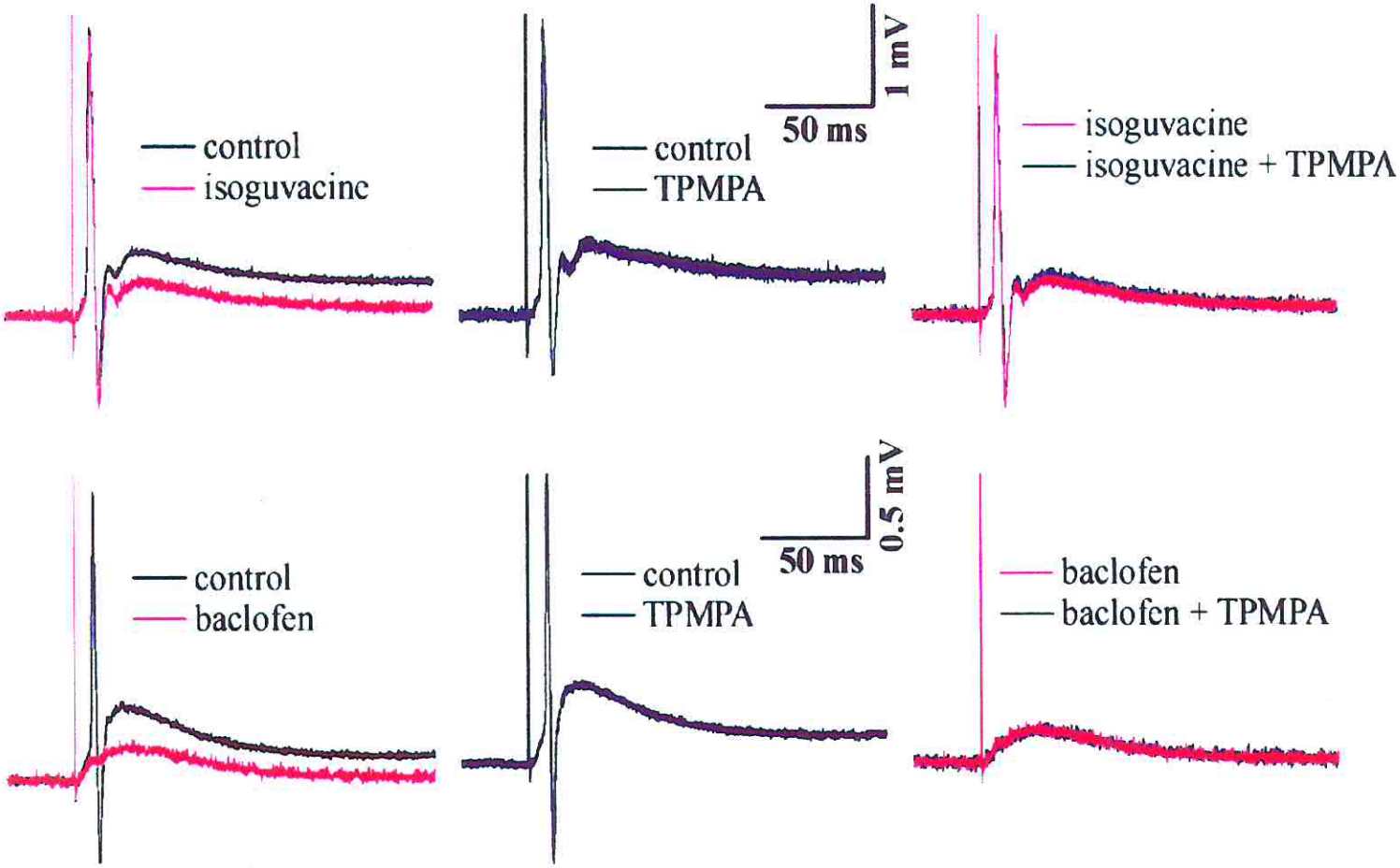

Fig. 11 The action of isoguvacine or baclofen on spinal cord responses is unaffected by TPMPA. **Top** row: the depression of reflex responses induced by 50 μM isoguvacine (left) is unaffected by application of 10 μM TPMPA (right) which *per se* does not change reflex activity (middle). **Bottom** row: the depression of the reflex responses induced by 2 μM baclofen (left) is unaffected by application of 10 μM TPMPA (right). For further details see Figure 1 legend.

Fig. 11 The action of isoguvacine or baclofen on spinal cord responses is unaffected by TPMPA

other GABA receptor classes in view of its chemical structure which resembles the GABA agonist isoguvacine and its reported ability (in high concentrations) to activate $GABA_B$ receptors (Murata *et al.,* 1996; Ragozzino *et al.,* 1996; Bormann, 2000; Chebib *et al.,* 1998). The issue of antagonism selectivity was therefore further investigated.

Fig. 11 (top row) shows that the depression by 50 μM isoguvacine of slow reflex activity (left) was unchanged in the presence of TPMPA (right) which *per se* had no effect on control reflexes (middle panel). Pooled data from 7 preparations (see Table 4) show that isoguvacine, receptor agonist preferential for $GABA_A$ receptors (Sivilotti and Nistri, 1991), depressed the reflex by 57±15 %, an effect quantitatively similar to the one induced by the submaximal concentration of GABA (0.5 mM), indicating that 50 μM isoguvacine did not saturate $GABA_A$ receptors. In the presence of TPMPA this effect of isoguvacine persisted (57±17 %). As far as the VR polarization response evoked by 50 μM isoguvacine was concerned, it did not differ (109±24 %) in TPMPA solution from the one observed in control.

Fig. 11 (bottom row) indicates an analogous approach used to study $GABA_B$ receptors functionally. The depression of the reflex induced by 2 μM baclofen (left) was unchanged in the presence of TPMPA (right) which *per se* had no effect on control reflexes (middle panel). On average (n=3) 2 μM baclofen depressed the reflex by 69±7 % and this effect was similar in the presence of TPMPA (74±11 % reduction; see Table 4). The reduction of the evoked events induced by baclofen in control solution did not differ (93±27 %) from the one induced in the presence of TPMPA. Note that a smaller concentration of baclofen (0.5 μM) had a lower depressant action on reflex activity (50±18 %) which was also not significantly altered (58±14 %) by TPMPA (n=3; Table 4). These observations suggest that the lack of TPMPA action on baclofen-induced effects was not due to saturation of $GABA_B$ receptors by the concentrations of baclofen used. Collectively, these results indicate that the concentration of TPMPA used in the present experiments did not have apparent effects on $GABA_A$ or $GABA_B$ receptor mediated responses.

Modulation by TPMPA of spinal bursting

Our approach to unmask a functional role of $GABA_C$ receptors in the spinal cord relied upon pharmacological block of $GABA_A$ receptors. Simply applying the antagonist bicuculline results in intense bursting so highly irregular (Bracci *et al.,* 1996a) that it seriously hampers subsequent electrophysiological studies. Nevertheless, when $GABA_A$ antagonism is

associated with glycine receptor antagonism by strychnine, a very regular, spontaneous pattern of bursting emerges and persists for many hours (see Bracci *et al.,* 1996a,b). Previous experiments have shown that this bursting activity results from the operation of an interneuronal circuit using predominantly excitatory synapses and not relying on $GABA_B$ receptor inhibition (Bracci *et al.,* 1996b). This phenomenon thus provides a convenient experimental model to assess in isolation the role of $GABA_C$ receptors in the spinal network supplying motoneurons.

Fig. 12A shows typical spontaneous bursting activity in strychnine (1 μM) plus bicuculline (20 μM) solution. Bursts appeared as all-or-none events from a stable baseline with regular cycle period. After 15 min application of TPMPA the burst amplitude was unchanged, whereas there was a clear lengthening of the bursting interval resulting in a slower cycle period. Note that, despite the clear effect of TPMPA on burst patterns, there was no detectable change in baseline polarization, suggesting that the observed result was not due to a direct action on motoneurons. Fig. 12B shows faster timebase traces of the bursts marked by asterisks in Fig. 12A. In particular, it became apparent that TPMPA increased the number of oscillations (from 7 to 10) present in each burst without changes in the frequency of such oscillations or in the decay phase of the bursts. On average raw data of cycle period before and after TPMPA application were (32±21 and 40±25 s, respectively) indicating a significant ($P<0.03$; pooled data from 5 preparations) deceleration of bursting activity. Recovery from the action of TPMPA was observed in 1/4 preparations at 60 min washout, confirming the very slow offset of the effect of TPMPA previously noted on reflex activity. TPMPA significantly ($P<0.005$) prolonged the duration (by 29±6 %; n=5) of individual bursts. Conversely, the intraburst oscillation frequency remained unchanged (2.3±0.2 Hz or 2.5±0.3 Hz before or after addition of TPMPA, respectively). The action of TPMPA on strychnine and bicuculline induced bursting did not depend on the fact that the block of $GABA_A$ receptors by bicuculline was transiently surmounted. In fact, application of the $GABA_A$ receptor modulator pentobarbitone (25 μM) did not enhance the inhibitory effect of TPMPA (102.5±3 % of the period in TPMPA; n=4), while the same concentration of pentobarbitone in control solution enhanced (by 88±29 %) the VR peak depolarization by 100 μM GABA.

The electrophysiological evidence for $GABA_C$ receptor activity prompted studies concerning in situ hybridisation of this receptor class and immunocytochemistry of its distribution.

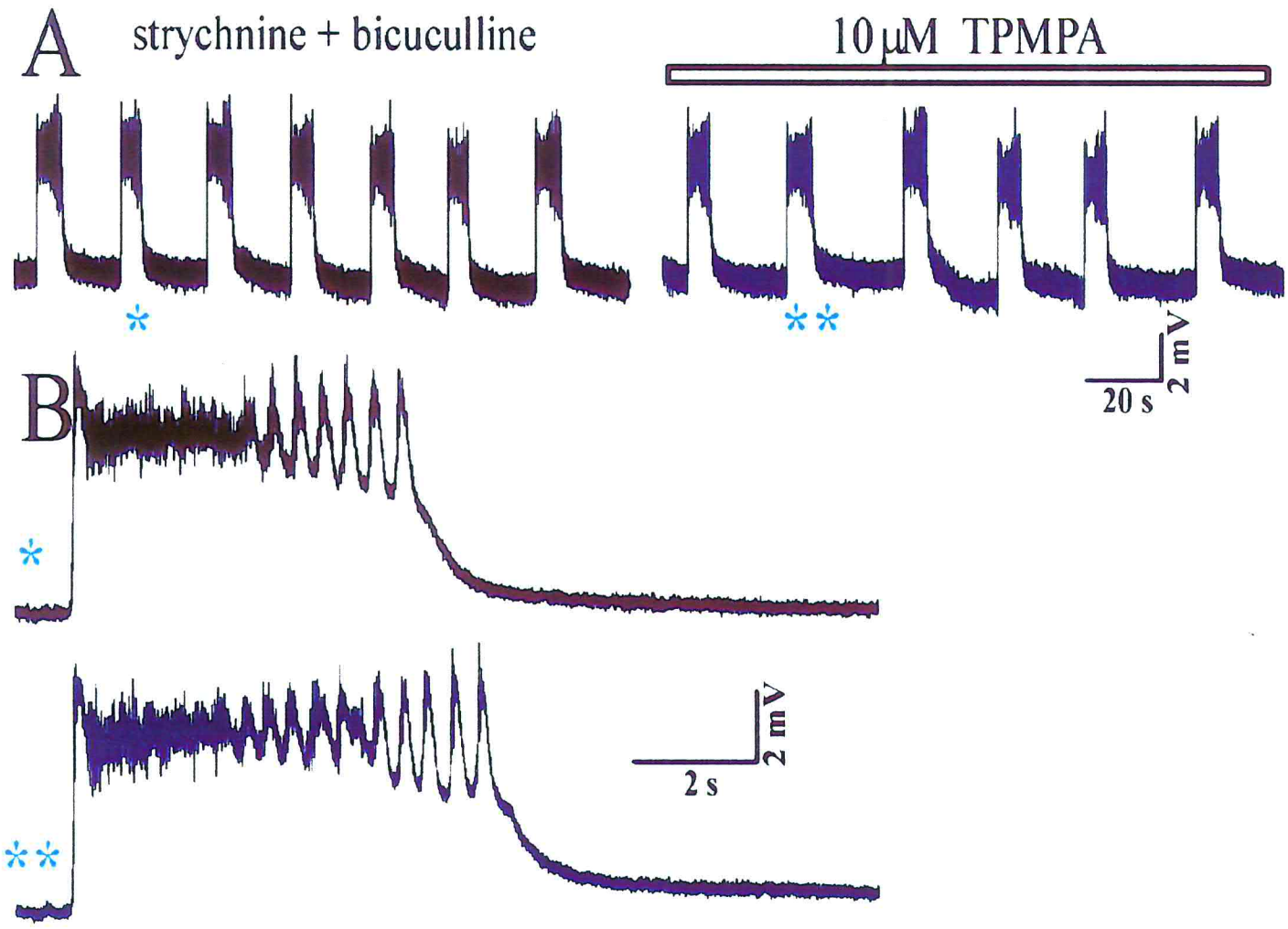

Fig. 12TPMPA affects bursting induced by strychnine and bicuculline

Fig. 12 TPMPA affects bursting induced by strychnine and bicuculline. **A**: slow records of spontaneous, regular bursting in the presence of 1 μM strychnine and 20 μM bicuculline. This activity is decelerated by TPMPA (15 min application) without change in burst amplitude. **B**: individual bursts marked by single or double asterisks (see A) are shown at faster speed to indicate enhancement of oscillatory behaviour in the presence of TPMPA. Voltage calibration refers to A as well.

Specificity of *in situ* hybridisation

The expression of ρ1 and ρ2 subunits of $GABA_C$ receptors in developing brain and spinal cord was investigated with a highly sensitive, non-radioactive *in situ* hybridisation technique previously developed in our laboratory (Tongiorgi *et al.,* 1998). The probes used for this purpose encompassed the 3' untranslated regions (3'UTR) of the cDNAs encoding for the ρ1 or the ρ2 subunits. The ρ1 3'UTR has already been characterised by Wegelius *et al.* (1996). Because the ρ2 3'UTR has not been described before, it was necessary to sequence it in the present study (see Fig. 13). Thus, the sequence published by Ogurusu *et al.* (1997) which consisted of 1757 nucleotides (data base access # D38494), was extended by our sequence analysis up to nucleotide 3170 (1413 additional nucleotides, accesion # AJ420757). The comparison between the new 3'UTR region of the ρ2 subunit with the available rat sequence of ρ1 cDNA, showed that they shared no significant sequence homology in a Blast comparison test. When tested in a Blast search against the non redundant DNA database, both the ρ1 3'UTR and the new ρ2 3'UTR regions did not possess any relevant homology with other known rat genes. When the same search was carried out against the dbEst database, the ρ1 3'UTR was confirmed to have no relevant homology to any EST sequence. However, the new ρ2 3'UTR region shown in Fig.13 was found to be almost identical to unidentified Est sequences isolated from rat ovary cDNA libraries (accession # AW142967, 99% identity), rat small intestine cDNA libraries (accession # AV065033, AV065152, 92% identity) and from mouse testis cDNA libraries (AI606408, 91% identity). From the same search against the ESTs database, the new rat ρ2 3'UTR was also found to be almost identical to one EST identified as the mouse ρ2 3'UTR (BF149062, 91% identity – 188 bp fragment). The latter result suggests that $GABA_C$ ρ subunits may be expressed in peripheral tissues as indeed recently demonstrated by the presence of the $GABA_C$ receptors in the gut (Jansen *et al.,* 2000). This realisation prompted us to explore whether rat ovary and testis could express ρ subunits because this possibility could readily explain the homology between the ρ2 subunit 3' UTR region and the EST unidentified gene sequences.

To examine whether the $GABA_C$ receptor was indeed expressed by rat gonads, a Western blot analysis (Fig.14) with the rho 63 polyclonal antibody (that recognises the three ρ1, ρ2 and ρ3 subunits; Enz *et al.,* 1996) was carried out on protein homogenates of testis and ovary in parallel with homogenates of brain and retina where $GABA_C$ is known to be expressed. Rho 63 antibody labelled a band of apparent molecular weight of 50 KDa in the ovary, a strong

```
1621 GACCTAATGA CCACACTTCC TACACCAGGC⇒CAAGCAGCTG CTCCTGGCTT GGAGGAGCCC
1681 AGGGACCTCC AGCTGCCCTC ACCCCATCTT CATGGCTCTT TTCCTAGTTC ACACTATTCC
1741 AGATCACACT TTTGACTtct ctgaacagag agctatcttc tgctgtgtgt gaacttgttc
1801 acaagaatcc accaccccac cccacccctt atcccccacc cccggtccca caccacttaa
1861 taaaagactc aaatgcctcc cagatgttct gagatgctca gtatgggaag aaagaaaata
1921 cagggcattc cgggtaagaa actagatgca aaaatctgtg aatttatcca gttggattaa
1981 ttaagtggca aggaaaaact ctcagaacgg agacaggaaa tgatttggcc taaacaaaac
2041 tggcagctga gatgatttta taaatgctag aggaagttat tcatttccct gttcattcaa
2101 tcattcatta aacactgagt tcccacccgg tgcctggaaa aaaaaaatcg cggtgaataa
2161 gtatgggagc caatcacaag agccaaacga gaagcccaag tatggacgga gaaagccatg
2221 gaccaaagag gaaaaaaaaa agaattaaga cactgtttag caggaaggaa ctacacgatt
2281 atacccaaag gaatgccggc⇒tcttgacaaa ataaataaaa caaaaggttc cttatagact
2341 tttaagctgt agatgaaaaa tacagttagc cagtcagttc atgcaactat agcgttgaga
2401 aagaaaagca atattgcact aaaaggaatt tcctaggctg⇐aatccacccc tgtcactgac
2461 tcaaagtcac cagccattcc tgtatgcatt ggcatacctg gcttgctcta cattccgaca
2521 agtagacaac acttgatcaa taaacttgtg ctccatctcc aggcctaggg agtctggagc
2581 tggggtccgc tttaggcgct tggtttcctg ggaatagcct tgcttgcttg agtcactcag
2641 tccgtctact tccattgcct gagatagctg agggctggtt ggaatctggt gcaagtcatt
2701 caaagctgcc ccagagcagt ctgcgggtga caggggagtc aagcttggag ggagcctgcc
2761 atttaagtga tgttgaaggt agaaaacgtg ccgcctgtga caccaaaggg tttcatgccc
2821 tggataggaa tcaataagat ctgtgcagaa ttccacctct tcttctagga gctggggaag
2881 actcacactg ggctcctctg ctgaggctgc tgctgctgct gcttctttcg gctcacattt
2941 caaagagttg tgctgcggta cagcattgtc tgtcgttgtc tggctaatca aggactttag
3001 caagaactgg cgatagtgaa atccactgtg gtctgagaca tgcacggacg cccagtgttt
3061 agtagaagat agttcatcaa gaaggatctt cagatccagc ttgcccacgt tctgtaacac
3121 ccagatgcga tgggaccagg cattatagtt gctgggatat ccatcacact ⇐SP6
```

Fig. 13 The 3'UTR cDNA sequence of ρ2. The new ρ2 3'UTR sequence (small, black letters) starts at nucleotide 1757 and ends at nucleotide 3170, i.e. 1413 nucleotides more than the previously published sequence (D38494) which is shown in capital grey letters. The underlined nucleotides indicate the position of the primers used to sequence this cDNA and arrows show their direction. SP6 means that an external SP6 primer was used. The sequence showed no homology with ρ1.

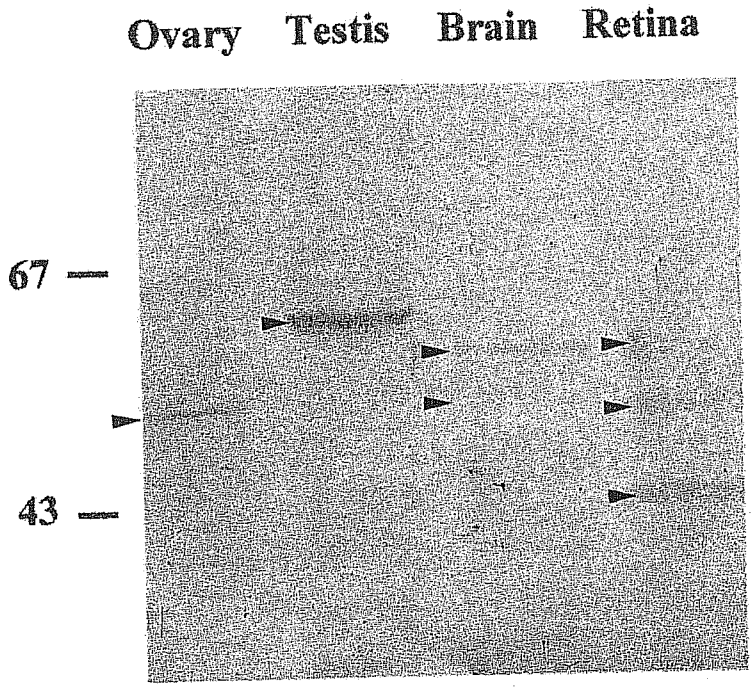

Fig. 14 Western blot analysis of ρ-peptides in adult rat homogenates. Homogenates from adult rat ovary, testis, whole brain and retina separated on a 8% gel and probed with the RHO63 polyclonal antibody that recognises ρ1, ρ2 and ρ3. Arrowheads indicates a 50KDa band in the ovary, a 60KDa band in testis, two bands at 55KDA and 50KDa in brain and three bands of 55, 50 and 43KDa in the retina. Numbers at the left indicate molecular weight standards in KDa.

single band of 60 KDa in testis, a band of 55 KDa and a faint band of 50 KDa in brain. In retina homogenates we observed the same two bands found in the brain plus an additional band of 43 KDa. These data confirmed the results obtained with the EST data screening and demonstrated that the ρ protein family is expressed also in rat ovary and testis. Furthermore, the present results support the use of our probes to specifically detect the distribution of the ρ subunits in rat tissues.

Further evidence in support of the use of such probes was sought by examining the ρ1 and ρ2 mRNA expression in adult rat cerebellum, and P7 and adult retina, which are structures where these patterns have been described before (Enz *et al.,* 1995; Boue-Grabot *et al.,* 1998; Wegelius *et al.,* 1998; Ogurusu *et al.,* 1999).

In the cerebellum, the two digoxigenin-labelled riboprobes for ρ1 and ρ2 labelled Purkinje cells intensely while leaving granule cells unstained (Fig. 15A, B, n=12 sections), a result which accords with previous data on ρ1 expression by Boue-Grabot *et al.* (1998) and, in addition, provides the first unequivocal detection of ρ2 mRNA in Purkinje cells. An additional, new finding was that both riboprobes labelled small cells scattered in the molecular (Fig. 15, A', B') and granular (Fig.15A, B) layers of the cerebellum. Judging from their location and dimension, such cells were likely to be basket cells. Further validation of the probe specificity was obtained by carrying out a competition experiment with a 20-fold excess of unlabelled ρ1 and ρ2 riboprobes. Under these conditions no staining of the cerebellum for ρ1 (Fig. 15C) and ρ2 (Fig. 15D) could be observed (n=14 sections).

In situ hybridisation analysis of P7 and adult retinas showed staining of the outer half of the inner nuclear layer for both ρ1 and ρ2 (n=15 for P7, Fig 16A, B; and n=21 for the adult; Fig. 16C, D). These results accord with previous experiments done on adult retina (Enz *et al.,* 1995; Albrecht *et al.,* 1997), although in the present study based on a non-radioactive method the ρ1 signal was stronger than the ρ2 one. In conclusion, these data demonstrated that these probes were highly specific tools to detect $GABA_C$ receptor ρ1 and ρ2 subunits mRNA in the developing nervous system.

Expression patterns of $GABA_C$ receptors in the developing spinal cord

To identify spinal neurons that could account for described functional $GABA_C$ receptor activity in the P3-P7 spinal cord (Fig. 9 and 12), we performed in situ hybridisations with ρ1

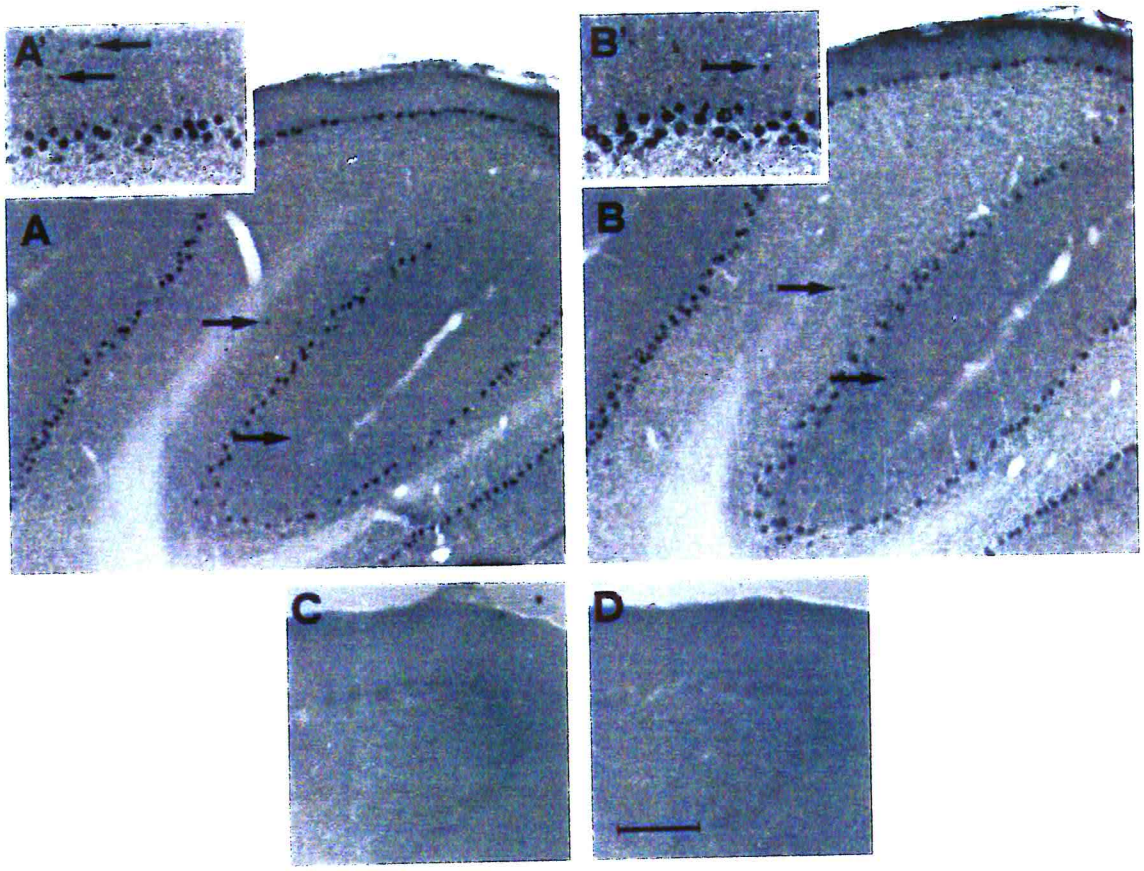

Fig 15 In situ hybridisation for ρ1 and ρ2 on adult rat cerebellum. **A**, cerebellar cortical section showing labelling of Purkinjie cell layer (also shown in A' at higher magnification) with ρ1 probe. Arrows in A' point to basket-like cells. **B**, corresponding section from the same cerebellar region labelled with ρ2 probe (higher magnification in B' shows basket-like cells, one of which is indicated by the arrow). **C**, **D**, sections from the same cerebellar region as in A,B but hybridised in the presence of 20 fold excess of unlabelled ρ1 or ρ2 probes, respectively. Calibration bar: 200 μm (A,B,C,D), 110 μm (A',B').

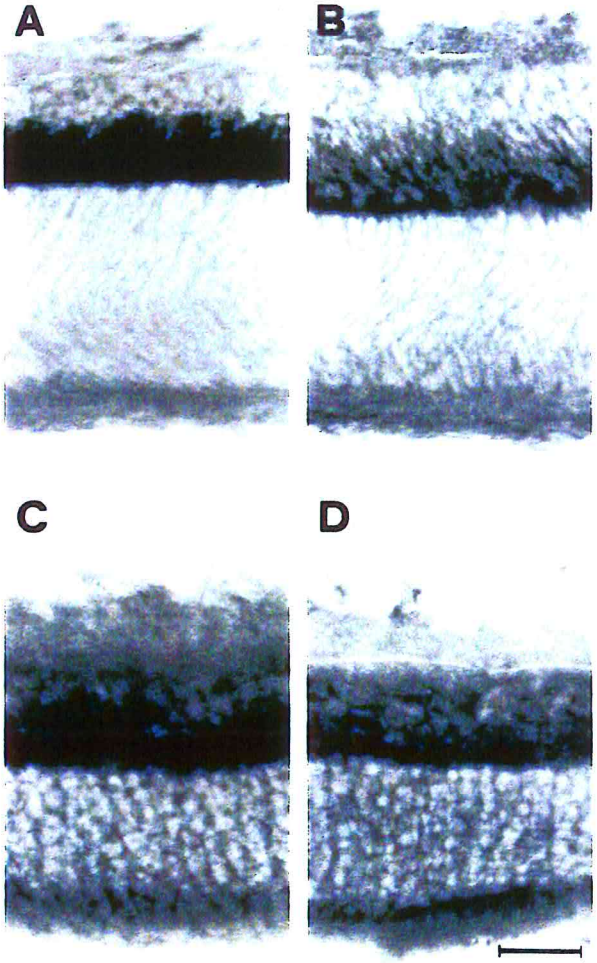

Fig. 16 Developmental expression of ρ1 and ρ2 in the retina. The in situ staining pattern was similar in the P7 (**A**,**B**) and adult retina (**C**,**D**), and the signal for both ρ1 (A,C) and ρ2 (B,D) was restricted to the outer half of the inner nuclear layer. Calibration bar: 25 μm.

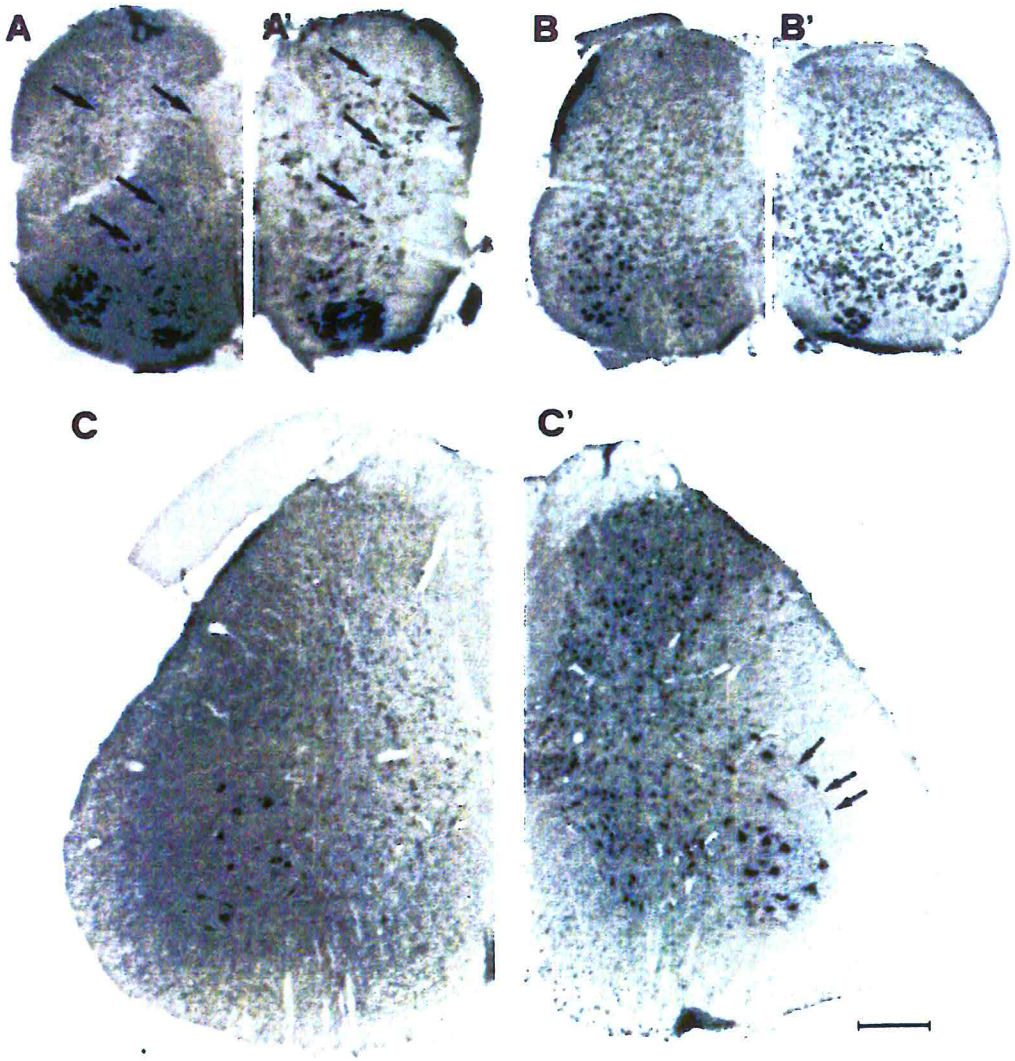

Fig. 17 ρ1 and ρ2 mRNA localisation in the developing rat lumbar spinal cord. **A, A'**, sections from P1 spinal cord labelled with ρ1 (A) or ρ2 (A') probes, showing strongly labelled motoneurons and sparsely labelled interneurons (examples are indicated by arrows). Note more intense signal with ρ2 probe. **B, B'**, similar sections from P7 spinal cord in which more diffuse cellular labelling is observed with either probe (B for ρ1 and B' for ρ2). **C, C'**, in the adult spinal cord the ρ1 (C) signal is weaker than the ρ2 (C') one with similar pattern of cellular labelling. Arrows (C') point to ρ2 labelled processes of single motoneuron. Calibration bar: 250 μm.

and ρ2 riboprobes on lumbar sections from the P1 (Fig. 17A, 17A', n=33 sections), P7 (Fig. 17B, 17B', n=37 sections) and adult (Fig. 17C, 17C', n=45 sections) rat spinal cord. For all three age groups the distribution of neurons positive to ρ1 and ρ2 riboprobes was similar, although the ρ2 staining was always stronger. On P1 sections, ρ1 (Fig. 17A), and ρ2 (Fig. 17A') mRNAs predominantly labelled cells in lamina IX which mainly contains motoneurons. In addition, only a few interneurons scattered over the deep dorsal horn and the intermediate grey matter expressed ρ1 mRNA weakly and ρ2 mRNA moderately (Fig. 17A, 17A', arrows). On P7 sections, the number of cells stained for ρ1 (Fig 17B) and ρ2 (Fig 17B') riboprobes was much higher than at P1 age whilst the staining intensity in lamina IX decreased. Motoneurons and interneurons of the adult lumbar spinal cord expressed less ρ1 than ρ2 mRNA (Fig. 17C, 17C'). Interestingly, a dendritic localisation of the ρ1 and ρ2 mRNAs (Fig. 17C', arrows) was observed. This result prompted us to quantify how far this mRNA could extend over the dendritic tree using as an index the MDDL value (see materials and methods).

Dendritic distribution of ρ1 and ρ2 mRNAs

In spinal motoneurons we found that, on average, ρ1 and ρ2 mRNAs were within the same range of distances from the cell soma: 62.20 μm and 62.16 μm for ρ1 and ρ2, respectively (Table 5, n=50). However, in several neurons the mRNAs for ρ1 or ρ2 could be found over than 100 μm away from the cell soma, indicating localisation to distal dendrites (Table 5). Fig. 18A (arrows) shows, on one motoneuron, an example of dendritic (MDDL=70 μm) localisation of ρ1 mRNA while Fig. 18B shows the dendritic (MDDL=80 μm) presence of ρ2 mRNA (arrows). Fig. 18C shows the strikingly punctate location of ρ2 mRNA (arrows) in correspondence with dendritic varicosities and branch points known to be preferential accumulation sites for dendritic mRNAs in vitro (Tongiorgi *et al.*, 1997). A clear dendritic localisation for ρ1 or ρ2 mRNAs could also be found in neurons of other adult brain regions such as hippocampal interneurons (unlike pyramidal cells), striatal neurons, substantia nigra neurons, deep cerebellar nuclei neurons (data not shown). In cerebellar Purkinje cells staining was however restricted to the cell soma (Fig. 15A, 15B).

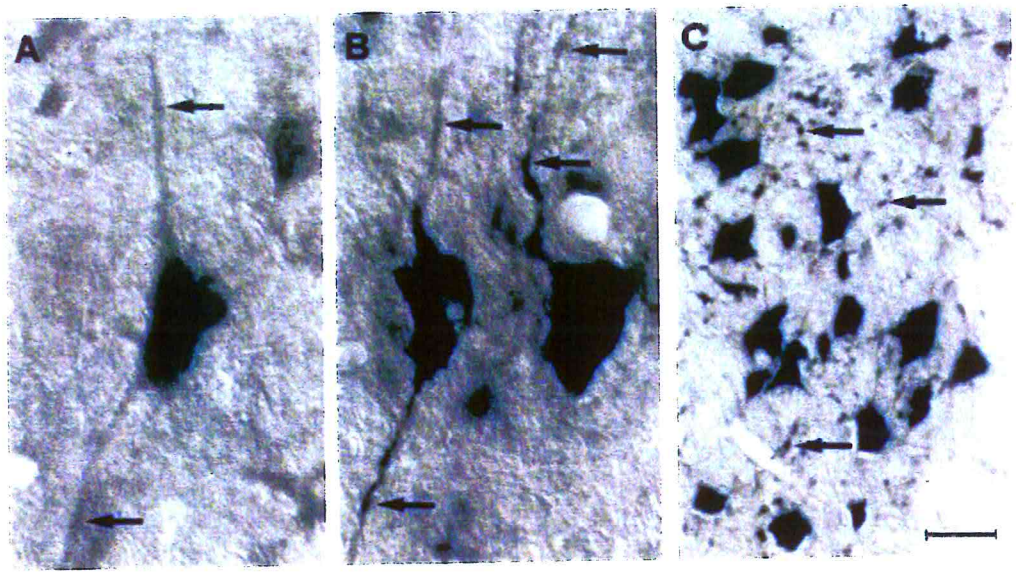

Fig. 18 Subcellular localisation of ρ1 and ρ2 mRNAs in adult spinal motoneurons. **A**, ρ1 labelling includes the cell body and dendritic processes marked by arrows. **B**, comparable data obtained with ρ2 probe showing stronger labelling of soma and dendrites (arrows). **C**, lower magnification of lamina IX stained for ρ2. Arrows point to examples of strong signals with punctate distribution even at long distances form cell bodies. Calibration bar: 25 μm (A, B) and 50 μm (C).

Table 5 Maximal Distance of Dendritic Labelling (MDDL) in spinal cord motoneurons

	Rho 1	**Rho 2**
MDDL (μm)	62.20 ±23.21	62.16 ±19.95
range (μm)	35.36-163.69	25.98-102.87
n	50	50

The MDDLs were measured in 50 dendritic processes from 4 sections from 2 different animals (total 8 sections).

Immunocytochemical localization of $GABA_C$ receptors in the spinal cord

Since the relation between mRNA expression level and density of encoded protein might be non linear, the actual presence of $GABA_C$ receptors in the spinal cord was established by detecting these receptors by immunohistochemistry. P1 lamina IX cells (presumably motoneurons) were virtually the only ones consistently stained by the $GABA_C$ receptor polyclonal antibody (Fig. 19A). At P7 stage (Fig. 19B), not only lamina IX motoneurons were stained (Fig. 19D) but also interneurons in the dorsal horn appeared labelled (Fig. 19C). Staining was mostly concentrated to the cell soma although faint staining of dendritic processes could be observed at P7 stage (Fig. 19D, arrows). In the adult labelled neurons were found in all laminae (Fig. 19E), including interneurons in the dorsal horn (Fig. 19F) and motoneurons (Fig. 19G, asterisks). On closer inspection, the staining pattern was found to be dramatically different with respect to the previous ages since intensely stained immunoreactive puncta were scattered throughout the whole grey matter region (Fig. 19G, large arrows) while staining of cell bodies was relatively weak and diffuse with occasional strongly labelled puncta (Fig. 19G, small arrows). These findings strongly confirmed the results obtained with in situ hybridisation demonstrating a close correlation between mRNA and protein expression.

Electrophysiology of $GABA_C$ receptors in the P1 rat spinal cord

The demonstration of the selective, strong expression of $GABA_C$ receptors on P1 motoneurons was an unexpected finding when considered in the light of previous data obtained from older rat spinal cords and which raised the issue of whether such receptors were

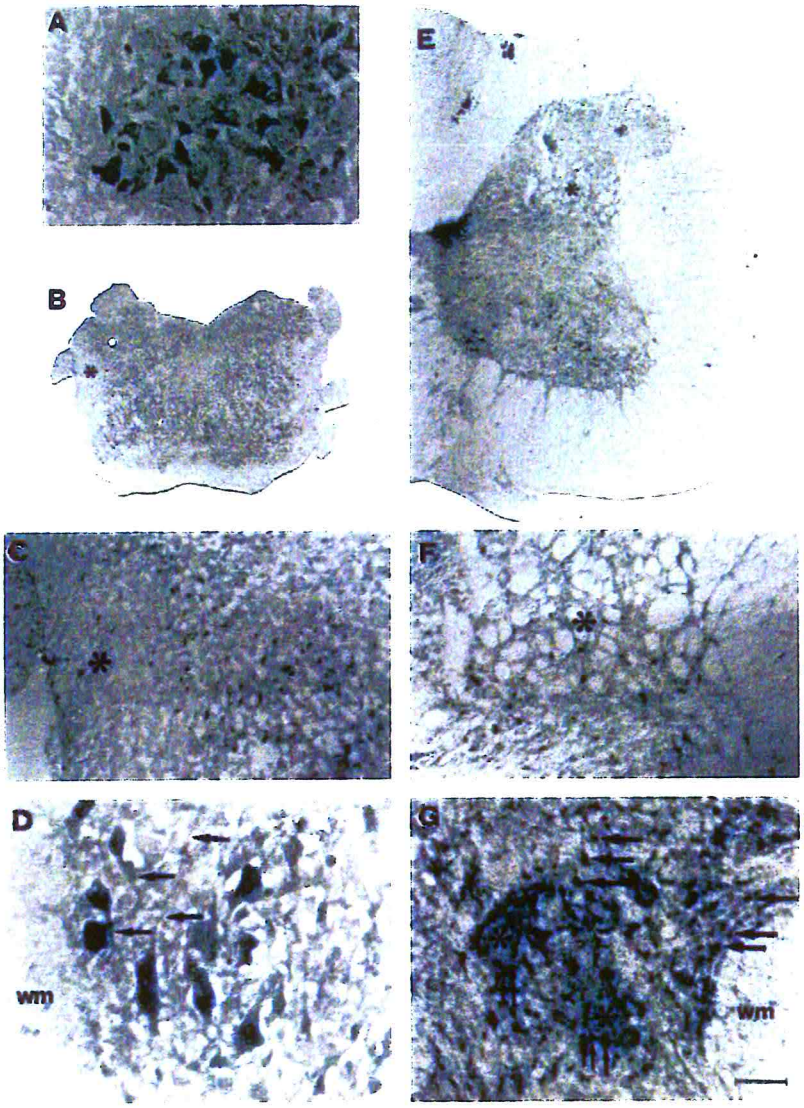

Fig. 19 $GABA_C$ receptor immunolocalisation in the developing rat lumbar spinal cord. **A**, P1 motoneurons stained with anti-ρ polyclonal antibody. **B**, low power view of the P7 spinal cord stained with anti-ρ antibody showing staining in the whole grey matter. **C**, high power magnification showing expression of $GABA_C$ receptor in the lamina III corresponding to the area marked by the asterisk in (B). **D**, comparative observation on P7 motoneurons. Labelling of processes is indicated by arrows. **E**, low power view of the anti-ρ staining on a section of adult spinal cord in which interneurons (lamina III enlarged in E) and motoneurons cell bodies (G) are stained. **G**, Note that motoneurons cell somas are weakly labelled (asterisks) while processes show punctate distribution of labelling (arrowheads). Small arrows point to occasional punctate staining of motoneuron somas. Calibration bar: 40 μm (A,C,D,F), 250 μm (B,E) and 20 μm (G).

functionally active. This question was explored with electrophysiological experiments in which responses induced by GABA were investigated in the presence of distinct GABA receptor blockers.

Fig. 20A shows one example of the averaged VR reflex (stimuli 10xT, 0.1ms, 1/30s) activity in control solution (left panel) and after 15 min application (middle panel) of the $GABA_C$ blocker TPMPA (10 μM; Murata *et al.,* 1996; Ragozzino *et al.,* 1996; Chebib *et al.,* 1998). No change in VR reflex could be detected (see also superimposed traces in right panel) either in terms of peak amplitude (4.48 or 4.24 mV in control or TPMPA solution, respectively) or of reflex area (49.3 or 46.7 mV*ms, respectively). On average the variation in reflex peak induced by TPMPA was 4±2 % ($P>0.05$). Likewise, the change in reflex area in the presence of TPMPA was 4±3 % ($P>0.05$; averages of trains of 10 responses repeated at least 3 times from 3 P1 spinal cords). Thus, there was no evidence for a role of $GABA_C$ receptors in synaptic transmission mediating DR-evoked VR reflexes.

To examine at this age if $GABA_C$ receptors, which were mainly observed on P1 motoneurons, were indeed functional, it was necessary to isolate pharmacologically motoneurons from the rest of the network. For this purpose preparations were continuously bathed with TTX solution (initially applied at 1 μM and then used at 0.25 μM as maintenance concentration).

Fig. 20B shows raw traces of VR depolarisations induced by GABA (250 μM) in TTX solution. The peak depolarisation was largely reduced (77 %) by the $GABA_A$ antagonist bicuculline (20 μM) and further decreased (5 % of control peak) by subsequent application of TPMPA (10 μM). The effect of TPMPA was reversible after 60-90 min washout (not shown).

Fig. 20C shows average log dose-response plots for GABA (50-500 μM range; 40 s application; black line and symbols) in the presence of TTX, of TTX + bicuculline (+Bic; red line and symbols) and of TTX + bicuculline + TPMPA (+TPMPA; blue line and symbols). Peak depolarizations evoked by 50-500 μM GABA were uniformly reduced by bicuculline throughout the concentration range (on average this reduction amounted to 67±18 %; n=5 spinal cords). This reduction was statistically significant ($p<0.0001$). Application of TPMPA (10 μM) further decreased the bicuculline-resistant GABA depolarisation (on average by 42±24 %; n=5; $p<0.002$) and displaced the plot downwards. The GABA response left in the presence of bicuculline and TPMPA was 20±10 % of the control GABA effect. This residual response after application of GABA antagonists bicuculline and TPMPA might have been caused by $GABA_B$ receptor activation. To test this hypothesis, saclofen (200 μM), a $GABA_B$ receptor antagonist, was added to the bath solution containing GABA receptor antagonists

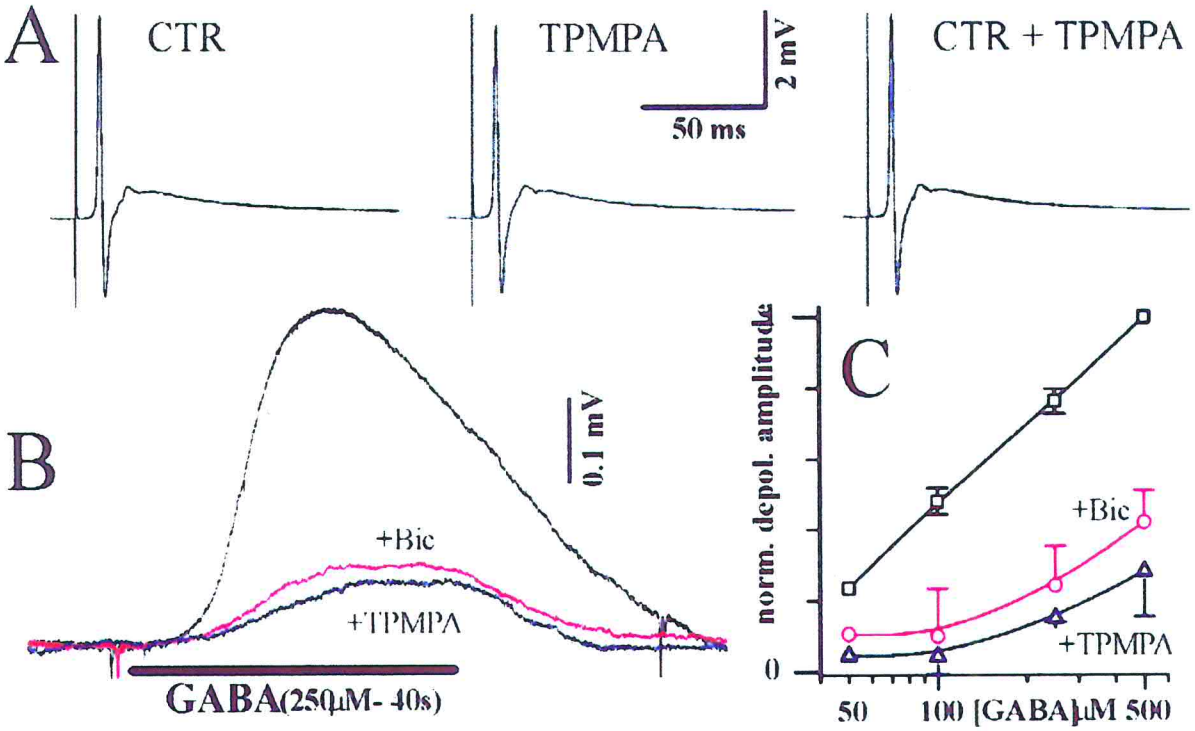

Fig. 20 Effect of TPMPA on spinal reflexes and on change in VR polarization level induced by exogenously applied GABA

Fig. 20 Effect of TPMPA on VR reflexes and on changes in VR polarization level induced by exogenously applied GABA. **A**: average VR reflex in control solution (left); lack of change in VR reflex in the presence of TPMPA (10 μM; middle); traces are superimposed (right panel) to aid comparison. **B**: slow time base VR responses, in the presence of 0.25 μM TTX, indicating depolarisation elicited by 250 μM GABA (applied for 40 s as shown by the horizontal filled bar). In control solution depolarisation peaks before end of GABA application and subsequently fades. After 20 min of exposure to 20 μM bicuculline (+Bic) the depolarisation induced by GABA is largely reduced and shows minimal fading. Further decrease appears in the presence of 10 μM TPMPA (15 min application). **C**: GABA log concentration-response plots in the presence of TTX, of TTX + bicuculline (+Bic) and of TTX + bicuculline + TPMPA (+TPMPA). The difference between control and +Bic or between +Bic and +TPMPA is statistically significant ($p<0.0001$ or $p<0.002$, respectively). Data are from 5 spinal cords.

and TTX. Under these conditions, the peak response to GABA (500 μM) was not significantly changed (-7.2 ± 16.5%; n=4). These data suggest that $GABA_C$ receptors were functional on P1 motoneurons, although much less so than $GABA_A$ receptors but apparently more than $GABA_B$ receptors.

Results II: Na^+/K^+ ATPase

Previous experiments showed a critical role of the Na^+/K^+ ATPase in spinal cord disinhibited rhythms (Ballerini *et al.,* 1997). These authors have shown that, among several sodium pump blockers tested, strophanthidin (4 μM) fully disrupts disinhibited bursting "which was fragmented into irregularly occurring paroxysmal activity mixed with short depolarizing events." (Ballerini *et al.,* 1997; see also Fig. 25).

One of the aims of the present study was to clarify the role of the electrogenic pump in the generation and/or maintenance of several forms of rhythmic activity during spinal circuit development, in particular whether synchronous activity in the absence of Na^+/K^+ ATPase could still be generated.

To address this issue, prior validation of strophanthidin potency in blocking sodium pump activity preparation was investigated.

Effectiveness of Na^+/K^+ ATPase inhibitors

A reliable method to quantify sodium pump activity is represented by monitoring $^{86}Rb^+$ uptake (Longo *et al.,* 1991; Bowen, 1992). Thus, we decided to measure the same parameter, namely $^{86}Rb^+$ uptake, by isolated neonatal spinal cord tissue in control solution or in the presence of saturating concentrations of ouabain, known as an irreversible blocker more potent than strophanthidin (Shen and Johnson 1998). Data were compared with results in the presence of 4 μM strophanthidin. All experiments were performed at room temperature.

In Fig. 21 mean values (obtained from 6 different preparations; P6-9) of $^{86}Rb^+$ uptake by spinal cord slices as function of time over a 12 min period are shown. In control conditions (black circles) radioactivity increased from 3029 ±500 (counts per min or cpm/mg of protein, 5 min incubation) to 5173 ±568 after 10 min and this increase was linear, as shown by linear regression values (r=1.00, SD= ±0.16).

The addition of ouabain at a saturating concentration (50 or 200 μM), known to completely inhibit Na^+/K^+ ATPase (Shen and Johnson, 1998; preincubation 20min; red circles), or addition of strophanthidin (preincubation 30 or 60 min; blue circles) significantly ($p<0.0001$)

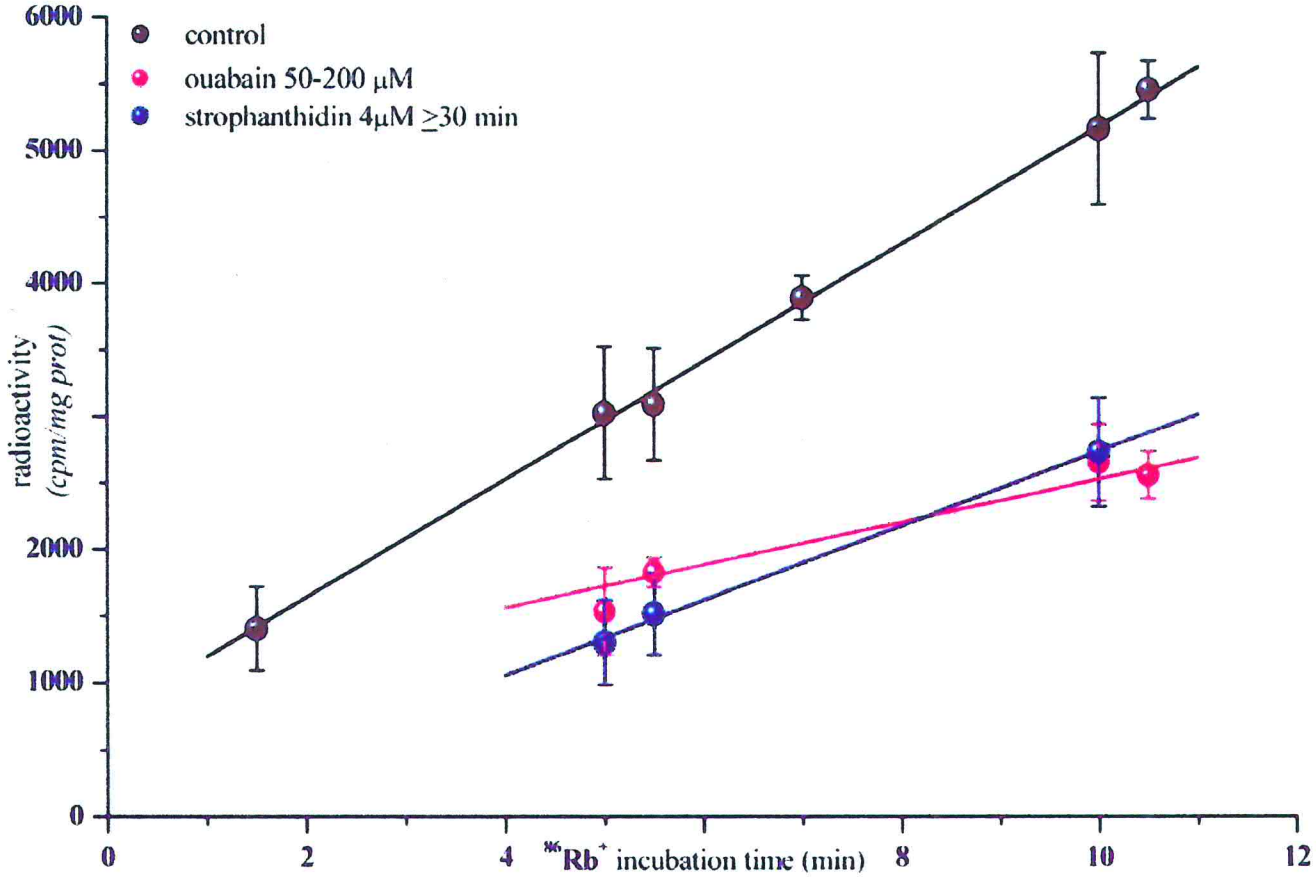

Fig. 21 Na^+/K^+ ATPase inhibition by 4 μM strophanthidin

Fig. 21 $^{86}Rb^+$ uptake by spinal cord slices as function of time. In control conditions (black circles) radioactivity (counts per min or cpm/mg of protein) increased linearly, as shown by linear regression values (r=1.00, SD= ±0.16). The addition of ouabain at a saturating concentration (50 or 200 μM; preincubation 20min; red circles), or of strophanthidin (preincubation 30 or 60 min; blue circles) significantly ($p<0.0001$) reduced at each time point $^{86}Rb^+$ uptake compared to controls. The two protocols induced the same block (n = 6; P6-9).

reduced (at each time point) $^{86}Rb^+$ uptake compared to controls. In fact, at 5 min incubation, the radioactivity detected was 1533 ±329 cpm/mg-prot in the presence of ouabain and 1301 ±315 cpm/mg-prot in strophanthidin; after 10 min incubation the values measured in the presence of ouabain or strophanthidin were significantly smaller than in controls (2656 ±289 cpm/mg-prot and 2735 ±412 cpm/mg-prot, respectively). These results demonstrated that $^{86}Rb^+$ uptake was strongly inhibited by both ouabain or strophanthidin at the tested concentrations, and that these concentrations of the two drugs were equally effective in blocking Na^+ pump activity after 30 or 60 min exposure.
This pharmacological block appeared to be nearly complete, leaving only a small residual activity, most likely reflecting passive redistribution of this isotope.

Since strophanthidin fully inhibited Na^+ pump activity in our preparation, we could investigate its effects on spinal cord excitability. This issue was investigated by means of electrophysiological recordings obtained from VR of the en bloc spinal cord (P3-P9).
Strophanthidin application induced a steady VR depolarization in 130 preparations (0.42 ± 0.31 mV, on a random sample of 10 preparations) as previously reported (Ballerini *et al.*, 1997), while spontaneous background activity was not changed by application of this agent (not shown).

Effects of strophanthidin on spinal reflexes

We studied the action of strophanthidin on VR responses induced by single pulses or by repetitive stimulations delivered to one DR (see methods).
Fig. 22A shows two superimposed traces: each trace represents the average of 10 consecutive responses to single pulses (10xTh, 0.1 ms, 1 every 30s) in control (black) and in the presence of strophanthidin (red). We compared the amplitude of the early response (7.4 ±0.9 ms after the stimulus) and the amplitude of the late response (> 13 ms after the stimulus). In this case the early peak was reduced from 1.66 to 1.11 mV, the late from 0.59 to 0.56 mV. Pooled data from 10 different preparations, on which different stimulus intensities were tested in control and in the presence of strophanthidin, are represented in Fig. 22C. In Fig. 22C (right) the late component of the reflex amplitude (normalized with respect to 5xTh control) was unaffected (-2% ±17%) by strophanthidin. A slight, not significant, reduction (-18 ±29%) in the early response is shown in Fig. 22C (left).

To evaluate a possible role of strophanthidin in impulse conduction by DR fibers we recorded the compound action potential (average of 30 pulses, 7-10xTh, 0.1ms, 1Hz) with or without Na^+ pump inhibition. In Fig. 22B two traces are superimposed for comparison. The compound action potential in control solution (black) was unaffected by strophanthidin (red; on average -3 ±16%, n=7).

To better characterize the functional role of the electrogenic sodium pump, we decided to investigate the effects of strophanthidin block in conditions when the operation of the pump should have been increased. To raise Na^+/K^+ pump activity, we applied trains of stimuli inducing strong depolarization and repetitive firing with associated major influx of Na^+, thus speeding up the pump rate.

Fig. 23A shows motoneuron responses to a train of 20 pulses (10xTh, 0.1 ms, 1Hz) in control condition (black) or in the presence of strophanthidin (red). Under control conditions, repetitive stimulation resulted in a cumulative depolarization (0.62 ±0.31 mV, 11 preparations) followed by slow decay (12.9 ±2.9 s half decay time). After strophanthidin incubation, the cumulative depolarization was severely reduced (0.24 mV vs 0.49 mV, see tracings in Fig. 23A), while the half decay time has strongly prolonged (29.7 s vs 11.5 s, Fig. 23A). Histograms in Fig. 23B and C show the average amplitude and half decay time values in control (n=11) and in the presence of strophanthidin (n=6).

In Fig. 23 (inset, right) the two traces shown in A are scaled and normalized (0-50 ms before the last pulse, see methods). Note that in control Krebs solution, after the first two stimuli, cumulative depolarization developed biphasically with an initially higher rate of rise; in the absence of sodium pump activity, cumulative depolarization instead developed monotonically (see also Fig. 20). To quantitate the difference in onset between these two conditions, we measured the cumulative depolarization velocity between 3rd and 7th stimulus ("early") and between 16th and 20th stimulus ("late"). On average, control cumulative depolarization velocity values were 35.7 ±22.3 μV/s (early) and 9.3 ±5.3 μV/s (late), whether in strophanthidin the two values were similar (7.6 ±5.7 μV/s and 9.1 ±3.5, respectively). Because the values of early and late components in the presence of strophanthidin were the same, we concluded that the depolarization apparently grew in monotonic fashion.

Trains of 10, 20, 30 and 60 pulses, with intensity of 2, 5 and 10xTh (0.1 or 1 ms duration), delivered at 0.33, 0.5 and 1 Hz frequency, gave similar results (not shown).

Could the strophanthidin induced network depolarization account for the described effects?

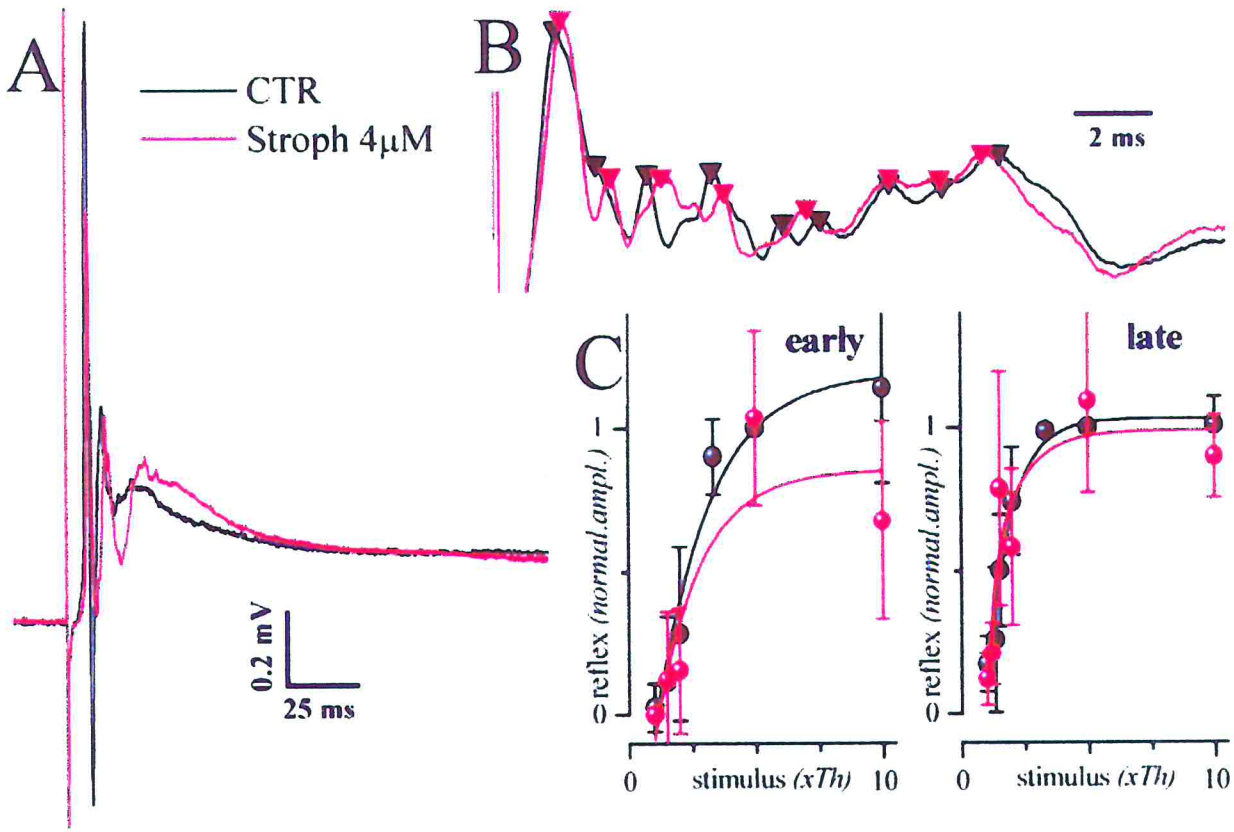

Fig. 22 Effects of strophanthidin on spinal reflexes

Fig. 22 Effect of strophanthidin on spinal reflexes.

A shows two superimposed traces: (average of 10 consecutive responses to single pulses; 10xTh, 0.1 ms, 1 every 30s), in control (black) and in the presence of strophanthidin (red). The early peak (7.4 ±0.9 ms after the stimulus) was reduced from 1.66 to 1.11 mV, the late (> 13 ms after the stimulus) from 0.59 to 0.56 mV. **B**: compound action potential of DR fibres (average of 30 pulses, 7-10xTh, 0.1ms, 1Hz) in control solution (black) was unaffected by strophanthidin (red; on average -3 ±16%, n=7). **C** shows pooled data from 10 different preparations, on which different stimulus intensities were tested in control and in the presence of strophanthidin (normalized with respect to 5xTh control). The early response (C left) presented a slight, not significant, reduction (-18 ±29%) by strophanthidin, the late one (C right) was unaffected (-2% ±17%).

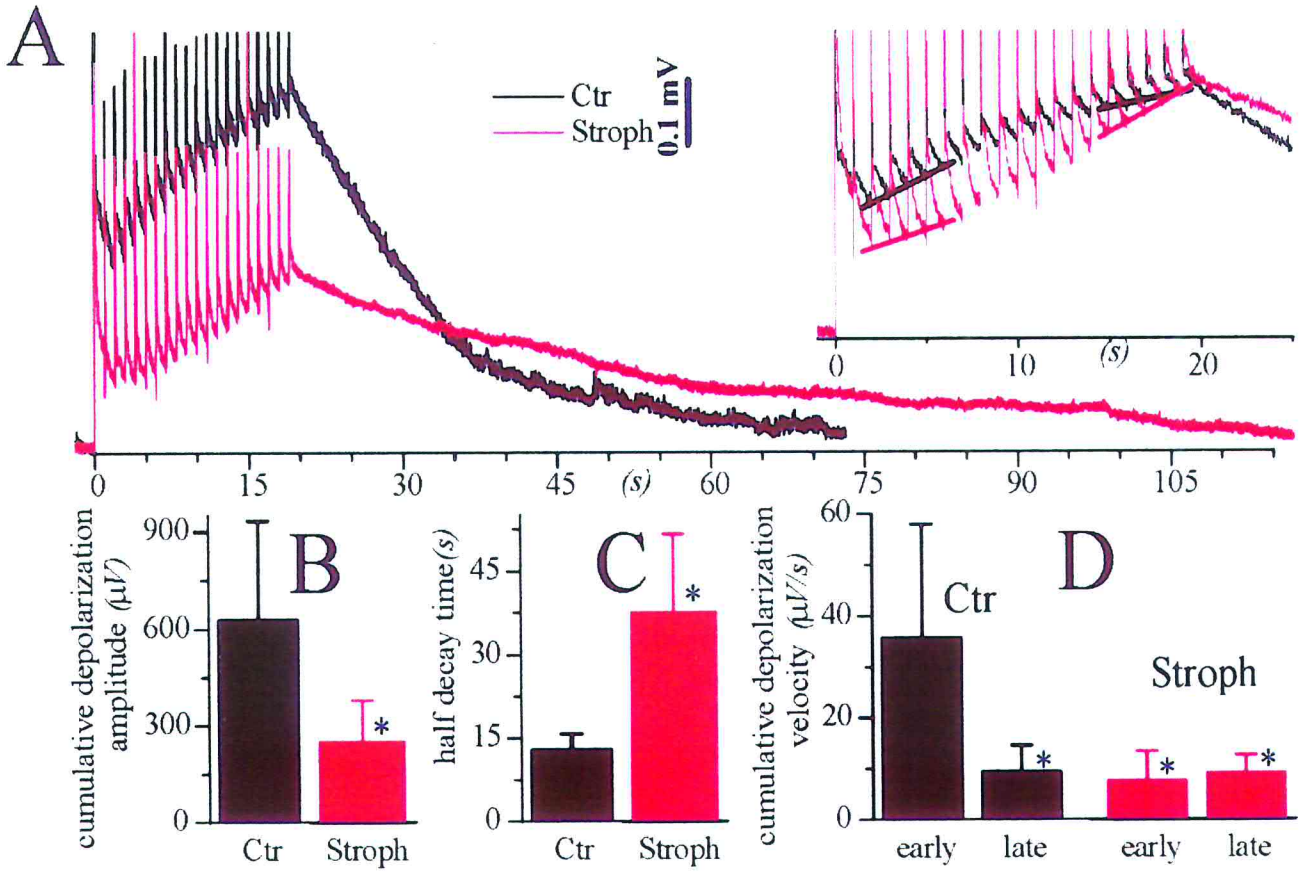

Fig. 23 Effects of strophanthidin on responses to repetitive stimulation. A shows motoneuron responses to a train of 20 pulses (10xTh, 0.1 ms, 1Hz) in control condition (black) or in the presence of strophanthidin (red). Histograms in B and C show the average amplitude and half decay time values in control (n=11) and after strophanthidin (n=6) incubation. The cumulative depolarization was severely reduced while the half decay time was strongly prolonged. Inset, right shows the two traces in A scaled and normalized. In control Krebs solution cumulative depolarization developed biphasically with an initially higher rate of rise; in the absence of sodium pump activity, cumulative depolarization instead developed monotonically. D shows compares cumulative depolarization velocity between 3rd and 7th stimulus ("early") and between 16th and 20th stimulus ("late").in the two conditions. In strophanthidin the two values were similar, the depolarization apparently grew in monotonic fashion (* = $p < 0.001$)

Fig. 23 Effects of strophanthidin on responses to repetitive stimulation

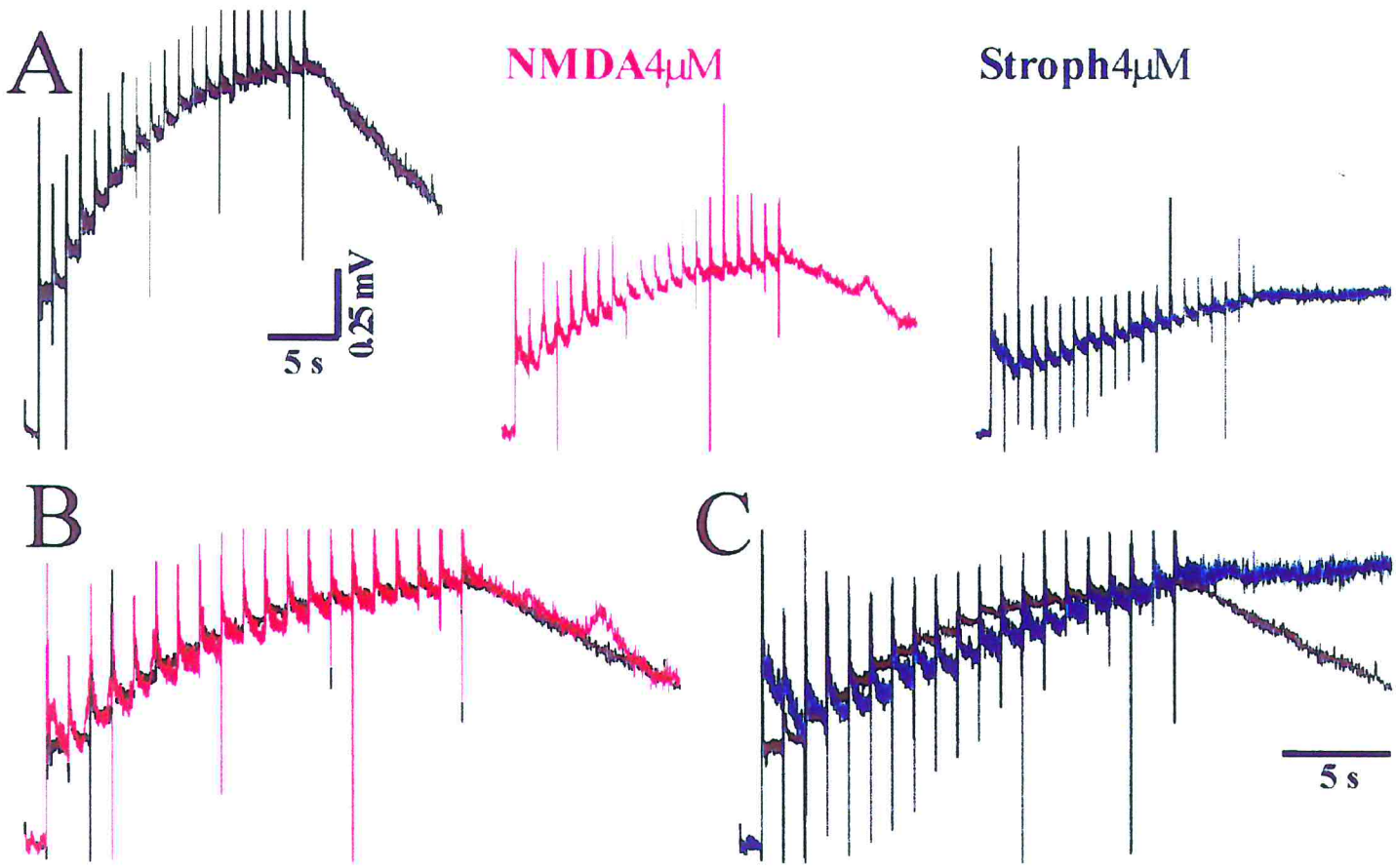

Fig. 24 Effects of NMDA on responses to high frequency stimulation

Fig. 24 Effects of NMDA on responses to high frequency stimulation. In A a stimulus train (20 pulses, 10xTh, 0.1 ms, 1Hz)) was applied in control solution(left), in the presence of NMDA (middle; 4 μM NMDA that induced a depolarization similar to subsequent strophanthidin one) and after strophanthidin application (right). In B traces in control (black) and in the presence of NMDA (red) are normalized and superimposed showing that NMDA baseline depolarization reduced the cumulative depolarization amplitude but it had no effect on the gradual decrease in cumulative depolarization velocity, as well as on the half decay time. In C traces in control (black) and in the presence of strophanthidin (blue) are scaled and superimposed, confirming all the previous described effects (n = 5 preparations).

To test this hypothesis we decided to induce a depolarization of similar amplitude with a different drug. To this aim we applied the glutamate receptor agonist NMDA (2-8 μM). Within this concentration range, NMDA induced (in 5 preparations) depolarization similar to the one obtained by strophanthidin application (range 0.21-1.32 mV).

Fig. 24A shows an example of one experiment in which the train of stimuli was applied in control solution(left), in the presence of NMDA (middle; in this case 4 μM NMDA induced a depolarization similar to subsequent strophanthidin one) and after strophanthidin application (right). NMDA baseline depolarization reduced the cumulative depolarization amplitude (by 53%) but it had no effect on the late decrease in cumulative depolarization velocity (in control 99.7 μV/s and 9.6μV/s early and late respectively; in NMDA 37.3 μV/s and 12.4 μV/s, early and late respectively), as well as on the half decay time (13.6 s in control vs 13.4 s in NMDA). In Fig. 24B tracings in control (black) and in the presence of NMDA (red) are normalized and superimposed to unmask these effects.

The train of stimuli after strophanthidin application, notwithstanding the comparable reduction in cumulative depolarization amplitude (by 64%), induced uniformly slow cumulative depolarization velocity (16.0 μV/s and 13.5 μV/s, early and late velocities respectively) and prolonged half decay time (46.3s in Strophanthidin). In Fig. 24C tracings in control (black) and in the presence of strophanthidin (blue) are scaled and superimposed, confirming the previous described effects. In these 5 preparations 4 μM strophanthidin induced a monophasic increment in cumulative depolarization (8.2 ±1.5 μV/s and 9.0 ±1.8 μV/s, early and late velocities respectively) as well as an increase in decay time (13.2 ±4.1 s and 34.3 ±9.1 s, half decay time in control and in strophanthidin respectively). Thus, strophanthidin effects on repetitive stimulation were not simply due to network depolarization like the one elicited by NMDA.

In summary, Na^+ pump inhibition had no significant effects on fiber impulse conduction, spontaneous activity, or spinal reflexes (evoked at low, 0.033 Hz, stimulus rate). When stimuli were delivered at higher rate (0.33– 1.0 Hz), Na^+ pump inhibition largely reduced cumulative depolarization, with monotonic growth. Moreover, once the train of stimuli terminated, in the presence of strophanthidin, baseline voltage returned to basal level with a 3-fold increase in half decay time. It may be concluded that Na^+/K^+ ATPase activity influenced the network signal summation velocity, and sped up recovery from excitation.

Long term strophanthidin application unmasked late bursting

We decided to investigate long term effects of Na^+ pump block on disinhibited spinal networks. We applied strychnine plus bicuculline to 130 isolated spinal cords from neonatal rats (P3-P9). After 20 min of Cl^--mediated transmission block, regular rhythmic bursting recorded from VRs was observed in 100% of cases. Disinhibited bursting was characterized by amplitude and duration values similar to the ones previously reported (see Table 6 and Bracci *et al.,* 1996a,b; Ballerini *et al.,* 1997). Application of strophanthidin always disrupted this rhythm within 15 min, as previously observed (Ballerini *et al.,* 1997). An example of rhythmic activity before and after strophanthidin application in the presence of strychnine and bicuculline is shown in Fig. 25A. In Fig. 25B and C the same recordings are displayed on faster time base in the absence or in the presence of strophanthidin, respectively. Note the loss of regular rhythmicity after Na^+ pump block, as confirmed by the large difference in CV values for periodicity (16% and 54%, respectively).

In 130 preparations strophanthidin application was prolonged for > 4 h up to a maximum of 12 h. In all cases, after the initial loss of bursting activity, a new bursting activity surprisingly appeared spontaneously in the continuous presence of strophanthidin (on average after 60 ± 10 min, see Fig. 26B, D).

Fig. 26 compares the features of bursting before and after long-term suppression of the electrogenic pump activity. The disinhibited rhythm shown in Fig. 26A was characterised by 24.3 ±4.9 s interburst interval (with 20% CV) and by 17.4 ± 3.1 s duration (with 18% CV). In C a single disinhibited burst (indicated by the star in A) is fully depicted. Note the presence of an initial plateau phase followed by intraburst oscillations (3.5 to 2.0 Hz; see Table 6 for pooled data) as previously shown (Bracci *et al.,* 1996a,b).

In Fig. 26B some spontaneous events, after about three hours of Na^+/K^+ pump block, are presented; this new activity was less regular and was characterized by 165.7 ±89.9 s interburst interval (with 54% CV) and by 84.8 ±54.3 s duration (with 64% CV). In D a single event (indicated by the star in B) is amplified: when compared it with the disinhibited burst shown in C (note the different time scale), the absence of an early plateau and the low frequency of continuos intraburst oscillations (1.0 to 0.1 Hz; see Table 6 for pooled data) becomes manifested.

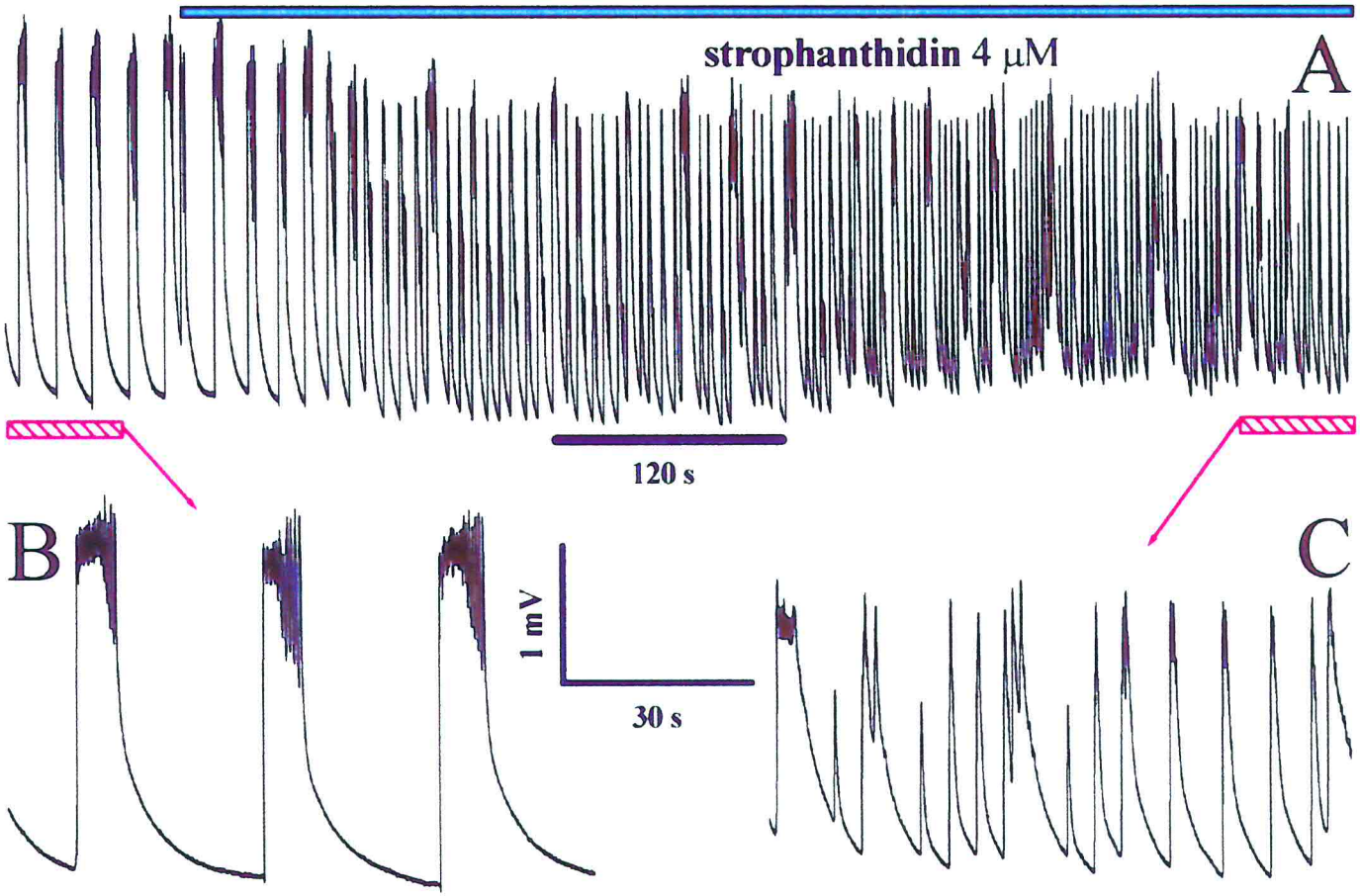

Fig. 25 Strophanthidin application fully disrupts disinhibited bursting

Fig. 25 Strophanthidin application fully disrupted disinhibited rhythm: A shows an example of rhythmic activity before and after strophanthidin application (indicated by the filled horizontal bar) in the presence of strychnine and bicuculline. In B and C the same recordings (red bars) are displayed at faster time base in the absence or in the presence of strophanthidin

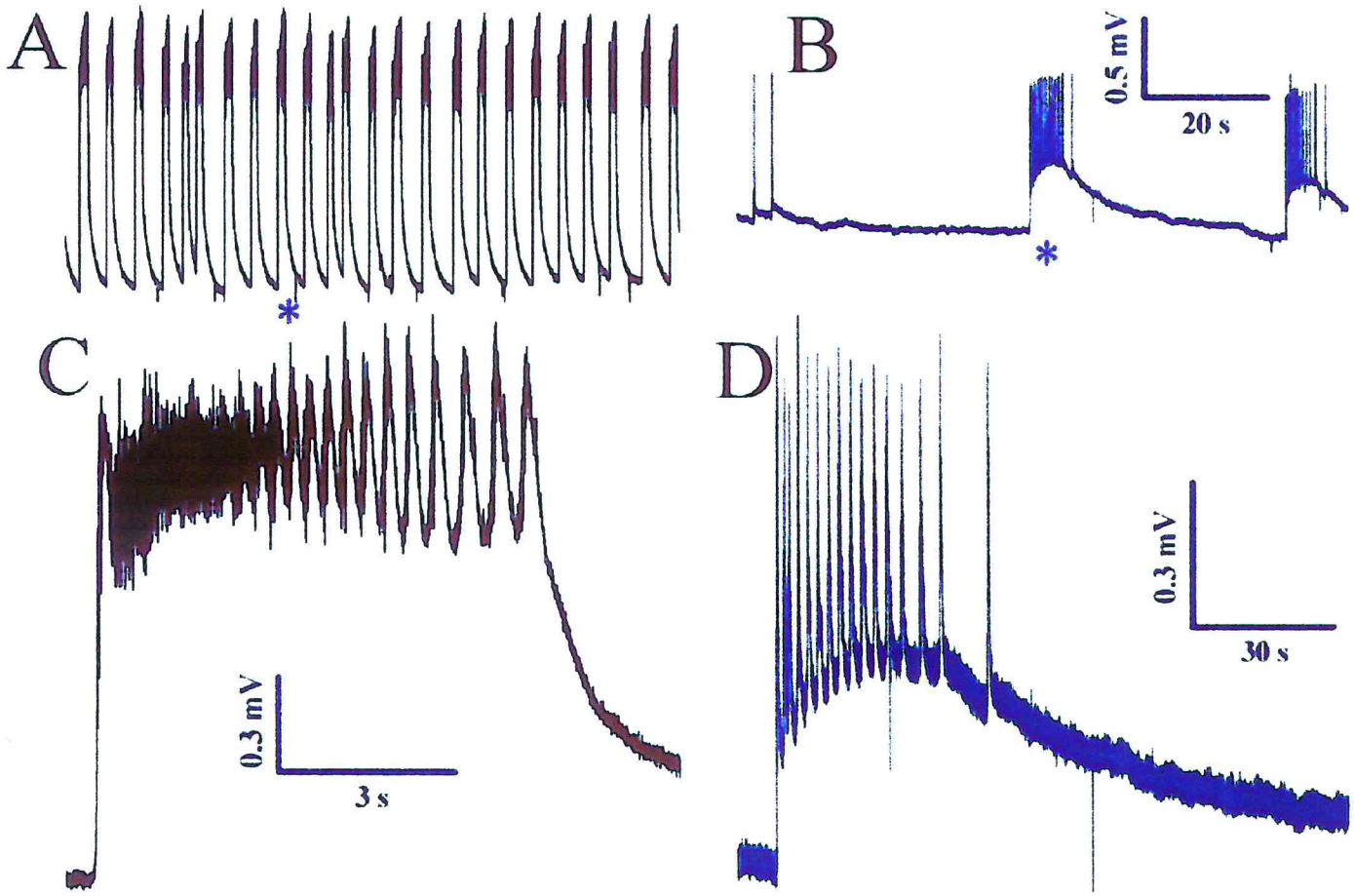

Fig. 26 Long term strophanthidin application unmasks late bursting

Fig. 26 Long term strophanthidin application unmasks late bursting. **A** shows an example of the disinhibited rhythm, while in **C** a single disinhibited burst (indicated by the star in A) is fully depicted. In **B** some spontaneous events, after about three hours of Na^+/K^+ pump block, are presented; and in **D** a single event (indicated by the star in B) is amplified. Note the different time scale between C and D.

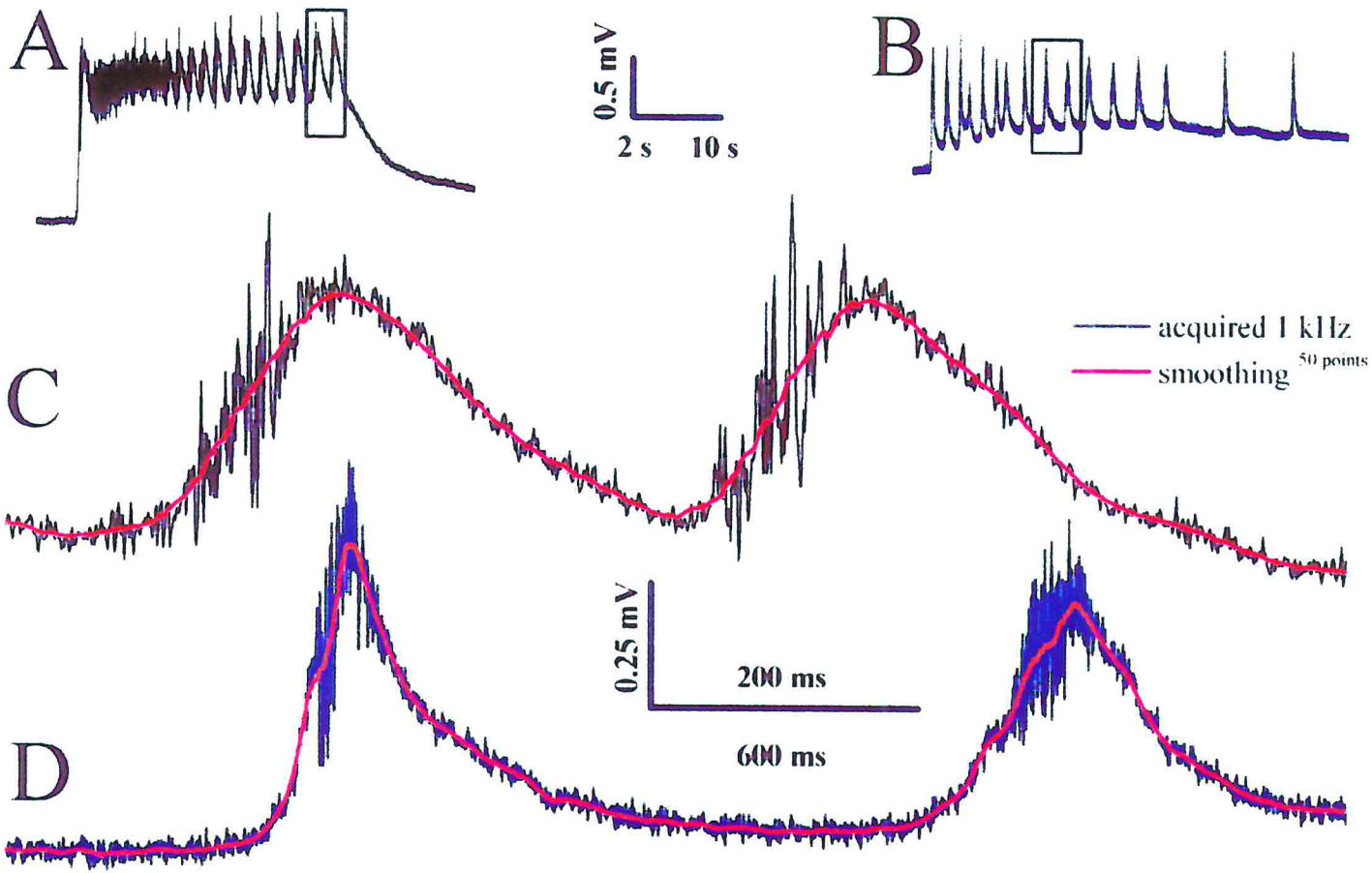

Fig. 27 Intraburst oscillations in disinhibithed rhythm and in strophanthidin bursting

Fig. 27 Intraburst oscillations in disinhibited rhythm and strophanthidin bursting. Intraburst oscillations during disinhibited rhythm (**A** and **C**, black line) or during strophanthidin bursting (**B** and **D**, blue line) are presented. Large spontaneous firing pattern occurred within the rising phase and peak of each oscillation in both conditions.

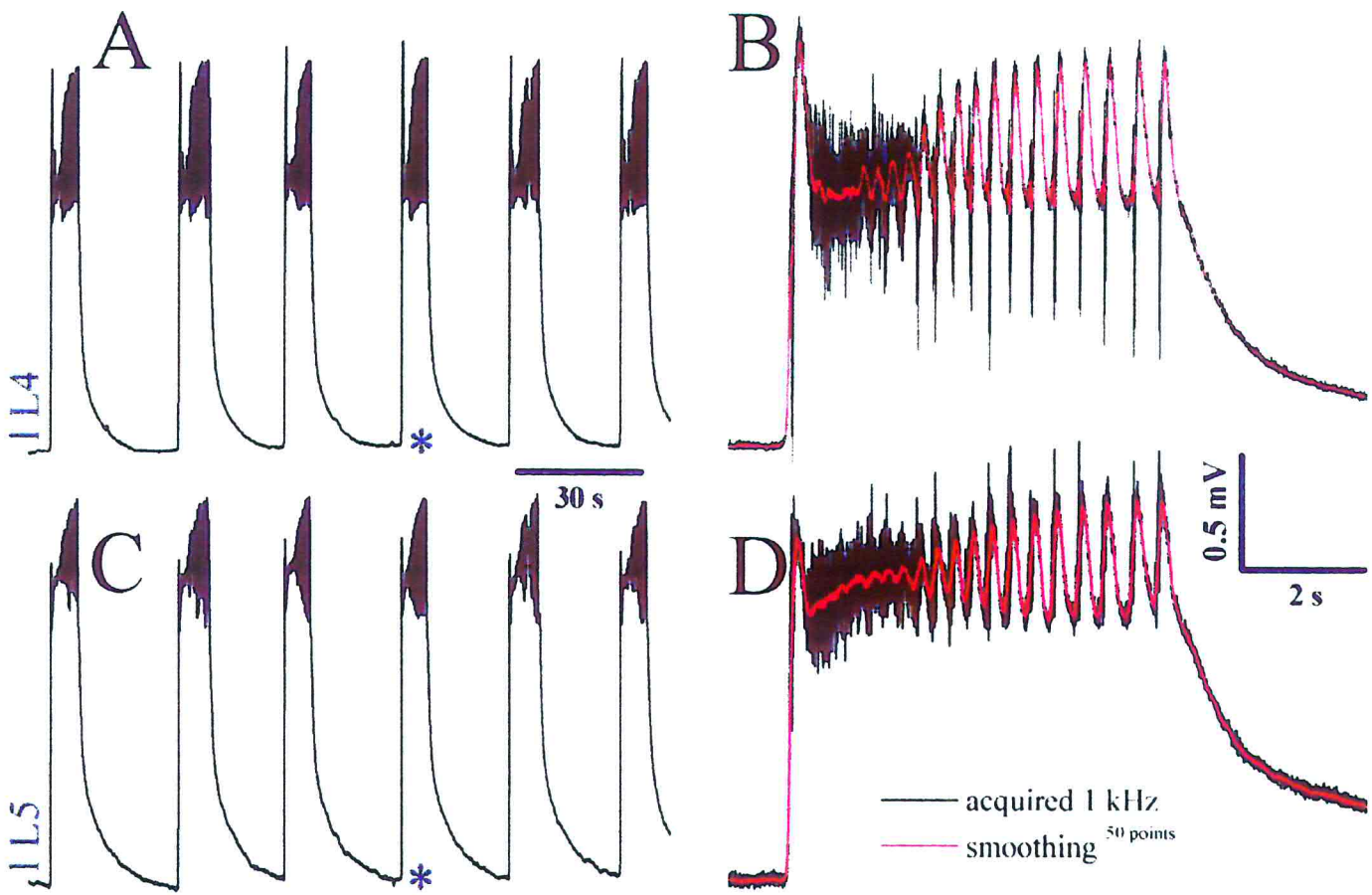

Fig. 28 Disinhibited rhythm recorded from two ventral roots

Fig. 28 Disinhibited rhythm recorded from two ventral roots. **A** and **C** shows two traces recorded from two VRs (left L4 and left L5) of the same preparation during disinhibited rhythmicity; the marked events (stars) are expanded on a faster time base in panels **B** and **D**. The black trace is the acquired one (1kHz), while the red trace is filtered by slow sampling (average every 50 points) to show the first oscillations after the initial plateau phase of the burst. The upstroke of each event was synchronous, like the intraburst oscillations (see also Bracci *et al.*, 1996a, b).

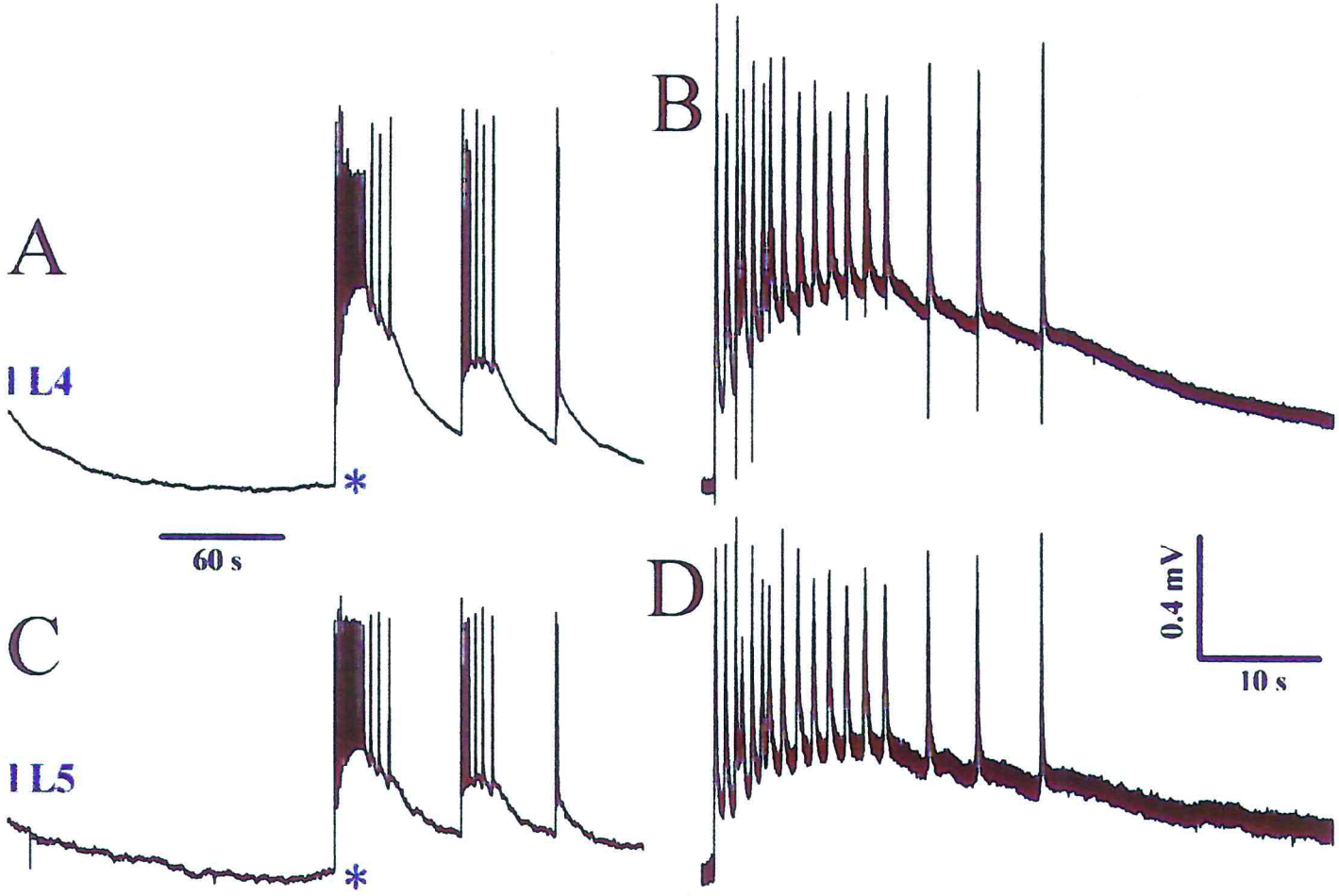

Fig. 29 Strophanthidin bursting recorded from two ventral roots

Fig. 29 Strophanthidin bursting recorded from two ventral roots. **A** and **C** shows the activity of the same preparation presented in Fig. 28 (left L4 and left L5), two hours after strophanthidin application, the marked events are expanded in **B** and **D**. The new bursting activity maintained abrupt onset and synchronous occurrence at segmental and inter-segmental level.

Table 6 Comparison between burst characteristics during disinhibited rhythm and during strophanthidin bursting.

	disinhibited rhythm	**strophanthidin bursting**
duration (s)	5.8 ±2.1	154 ±72
plateau ampl. (mV)	1.48 ±53	0.89 ±0.43
interburst interval (s)	26.3 ±9.2	412 ±373
intraburst oscill. freq. (Hz)	3.2 ±0.8	1.00 ± 0.79
decay time (s)	5.5 ±1.1	138 ±64

Averages ±standard deviations from 7 preparations.

This spontaneous discharge continued as long as the strophanthidin application was maintained (together with strychnine and bicuculline) and was the prototype of a novel form of long-lasting activity, thereafter termed "strophanthidin bursting". This activity was clearly different from former disinhibited bursting generated by the same preparation. In fact, the interburst interval was highly irregular and was more than ten times longer, the burst duration became irregular and longer while the intraburst oscillations changed shape and frequency. These properties are summarized in Table 6 for a sample of 7 spinal cords.

Closer inspection of intraburst oscillations before and after long term application of strophanthidin was performed. Fig. 27 shows the faster characteristics of intraburst oscillations during disinhibited rhythm (A and C, black line) or during strophanthidin bursting (B and D, blue line). On a random sample of 7 preparations each oscillation displayed a time window on which large spontaneous firing was present. In all conditions such a firing pattern occurred within the rising phase and peak of each oscillation (see Fig. 27C and D, respectively).

Further comparison between disinhibited rhythm and strophanthidin one was carried out.

Fig. 28A and C shows two traces recorded from two VRs (left L4 and left L5) of the same preparation during disinhibited rhythmicity; the marked events (stars) are expanded on a faster time base in panels B and D. In B and D the black trace is the acquired one (1kHz), while the red trace is filtered by slow sampling (average every 50 points) to show the first

oscillations after the initial plateau phase of the burst. As previously reported (Bracci *et al.*, 1996a,b), the upstroke of each event was synchronous, like the intraburst oscillations.
Fig. 29A and C shows the activity of the same preparation presented in Fig. 28, two hours after strophanthidin application, the marked events are expanded in B and D. Although the amplitude reduction induced by strophanthidin was stronger in lower trace, the new bursting activity maintained abrupt onset and synchronous occurrence at segmental and inter-segmental level.

Strophanthidin bursting was not due to a gradual metabolic disturbance of the spinal cord due to deleterious effects of sustained Na^+/K^+ pump inhibition. In fact, this form of bursting was continuously observed for at least 12 h without significant change in burst characteristics. In particular, bursts in the second hour in strophanthidin solution were as large as those during the tenth hour (0.8±0.4 vs 0.9±0.4 mV, respectively), had similar periodicity (383±209 vs 508±267 s, respectively) and average duration (130±70 vs 177±75 s, respectively).

Pharmacology of strophanthidin bursting

Glutamatergic transmission was shown (Bracci et al.1996a) to play a prominent role in the disinhibited rhythm since bursts were suppressed by the non NMDA receptor antagonist CNQX and were abolished (or slowed down) by the NMDA receptor antagonists D-APV or CPP.
Fig. 30 shows a rapresentative example of the effect of the non NMDA receptor blocker CNQX (10 μM, n=8) on strophanthidin bursting. In panel A CNQX (indicated by the filled horizontal bar) completely blocked spontaneous activity within a few minutes, although DR stimulation (indicated by stars) evoked a VR response. Note the absence of oscillations in the evoked events in the presence of CNQX. During blocker washout, the amplitude of the evoked events progressively increased and finally, after about 15 min, also spontaneous activity was completely recovered.
In Fig 30B, C and D the spontaneous and evoked events (indicated by the arrows in trace A), were amplified to show events before, during and after the CNQX block.
In Fig. 31 the NMDA receptor blocker D-APV (50 μM) blocked bursting in a reversible fashion. The experimental protocol was similar to the preceding one and gave analogous results (n= 9). In panel A the D-AP5 application (indicated by the filled horizontal bar)

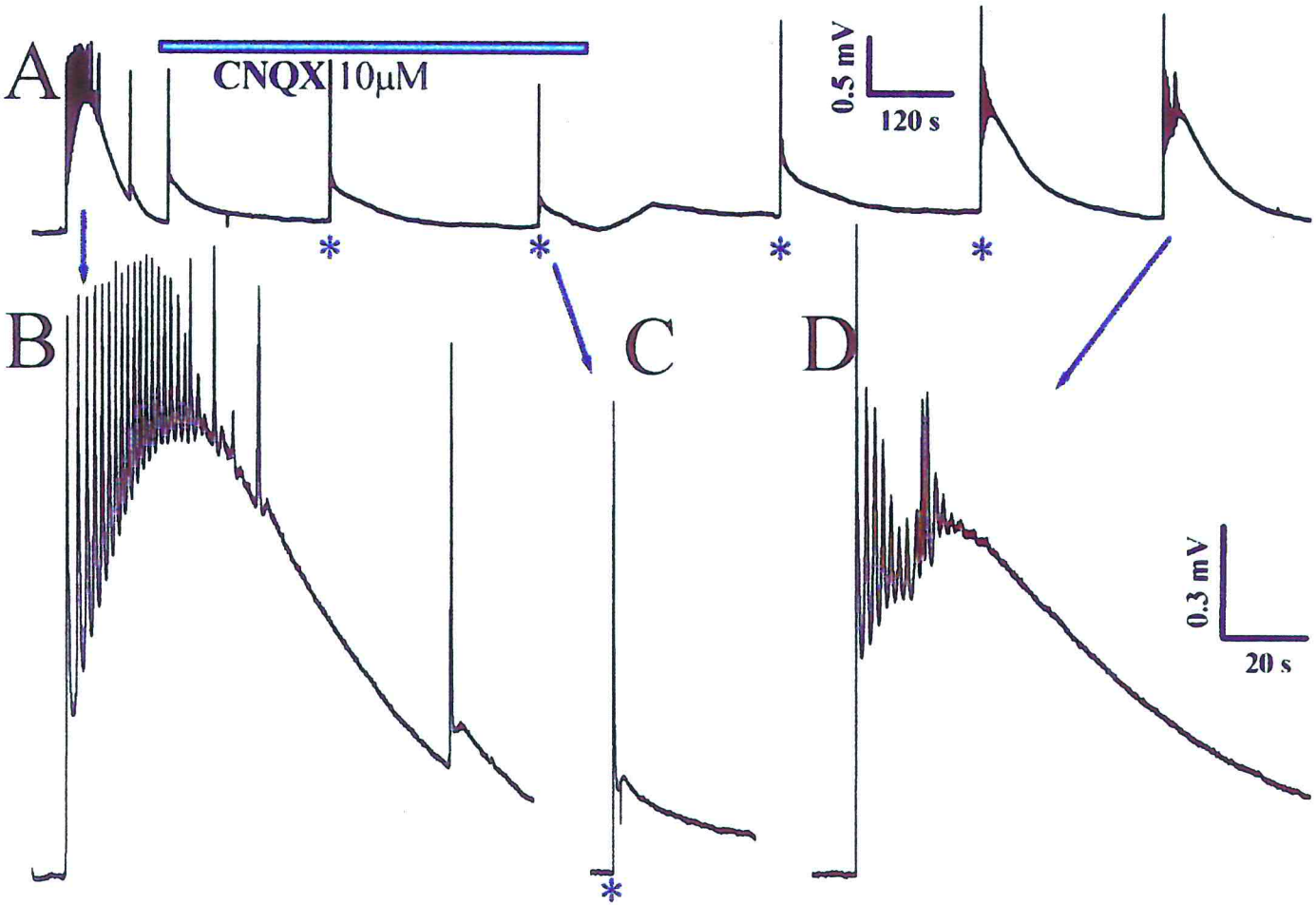

Fig. 30 Effects of CNQX (10 μM) on strophanthidin bursting

Fig. 30 Effects of CNQX on strophanthidin bursting. In panel **A** CNQX (non NMDA receptor blocker; 10 μM; indicated by the filled horizontal bar) was applied on strophanthidin bursting and completely blocked spontaneous activity within a few minutes, although DR stimulation (indicated by stars) evoked a VR response. In **B**, **C** and **D** the spontaneous and evoked events (indicated by the arrows in trace A), were amplified, note the absence of oscillations in the evoked events in the presence of CNQX (n=8).

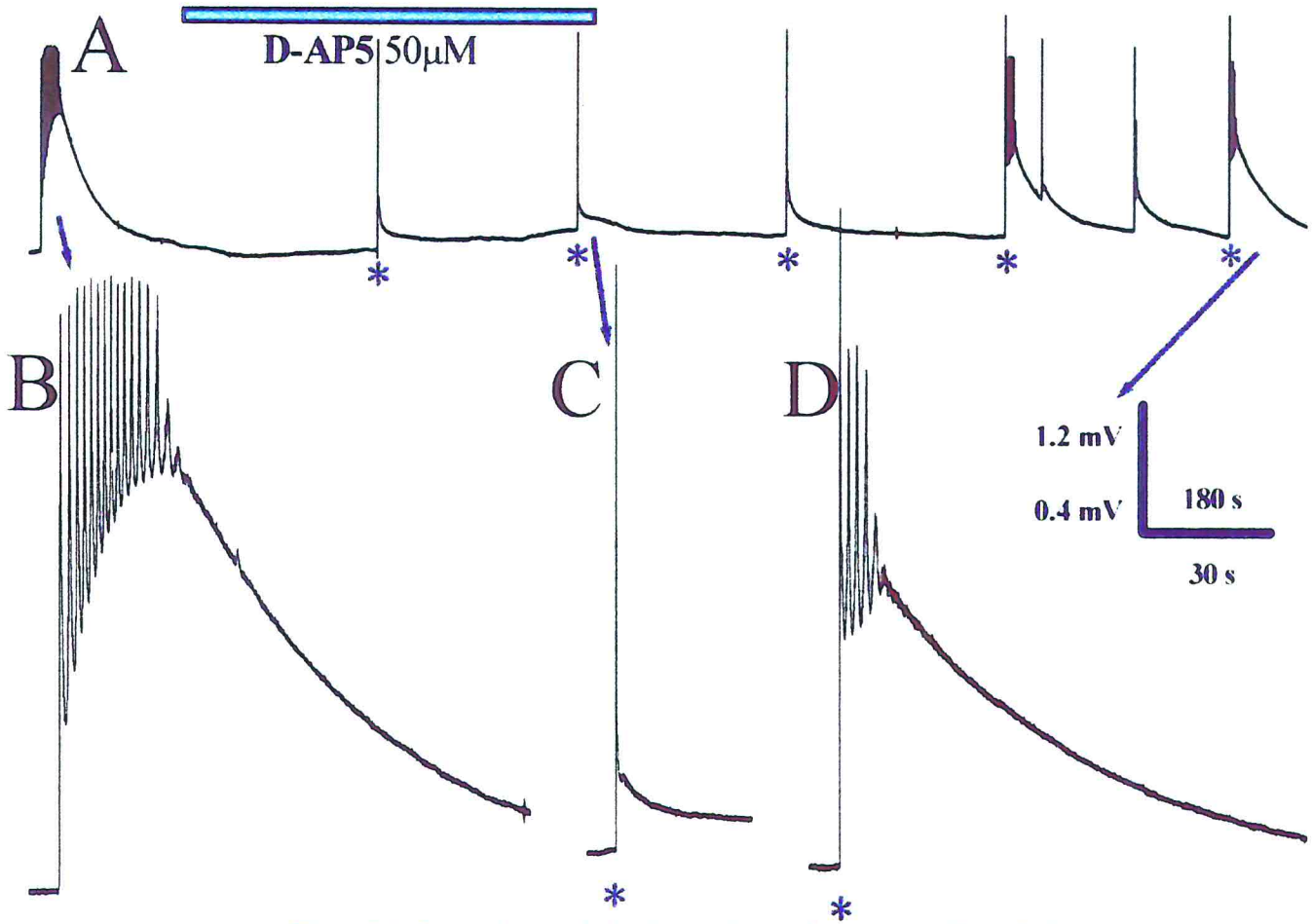

Fig. 31 Strophanthidin bursting bloked by D-AP5

Fig. 31 Strophanthidin bursting blocked by D-AP5. In panel **A** the NMDA receptor blocker D-APV (50 μM; indicated by the filled horizontal bar) blocked bursting in a reversible fashion. The experimental protocol was similar to the preceding one and gave analogous results. DR stimuli could not evoke a structured strophanthidin burst, but only small responses (stars; expanded in **C**, compare with spontaneous in **B**). After washout, spontaneous events reappeared and a DR stimulus could again induce a burst with intraburst oscillations (n= 9).

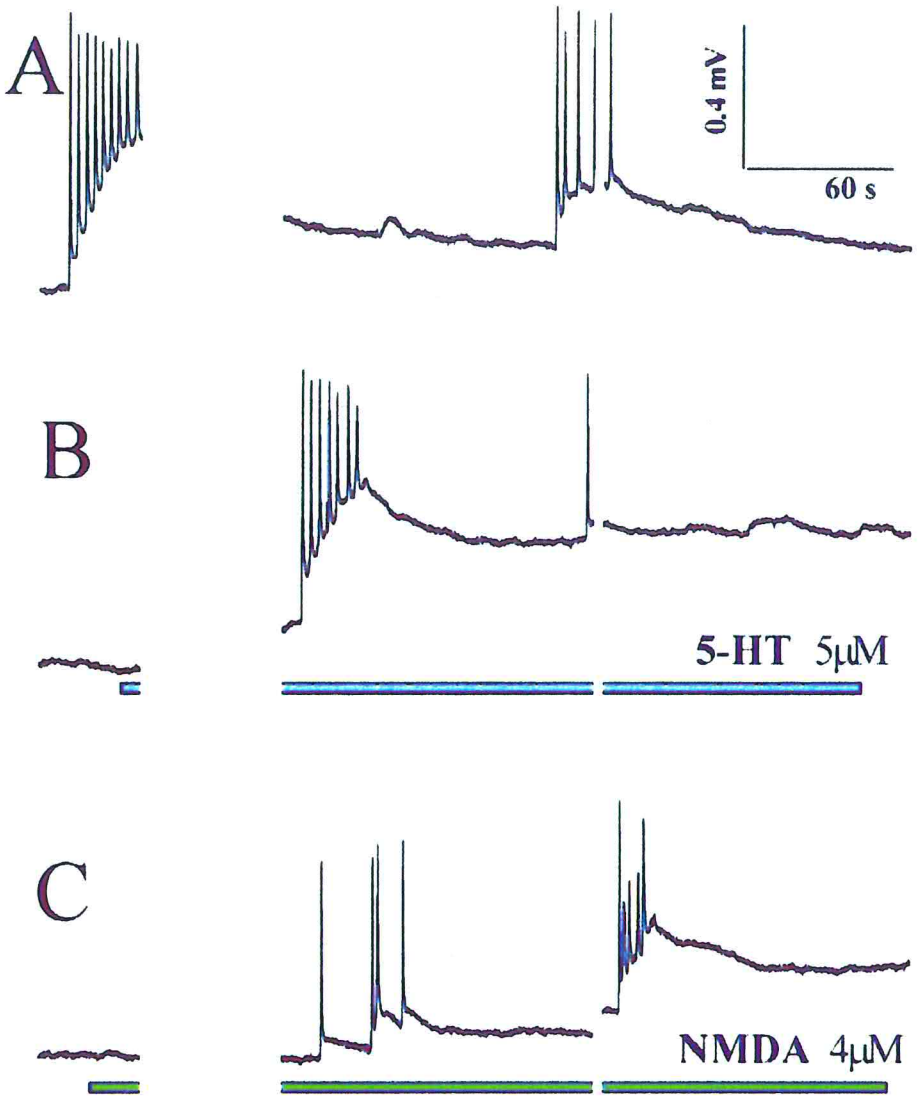

Fig. 32 Effect of excitatory agents applied during strophanthidin bursting

Fig. 32 Effects of excitatory agents applied during strophanthidin bursting. In panel **A** two spontaneous events are depicted, **B** shows that, during strophanthidin bursting, 5-HT (5 μM) application (indicated by the filled horizontal bar), induced a burst followed by a persistent plateau without oscillations. Similar effects were observed in **C** with NMDA (4 μM) application to the same preparation.

blocked spontaneous activity (see spontaneous event expanded in B). DR stimuli could not evoke a structured strophanthidin burst, but only small responses (stars; expanded in C). After washout, spontaneous events reappeared and a DR stimulus could again induce a burst with intraburst oscillations.
Strophanthidin bursting was therefore completely dependent on intact glutamatergic transmission because application of the AMPA/kainate receptor antagonist CNQX or the NMDA receptor antagonist D-APV rapidly abolished it.

Strophanthidin bursting was promptly suppressed by TTX (0.25-1 μM; n= 8) without leaving any residual, spontaneous or evoked activity recorded from VRs (not shown). The gap junction blocker carbenexolone (200 μM) did not inhibit bursting. These observations indicate that strophanthidin bursting was a network mediated phenomenon, depended on glutamatergic transmission and conveyed to motoneurons via spike-dependent activity.

We also investigated if strophanthidin bursting could be upregulated by excitatory agents like NMDA (4-8 μM; n=9), 5-HT (4-12 μM; n=8) or high K^+ (5.5-8.5 mM; n=5), all of which accelerate both fictive locomotor rhythms and disinhibited bursting (Bracci *et al.,* 1996a).
Fig. 32B shows that, during strophanthidin bursting, 5-HT (5 μM) application (indicated by the filled horizontal bar), induced a burst followed by a persistent plateau (about 0.4 mV in amplitude, compare it with two spontaneous events in trace A) without oscillations. After drug washout (5-10 min), baseline recovery was obtained. Similar effects were observed with NMDA (4 μM) application to the same preparation (Fig. 29C) in which a post-burst plateau depolarization (about 0.3 mV) persistently appeared.
Likewise, high K^+ solution produced a stereotypic response consisting of a burst which reached plateau, lost its oscillations and remained depolarized as long as the excitatory agent was applied. Recovery to baseline and return of spontaneous bursting were, however, always obtained after washout (5-10 min). Despite fine titration of the concentration range of these excitatory agents, it was never possible to maintain bursting. Hence, concurrent block of Cl^- mediated inhibition and of the Na^+ pump caused spinal networks to respond to bath applied excitatory agents with a large, sustained depolarization.

General properties of strophanthidin bursting

Fig. 33 (top) shows histograms relative to 106 consecutive events of strophanthidin bursting recorded from one preparation with stable activity for at least 12 h. All the parameters are widely distributed: the interburst interval has a mean value of 392.5 ±226.3 s (CV = 58%), duration of 146.3 ±69.4 s (CV = 47%) and amplitude of 0.86 ±0.37 mV (CV = 44%). Because of this high variability we attempted to study if there was any correlation between various parameters of strophanthidin bursts, especially looking for the influence of any event on the subsequent one. Fig. 33 (bottom) shows plots of burst amplitude, or preceding pause or subsequent pause versus burst duration for the same data shown in Fig. 33 (top). Burst duration was strongly correlated to burst amplitude ($r = 0.91$, $p < 0.0001$) and to length of the preceding pause ($r = 0.76$, $p < 0.0001$), but not to its subsequent pause ($r = 0.29$, $p = 0.0022$, expressing "high" probability that r is zero). Thus, burst duration, which reflects sustained network activity, depended on the intensity of neuronal activation (i.e. burst amplitude) and was a non-markovian process shaped by the ongoing activity during the preceding pause, and without influence on subsequent network behavior.

The data shows in Fig. 33 and the data collected from another preparation (both continuously recorded over 12 hours in the presence of strophanthidin, strychnine and bicuculline solution) were evaluated by Dr Gilda Abbate and used for her thesis project on Statistical Mathematics at the "A. Avogadro" University of Western Piedmont. On the basis of the principal component analysis she confirmed the present correlations (Abbate, 2001). Table 7 shows the average values of those burst components measured between the 2nd and the 12th hour of strophanthidin application in both preparations. Table 8 shows some correlations exhibited by one preparation (the same presented in Fig. 28 and listed as P3 in Table 7).

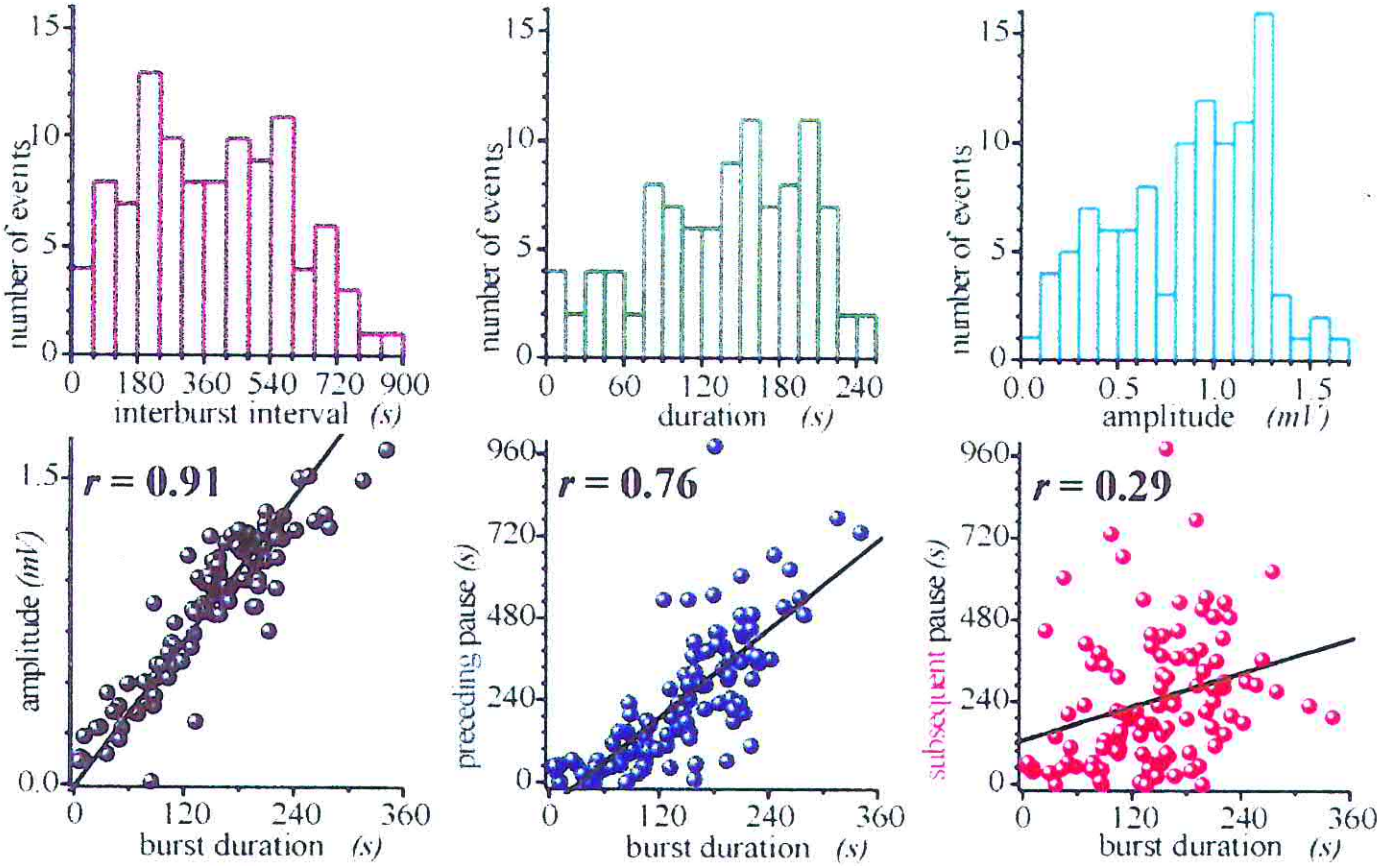

Fig. 33 Strophanthidin bursting: histograms and correlation between various parameters

Fig. 33 Histograms and correlation between various parameters in strophanthidin bursting. **Top** panels shows histograms relative to 106 consecutive events of strophanthidin bursting continuously recorded from one preparation with stable activity for at least 12 h. All the parameters are widely distributed (interburst interval: 392.5 ±226.3 s, CV = 58%; duration 146.3 ±69.4 s, CV = 47%; amplitude 0.86 ±0.37 mV, CV = 44%). **Bottom** panels show plots of burst amplitude, or preceding pause or subsequent pause versus burst duration for the same data. Burst duration was strongly correlated to burst amplitude ($r = 0.91$, $p < 0.0001$) and to the length of the preceding pause ($r = 0.76$, $p < 0.0001$), but not to its subsequent pause ($r = 0.29$, $p = 0.0022$).

Table 7 Average values of burst component measured between the 2nd and the 12th hour of strophanthidin application in two different preparations.

strophathidin bursting	**P3** (106 events)		**P4** (166 events)	
	mean ±SD	CV %	mean ±SD	CV %
amplitude *(mV)*	0.86 ±0.37	44	0.89 ±0.46	52
duration *(s)*	146.3 ±69.4	47	99.8 ±67.7	68
time to plateau *(s)*	23.9 ±14.3	60	19.1 ±14.5	76
recovery time *(s)*	122.4 ±61.0	50	80.7 ±57.5	71
pause *(s)*	246.5 ±195.7	79	143.9 ±144.9	101
interburst interval *(s)*	392.5 ±226.3	58	243.7 ±173.7	71

Table 8 Correlation matrix of P3 preparation (106 events) (from Abbate, 2001)

	amplitude	duration	time to plateau	recovery time	interburst interval	pause	preceding interburts int.	preceding pause	preceding duration
amplitude	1.000								
duration	0.910	1.000							
time to plateau	0.607	0.652	1.000						
recovery time	0.893	0.984	0.505	1.000					
interburst interval	0.498	0.552	0.261	0.566	1.000				
pause	0.251	0.281	0.070	0.303	0.955	1.000			
prec. interb. int.	0.754	0.754	0.498	0.741	0.408	0.203	1.000		
preceding pause	0.806	0.766	0.516	0.750	0.404	0.193	0.955	1.000	
preceding duration	0.182	0.294	0.167	0.295	0.189	0.113	0.559	0.287	1.000

Effects of DR stimulation during strophantidin bursting

Because bath applied excitatory agents did not modulate bursting, we wondered whether synaptically-released transmitters could. To explore this issue we examined the effect of DR stimulation on strophanthidin bursting.

We first tested the effect of a single DR stimulus in control condition, during disinhibited rhythmicity (Bracci *et al.*, 1997) or during strophanthidin bursting activity.

Fig. 34 shows the spinal cord response to very weak (1xTh, 0.1ms) DR stimulus in the three experimental conditions, in the same preparation. In standard control solution (B) the response evoked by 1xTh was the smallest detectable one (see definition of "threshold" in Methods). In Fig. 34A, the evoked event (at higher gain) is visible ~ 10 ms after the stimulus artifact (star); its amplitude was 0.105 mV, area 0.0035 mV x s and duration about 70 ms.

The evoked event induced during a silent period of the disinhibited rhythm (Fig. 34C) was a stereotypic event, similar to a spontaneous one (Bracci *et al.*, 1997) and unrelated to the stimulus intensity; in this example area was 12.215 mV x s (plateau amplitude 1.45 mV, duration 9.4 s).

Likewise, the response induced in a silent period of the strophanthidin bursting (Fig. 34D) was an event unrelated to stimulus intensity and similar to a spontaneous one, although high response variability did not allow constructing a stereotypic burst template in term of duration or amplitude. The evoked event area presented in D was 107.734 mV x s (plateau amplitude about 1.32 mV, duration 157.8 s). During either rhythm, each single pulse (above threshold) applied during a silent period, was able to generate a network response similar to a spontaneous burst and never induced a response similar to a control reflex. These observations suggest that the spinal network became hyperexcitable after strychnine + bicuculline application and that such hyperexcitability was preserved long after strophanthidin application. Neither pharmacological treatment made the spinal network inaccessible to afferent inputs.

Like the observations on disinhibited rhythm (Bracci *et al.*, 1997), also for the strophanthidin bursts the latency after a DR stimulus was progressively reduced by increasing the stimulus intensity. Fig. 35A and C shows two evoked bursts induced by 2 and 5xTh stimulation, respectively. In E the two traces reported in A and C are superimposed to demonstrate a time-to- peak decrease from 345 ms to 300 ms when the stimulus intensity increased from 2 to 5xTh.

Furthermore, the stimulus intensity modulated also the intraburst oscillation frequency that increased progressively and saturated at 8-9xTh. Fig. 35B and D depicts the same events

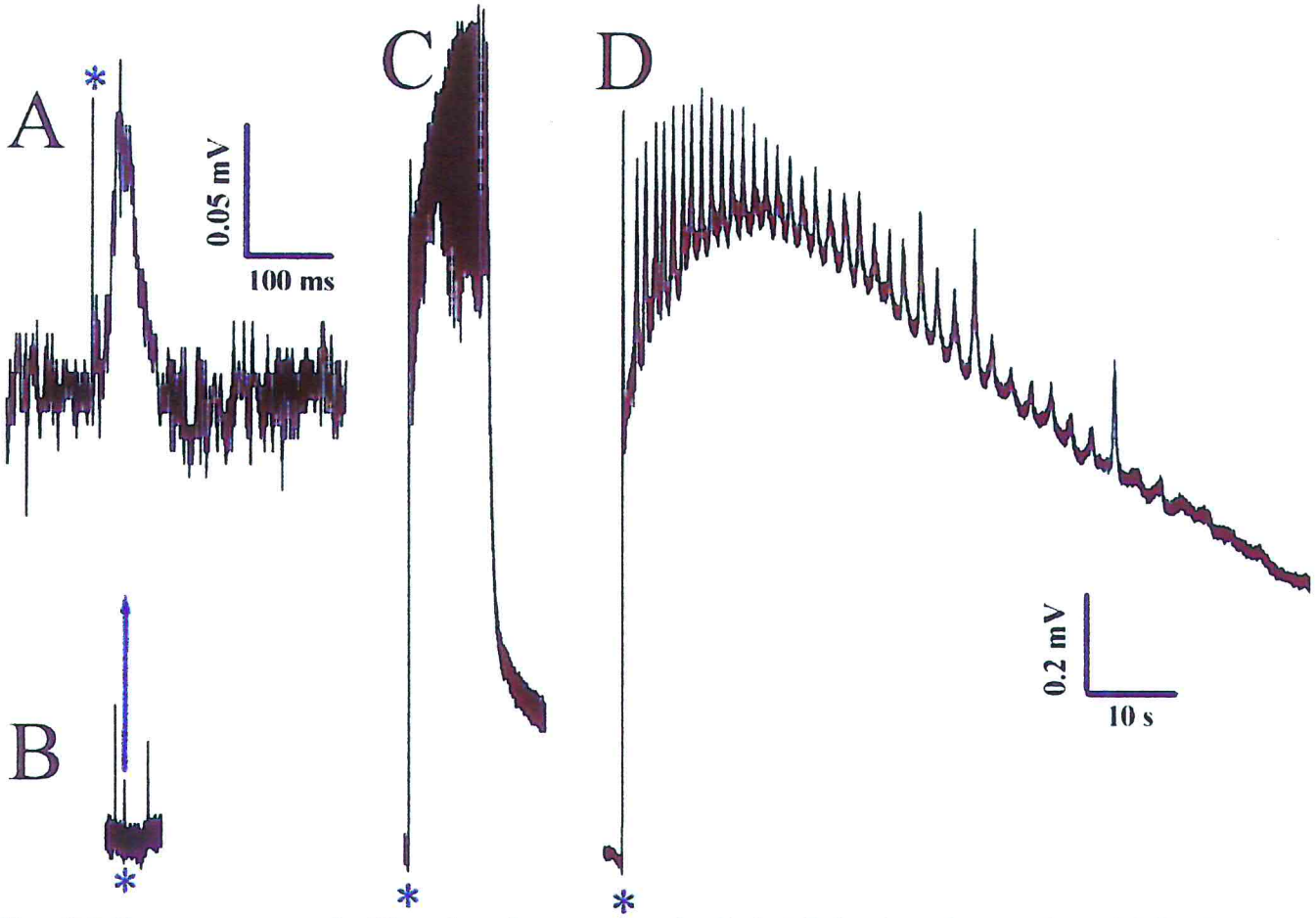

Fig. 34 Responses to 1xTh stimulus: control, disinhibited and strophanthidin bursting

Fig. 34 Responses to 1xTh stimulus in control, and during pause in disinhibited and strophanthidin bursting. In standard control solution (**B**) the response evoked by 1xTh (0.1ms) was the smallest detectable one, and at higher gain (**A**) was visible ~10 ms after the stimulus artifact (star). **C** shows the evoked event induced during a silent period of the disinhibited rhythm, a stereotypic event, similar to a spontaneous one (see Bracci *et al.*, 1997) unrelated to the stimulus intensity. **D** shows that, also the response induced in a silent period of the strophanthidin bursting was an event unrelated with the stimulus intensity and similar to a spontaneous one.

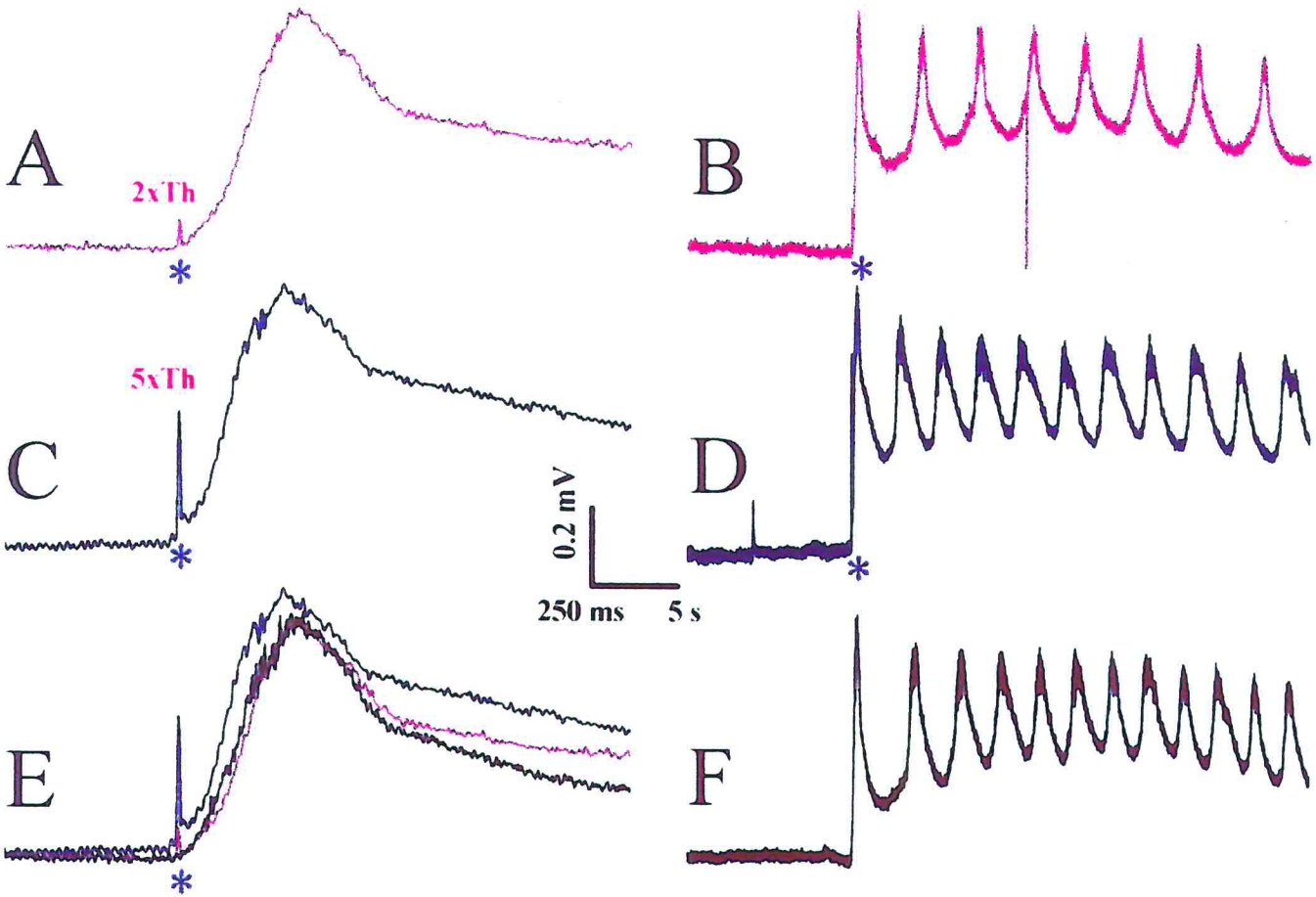

Fig. 35 Effects of different intensity DR stimuli on strophanthidin bursting

Fig. 35 Effects of different intensity DR stimuli on strophanthidin bursting. A and C shows two evoked burst induced by a stimulus 2 and 5xTh respectively. In E the two trace reported in A and C, and a spontaneous event, are superimposed showing a time to peak decrease when the stimulus intensity increased. B and D depict the same events displayed in A and C on a different timescale, F the spontaneous one in E. Stimulus intensity also modulated the intraburst oscillation frequency that increased progressively, but remained in the same range of the spontaneous events.

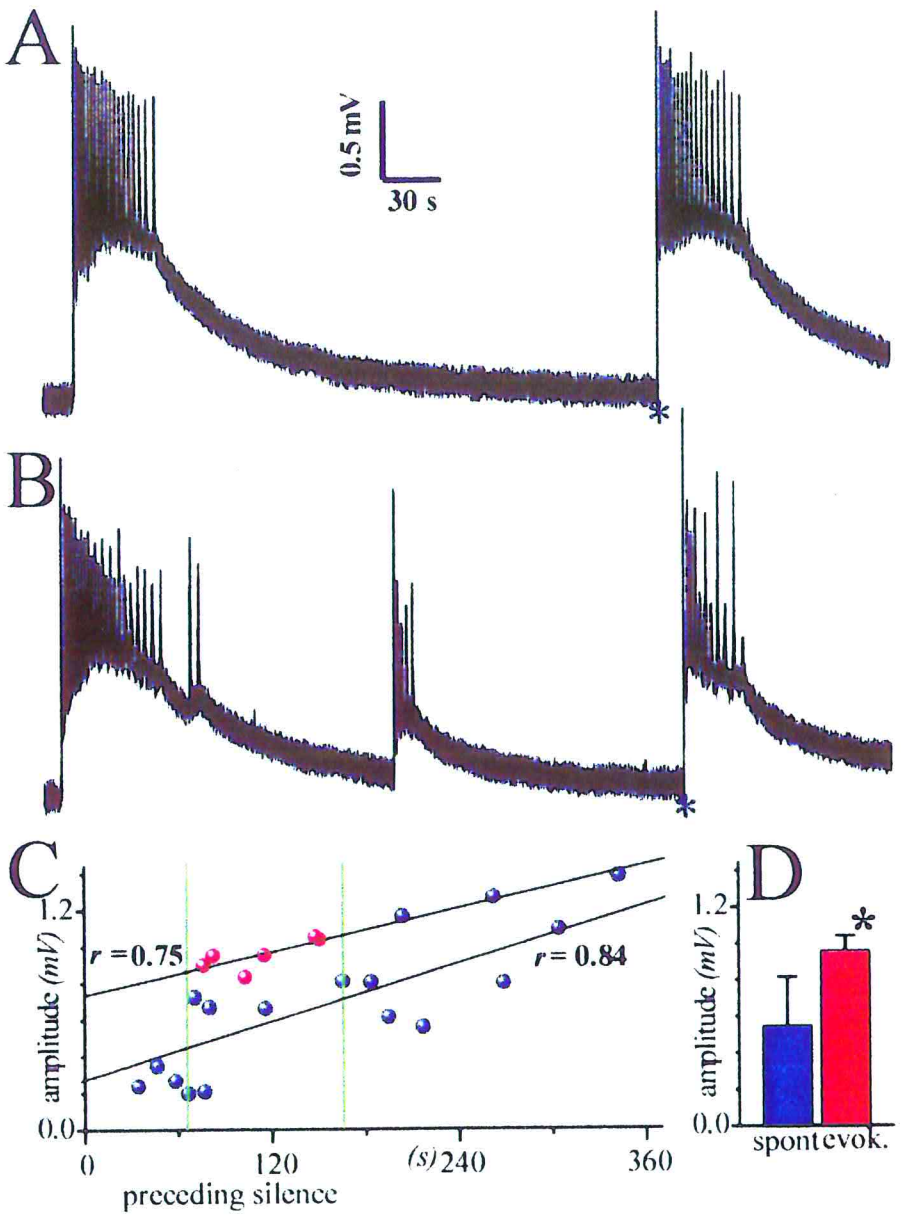

Fig. 36 Effects of DR stimuli during strophanthidin bursting

Fig. 36 Effects of DR stimuli during strophanthidin bursting. **A** and **B** shows two traces, depicting one evoked event (stars; 2xTh, 0.1 ms) after a spontaneous one. **C** shows, spontaneous (blue) and evoked (red) event amplitudes (always measured after a spontaneous event) plotted versus preceding silence. The relation was linear in both cases and with similar slope. The events between green line (100s) in C are reported in **D** showing that the evoked one shown higher amplitude compared with spontaneous ones with similar preceding pause.

displayed in A and C on a different timescale. The intraburst frequency increased from 0.29 Hz (B trace) to 0.38 Hz (D trace) for 2xTh and 5xTh stimuli, respectively. The intraburst oscillation frequency induced by DR stimuli was in the same range of values measured for the spontaneous events, as shown in Fig. 35F (oscillation frequency was about 0.44 Hz).

Increasing the intensity of the DR stimulus did not influence the overall duration of the DR evoked burst, which continued to be strongly determined by the preceding silente period. Fig. 36A and B shows two traces, depicting one evoked event (stars; 2xTh, 0.1 ms) after a spontaneous one. In the upper trace, after about 187 s of silence the stimulus (2xTh, 0.1ms) induced an event with plateau amplitude of 1.038 mV, very similar to the preceding spontaneous one. In the lower trace (same preparation) after only 89 s of pause, the same stimulus could not induce a similar response (burst amplitude 0.764 mV). Fig. 36C shows, for the same preparation, spontaneous (blue) and evoked (red) event amplitudes (always measured after a spontaneous event) plotted versus preceding silence. The relation between preceding pause and subsequent events was linear in both cases (r= 0.75 vs 0.84, evoked vs spontaneous events, respectively) and with similar slope (0.0020 vs 0.0026 linear regression slope coefficient). The evoked events shown higher amplitude compared with spontaneous ones associated with similar preceding pause. Considering a time range of 100 s, the mean amplitude is 0.96 ±0.08 mV vs 0.55 ±0.27 mV (evoked vs spontaneous events, respectively); the decrease in CV is from 49 to 9%. Similar results were obtained in three other preparations.

Effects of DR stimulation during disinhibited or strophanthidin bursts

The above reported data suggested to investigate also the refractoriness of the disinhibited rhythm to DR stimuli applied at short intervals after a burst.

In Fig. 37A a burst was evoked (blue star, 5xTh, 0.1 ms) in a silent period between two spontaneous events: the evoked burst was generated 31.7 s after the first spontaneous event and after further 31.4 s a new spontaneous event appeared. In trace B and C the first two events (arrows) are amplified to compare the spontaneous burst (B) with the evoked one (C). The upstroke was faster in the evoked events, but the area (12.6 mV x s in B vs 12.1 mV x s in C), the plateau amplitude (1.46 mV in B vs 1.54 mV in C) and the duration (8.5 s in B vs 8.4 s in C) of the two events were very similar, as reported also by Bracci *et al.* (1997).

Fig. 38A shows the effect of a stimulus (star, 5xTh, 0.1 ms) applied about 500 ms after the last oscillation; the pulse was delivered about 0.95 mV over the resting baseline (60% of

plateau depolarization, 1.58 mV), and induced a response comparable to the spontaneous one, albeit with fewer oscillations. Evoked event area was 12.8 mV x s vs 14.1 mV x s spontaneous area; plateau amplitude was 1.82 mV vs 1.58 mV, respectively, and the duration 7.6 s vs 9.1, respectively.

In Fig. 38B, we applied repeated stimuli, as close as possible to the last oscillation of each burst (between 135 and 460 ms). After three pulses the last burst was shorter (1.7 s, measured between stimulus artefact and a time corrsponding to the level of depolarization at which the first burst of the series terminated) than the spontaneous one (8.8 s, between onset and stimulus; star) and did not generate intraburst oscillations. Plateau amplitude of the three evoked events was similar to the spontaneous one (1.74, 1.90, 1.79 and 1.76 mV), whereas burst duration decreased progressively (8.8, 4.2, 2.2 and 1.7 s). Similar results were obtained from all 5 preparations tested.

Fig. 38C shows the effect of a single stimulus (star; 5xTh, 0.1 ms) applied before the end of a spontaneous strophanthidin burst (28 s after the last oscillation and corresponding to a 26 % plateau depolarization). While burst depolarization amplitude was similar to the spontaneous one, it lacked oscillations and was much shorter. Evoked event area was 22.6 mV x s vs 40.0 mV x s spontaneous area; plateau amplitude was 0.610 mV vs 0.605 mV, respectively, and the duration 59.6 s vs 90.0, respectively.

In conclusion, single DR stimuli were able to induce, during disinhibited rhythm, sustained plateau bursts due to synaptic activity by the interneuron network, indicating that fatigue was not a major factor to end each burst. Conversely, during strophanthidin bursting, a stimulus could not generate (even after many seconds from the last oscillation) a discharge comparable to the preceding spontaneous one, suggesting relevant fatigue in the interneuron network.

Effects of DR stimulus train during strophantidin bursting

Previous experiments have indicated that disinhibited bursts could be entrained, on a 1:1 basis, by a train of DR pulses applied at various frequencies (Bracci *et al.,* 1997). We next examined if strophanthidin bursting could show similar properties. Fig. 39A and B shows examples of responses induced by electrical stimuli applied every 45 or 15 s respectively.

At the lower frequency (Fig. 39A) the first pulse induced a burst while subsequent ones (all indicated by a blue star) evoked shorter VR discharges (comprising one or more peaks) superimposed on a declining baseline. At the higher frequency (Fig. 39B) each pulse after the

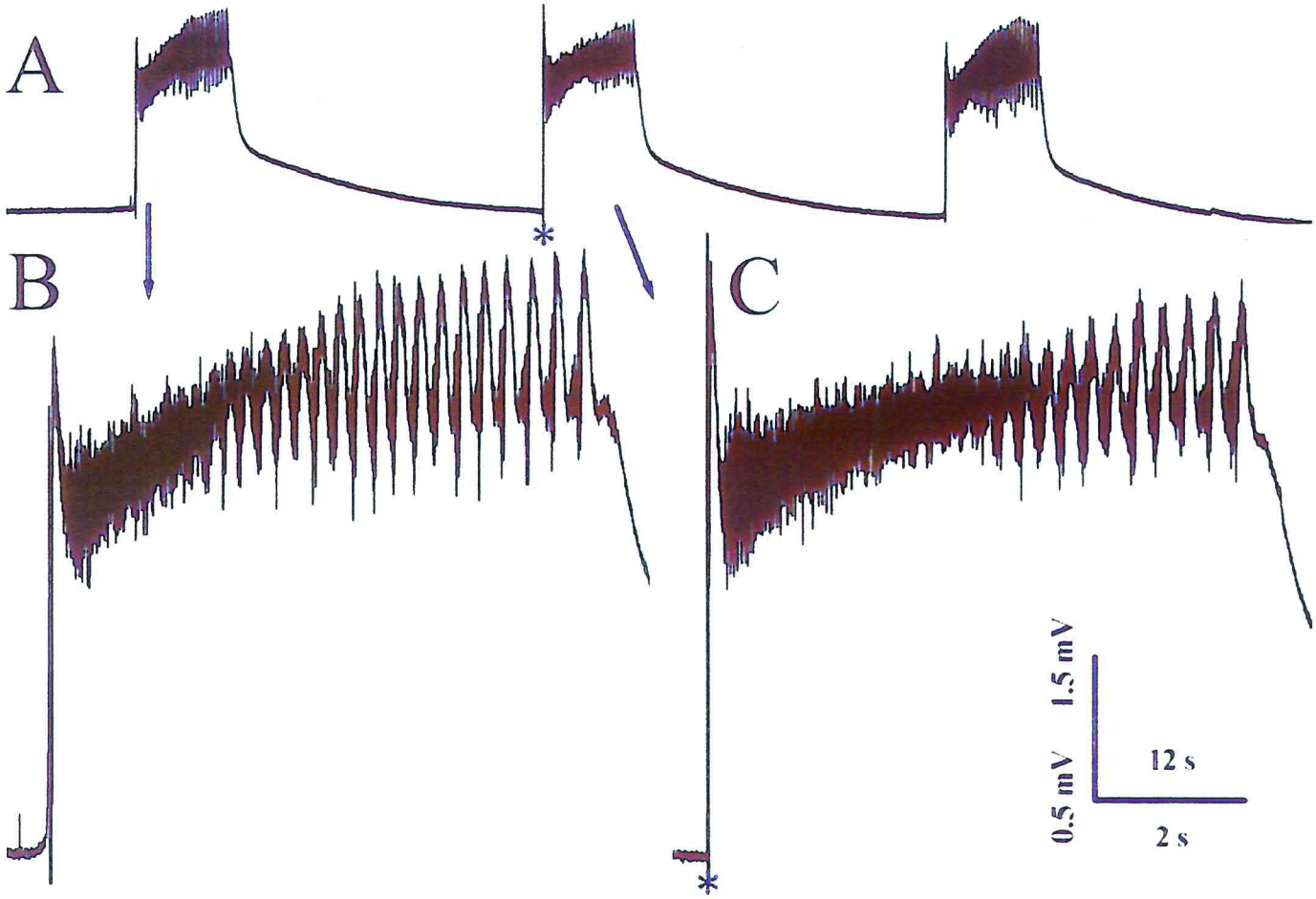

Fig. 37 Spontaneous and evoked events in disinhibited rhythm

Fig. 37 Spontaneous and evoked events in disinhibited bursting. **A** a burst was evoked (blue star, 5xTh, 0.1 ms) in a silent period between two spontaneous events. In trace **B** and **C** the first two events (arrows) are amplified to compare the spontaneous burst (B) with the evoked one (C): the two events were very similar, as reported also by Bracci *et al.* (1997).

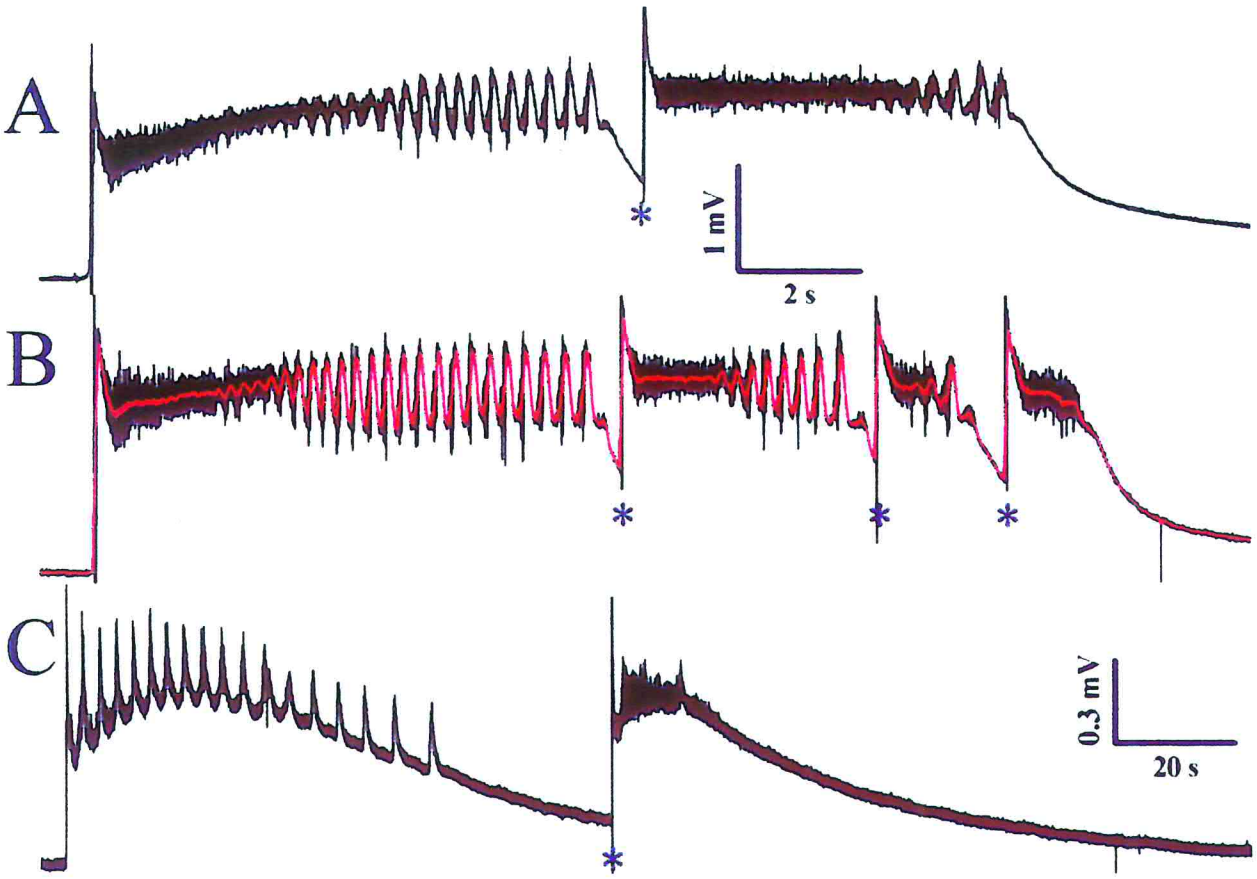

Fig. 38 Effects of stimuli delivered during disinhibited or strophanthidin bursting

Fig. 38 Effects of stimuli delivered during disinhibited or strophanthidin bursts. **A** shows the effect of a stimulus (star, 5xTh, 0.1 ms) applied about 500 ms after the last oscillation of a disinhibited spontaneous event. The pulse induced a response comparable to the spontaneous one, albeit with fewer oscillations. In **B**, repeated stimuli were applied at the end of a disinhibited burst, as close as possible to the last oscillation of each burst (between 135 and 460 ms). After three pulses the last burst was shorter than the spontaneous one and did not generate intraburst oscillations. **C** shows the effect of a single stimulus (star; 5xTh, 0.1 ms) applied before the end of a spontaneous strophanthidin burst (28 s after the last oscillation). While burst depolarization amplitude was similar to the spontaneous one, it lacked oscillations and was much shorter.

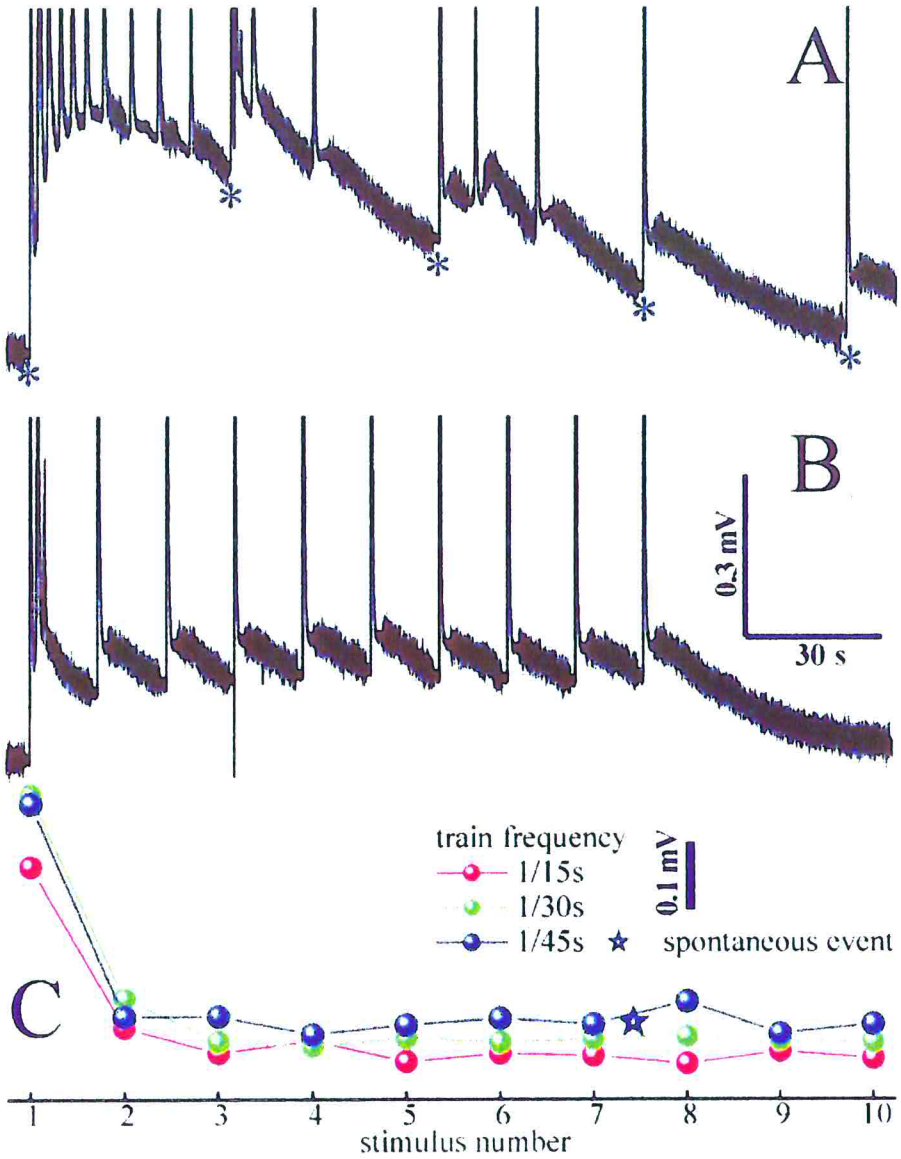

Fig. 39 Effects of stimulus train on strophantidin bursting

Fig. 39 Effects of stimulus train on strophanthidin bursting. **A** and **B** shows examples of responses induced by electrical stimuli (stars in A) applied every 45 or 15 s respectively. Note that at the higher frequency (B) each pulse after the first one elicited a single discharge, riding over a persistent baseline depolarization. **C** shows the relative amplitude of slow responses (measured from the immediately preceding level of polarization) for a series of DR pulses at varying frequency.

first one elicited a single discharge made up by a fast transient followed by a slow component, riding over a persistent baseline depolarization. Fig. 39C shows the relative amplitude of slow responses (measured from the immediately preceding level of polarization) for a series of DR pulses at varying frequency. Despite changing frequency, each pulse generated a slow response that remained at relatively stable amplitude throughout the stimulus train. The average amplitude (3^{dh} –10th pulse) of the responses induced by trains (1 every 15 to 1 every 120 s) are reported in Table 9. p values (marked with one or two stars, depending on the level of significance, <0.002 and <0.0003, respectively) were calculated for each set of data with respect to the data obtained with the preceding higher frequency of stimulation. All the 4 preparation gave similar results.

Table 9 Effects of stimulus train on strophanthidin bursting.

stimulation frequency	amplitude (mV)	spontaneous events
1/15 s - 4h stroph.	0.062 ±0.008	
1/15 s - 6h stroph.	0.061 ±0.010	
1/30 s	0.081 ±0.004**	
1/45 s	0.107 ±0.014**	1
1/60 s	0.106 ±0.023	1
1/90 s	0.181 ±0.050*	2
1/120 s	0.188 ±0.092	1

When the pulse interval was set at 45 s, occasional spontaneous bursts could appear (as shown by the star in Fig. 40C) but never in coincidence with the earliest part of the evoked event. At the faster rates of stimulation, spontaneous bursts did not appear. Table 9 lists spontaneous events appearing within the first 10 stimuli.

Discussion

Discussion I:

$GABA_C$ receptors expression and function

The principal finding of the first part of the present study is the demonstration of the presence in the spinal cord network of functional $GABA_C$ receptors, showing different localisation at different ages. In P0-P1 rats the $GABA_C$ receptors are mainly expressed by motoneurons and contributed to the direct motoneuron inhibitory action of GABA, without apparent influence on network activity. From P3 age onwards $GABA_C$ receptors highly expressed by interneurons and the novel $GABA_C$ receptor antagonist TPMPA decreased the inhibitory action of exogenous GABA on evoked synaptic transmission and retarded disinhibited bursting. Such a slowing down of spontaneous bursting was associated with a striking prolongation of individual bursting events. Collectively, the data suggest that in the neonatal rat spinal cord there are functional $GABA_C$ receptors whose activity is highlighted after block of the predominant $GABA_A$ receptor population.

Characteristics of TPMPA antagonism

Any investigation into a possible role of $GABA_C$ receptors in the >P3 spinal cord ought to be focussed on the interneuronal network (Allan *et al.,* 1980; Johnston, 1976). In fact, the large majority of GABA receptors on motoneurons belong to the $GABA_A$ class as shown by their strong block by bicuculline (Evans, 1978; Long *et al.,* 1989). Nevertheless, in the in situ preparation the sparse location of the interneuronal network in the ventral and dorsal horn and its heterogeneous cell population make it unsuitable to electrophysiological studies. This realisation thus led us, as a first approach, to study GABA responses in a spinal cord preparation with fully preserved polysynaptic reflexes generated by the spinal network: polysynaptic reflexes thus represented a simple but effective index of network operation. When these electrically evoked synaptic responses were recorded in the presence of GABA, it was apparent that TPMPA decreased the extent of the depression by exogenous GABA of the slow polysynaptic reflex, a phenomenon thus relying in part on $GABA_C$ receptor activity at network level. Since TPMPA *per se* had no effect either on baseline VR polarisation or control reflexes, it does not seem likely that $GABA_C$ receptors were involved in the maintenance of the average potential of a large pool of motoneurons or were synaptically activated by endogenous GABA through the type of DR stimulation used for those experiments. As TPMPA had no effect on depolarisations elicited by exogenously applied GABA, these VR responses were unlikely to involve $GABA_C$ receptor activation.

Under standard experimental conditions the role of $GABA_C$ receptors in the neonatal rat spinal cord was a minor one when compared with that of $GABA_A$ receptors.

Selectivity of TPMPA antagonism

Previous studies have shown that, in high concentrations, TPMPA could activate $GABA_B$ receptors (Murata *et al.,* 1996; Ragozzino *et al.,* 1996; Chebib *et al.,* 1998) and inhibit $GABA_A$ receptors.

The present experiments were carried out with the recommended concentration of TPMPA to retain selectivity of action towards $GABA_C$ receptors (Murata *et al.,* 1996; Ragozzino *et al.,* 1996). Homo-oligomers of ρ_2 subunits showed a very high K_b (15.6 μM; over 7 times ρ1 value), but apparently they do not exist in nature and also their expression in *Xenopus* oocytes is very difficult to obtain (Chebib *et al.,* 1998).

The possibility of $GABA_B$ receptor agonism was explored using the $GABA_B$ agonist baclofen which evoked responses unchanged by TPMPA. Similarly, the responses induced by the

selective $GABA_A$ agonist isoguvacine were insensitive to TPMPA. Like GABA, baclofen (0.5-2.0 μM) depressed all components of the reflex, although the effect on the monosynaptic one was stronger. Since the action of baclofen was dose-dependent and consistently unaffected by TPMPA, its insensitivity to TPMPA antagonism could not be simply caused by full occupancy of $GABA_B$ receptors from which TPMPA was unable to displace this agonist. A more likely explanation is that the test dose of GABA had relatively minor effects via $GABA_B$ receptor activation (perhaps because these receptors were comparatively less sensitive to GABA than to baclofen and mainly located at presynaptic level; Sivilotti and Nistri, 1991) and that it activated predominantly $GABA_A$ and partly $GABA_C$ receptors. In P3-P7 rat tissues, the lack of change by TPMPA alone in the fast reflex amplitude, which represents mainly a monosynaptic component mediated by glutamate receptor activation, indicates that this drug did not interfere with excitatory transmitter receptors. All together, these observations concur to validate the selectivity of antagonism by TPMPA against the ρ subunits which are thought to make up the $GABA_C$ receptor (Bormann, 2000; Chebib *et al.,* 1998).

Bursting activity is decreased by TPMPA

Pharmacological isolation of $GABA_C$ receptor mediated responses requires application of a $GABA_A$ antagonist such as bicuculline which invariably triggers chaotic bursting activity. If the glycine receptor antagonist strychnine is also applied, a very regular, spontaneous bursting pattern emerges which continues unabated for many hours at a slow cycle period. This experimental paradigm, extensively tested in our laboratory (Bracci *et al.,* 1996a,b; Ballerini *et al.,* 1997; Bracci *et al.,* 1997), provided us with a network expressing excitatory behaviour via activation of glutamatergic synapses and devoid of conventional GABA receptor activity since no significant role of $GABA_B$ receptors is present in this phenomenon (Bracci *et al.,* 1996b): this situation should thus maximize the chances of detecting any role of $GABA_C$ receptors. Under these conditions TPMPA again did not alter VR polarization, but it increased the cycle period of these bursts. This deceleration was not mirrored by any change in burst amplitude (also confirmatory of lack of antagonism of excitatory transmission) or decay, while there was a noticeable increase in the number of intraburst oscillations. The depressant action of TPMPA did not involve transient relief of the bicuculline block of $GABA_A$ receptors. In fact, should this be the case, the response would be enhanced by a typical modulator of $GABA_A$ receptors such as pentobarbitone (Sivilotti and Nistri, 1991). In contrast

with this possibility, we observed that, while 25 μM pentobarbitone increased the VR depolarization by GABA, it did not alter the slowing down of bursting activity by TPMPA. This result suggests that pharmacological block of $GABA_A$ receptors was saturating under the present conditions.

Strychnine and bicuculline induced bursting is known to depend on the operation of a rhythm generator localized within the anteroventral quadrant of the spinal cord which uses motoneurones as output elements of the system (Bracci *et al.,* 1996b). Such bursts, which are synaptically originated events arising from a stable baseline with great regularity, comprise a rapid depolarizing upstroke followed by a variable number of intraburst oscillations. So far it has been possible to identify only a limited number of processes responsible for burst generation, duration and termination (Ballerini *et al.,* 1997). It is now possible to suggest that activation of $GABA_C$ receptors contributed to bursting as indicated by the present experiments with TPMPA. As the rhythm generator interneurones have up to now escaped identification, it is not yet possible to postulate where, within a complex network, such $GABA_C$ receptors are found. However, some insight into their functional significance might come from observing the characteristic facilitation of intraburst oscillations by TPMPA against a background of slower bursting activity. From this it seems plausible to infer that synaptically activated $GABA_C$ receptors facilitated bursting episodes and at the same time restricted the oscillatory property of the network. This apparently paradoxical function might be explained by supposing that $GABA_C$ receptors mediated network excitation. This notion is supported by the analogous effects of disparate depolarizing agents such as *N*-methyl-D-aspartate (NMDA) or serotonin which speed up bursting but consistently shorten intraburst oscillations Bracci *et al.,* 1996a,b). This dissociation is probably due to the fact that network depolarization triggers bursting by reducing firing threshold in interneurones, but, at the same time, it curtails intraburst oscillations which require for their full expression recovery of Na^+ (and Ca^{2+}) currents from voltage-dependent inactivation (Ballerini *et al.,* 1997;). In summary then, it is suggested that blocking $GABA_A$ (and glycine) receptors unveiled a significant contribution by $GABA_C$ receptors to bursting activity and that their role was presumably an excitatory one as also reported for the hippocampus of neonatal rats (Strata and Cherubini, 1994). In analogy with the proposed excitatory action of $GABA_C$ receptors during bursting episodes, we can hypothesize that a similar interneuronal depolarization mediated by $GABA_C$ receptors, activated by bath-applied GABA, inhibited reflex activity via a combination of shunting and inactivating excitatory membrane currents as proposed for other actions of synaptically released GABA (Stuart and Redman, 1992; Graham and Redman, 1994).

Mapping $GABA_C$ receptors in the CNS

The main findings of the present study with *in situ* hybridisation and immunohistochemistry are that in the rat spinal cord ρ1 or ρ2 subunits (which make up $GABA_C$ receptors; Bormann, 2000) have a much wider distribution than suspected before, and that these two subunits were differentially expressed depending on the cell type, region and age.

The ρ family in neural and non-neural tissues

In the present study, both EST database screening and Western blot analysis suggest the presence of ρ subunits in non neural tissues such as ovary and testis. In these two tissues the bands detected were of apparent MW similar to that of bands found also in the rat brain and retina homogenates (50 and 60 KDa). The molecular weights (MW) of the three $GABA_C$ receptor subunits can be calculated from the available sequences as 52 KDa for ρ1, 51 KDa for ρ2, and 48 KDa for ρ3. While the experimentally observed MW of ρ1 is 55 KDa (Boue-Grabot *et al.,* 1998), the other values are indirect because no data were available prior this study concerning the native proteins recognised by the rho 63 polyclonal antibody on rat tissue homogenates. The presence of a low MW band (43 KDa) in the retina homogenate is compatible with its identification as the ρ3 subunit since this protein has the lowest predicted MW amongst the ρ proteins and has been described at high levels in the retina of the adult rat (Ogurusu *et al.,* 1997). The discrepancies between the expected and the observed MW might be due to posttranslational modifications which were not further investigated in the present study. The presence of $GABA_C$ receptors in peripheral tissues is not surprising since they have already been described in the gut (Jansen *et al.,* 2000). In addition, $GABA_A$ and $GABA_B$ receptors are also expressed in a number of non-neural tissues including spleen, kidney, gonads, stomach and intestine (Akinci *et al.*, 1999; Belley *et al.,* 1999).

$GABA_C$ receptor distribution in the central nervous system

In recent years, RT-PCR based evidence has shown $GABA_C$ receptor ρ1 and ρ2 subunits in rat adult cortex, striatum, hippocampus, superior colliculus, cerebellum, brain stem and spinal cord (Enz *et al.,* 1995; Boue-Grabot *et al.,* 1998; Wegelius *et al.,* 1998). However, the precise cellular localisation of the ρ1 and ρ2 subunits in most of these structures remains controversial or unavailable (Enz *et al.,* 1995; Ogurusu *et al.,* 1997, 1999; Boue-Grabot *et al.,*

1998). The present study was targeted to identify the cells stained for ρ1 or ρ2 subunits and did not rely on a quantitative evaluation of the staining level. Further analysis of the relative preponderance of each subunit in various discrete areas will require new antibodies (not yet available) selective against each subunit.

Although earlier work had concluded that the two ρ subunits are expressed in adult Purkinje cells tested with mixture of the ρ1 and ρ2 probes or with an anti ρ1 antibody (Boue-Grabot et al., 1998), the presence of two distinct ρ subunits in other cerebellar neurons was not reported. The present *in situ* hybridisation experiments carried out on adult cerebellum demonstrated that Purkinje cells and basket-like cells expressed ρ1 and ρ2 subunits.

Spinal cord

In the spinal cord, the presence of $GABA_C$ receptors has been inferred from our electrophysiological studies of early postnatal preparations or by RT-PCR in the adult (Enz *et al.,* 1995). So far no data on the actual topographical distribution of this receptor have been available. We demonstrated that the P1, P7 and adult spinal cord expressed the $GABA_C$ receptor subunits ρ1 and ρ2. The expression patterns for these two subunits were essentially overlapping although ρ2 was always stronger than ρ1, in agreement with the RT-PCR data indicating that in the adult spinal cord the mRNA for ρ2 is more abundant (Enz *et al.,* 1995). Furthermore, our results confirm previous electrophysiological work indicating that at P3-7 stage $GABA_C$ receptors were diffusely distributed within the spinal network responsible for rhythmic bursting.

An intriguing, observation was the intense motoneuron staining at P1 stage while at P7 stage these two subunits were expressed by interneurons as well as motoneurons. These changes in the mRNA expression pattern were accompanied by developmental changes in ρ proteins. In order to clarify if P1 $GABA_C$ receptors were functional, we performed electrophysiological experiments which showed how P1 motoneurons did possess functional $GABA_C$ receptors sensitive to exogenous GABA but apparently not accessible to synaptically released GABA during DR evoked reflex activity. Since the affinity of $GABA_C$ receptors for GABA is higher than the one of $GABA_A$ receptors (Bormann, 2000), our experiments used concentrations of GABA (50-500 μM) which should have co-activated both receptor classes. However, $GABA_A$-mediated responses were readily suppressed by 20 μM bicuculline, a concentration which completely eliminates $GABA_A$ receptors mediated responses induced by doses of

GABA as high as 1 mM (Bracci *et al.,* 1996b). The bicuculline-resistant GABA response was partly mediated by $GABA_C$ receptors as it was reduced by TPMPA (a $GABA_C$ receptor blocker; Murata *et al.,* 1996; Ragozzino et al., 1996; Chebib *et al.,* 1998) at a concentration apparently devoid of non-selective antagonism on other GABA receptors. The fact that spinal motoneurons required at least 50 μM GABA to generate threshold activation of $GABA_{(A,C)}$ receptors does not imply a low sensitivity of $GABA_C$ receptors to GABA. A more likely explanation would be that uptake and diffusional barriers restricted the access of exogenous GABA to those receptors.

Despite applying relatively high doses of GABA, $GABA_C$ receptors of P1 motoneurons seemed to be responsible for a relatively small component of the overall GABA-induced depolarisation which did not comprise $GABA_B$ receptor activity in view of its resistance to the $GABA_B$ antagonist saclofen and might instead have been contributed by electrogenic transport of GABA (Fykse and Fonnum, 1996). It is possible to hypothesize that at the P1 stage $GABA_C$ receptors could be activated by synaptic GABA released by yet unidentified pathways not accessible to DR projections, or that $GABA_C$ receptors, though functional, had a vestigial role (like $GABA_A$ receptors on dorsal root ganglion cells; Sivilotti and Nistri, 1991), having perhaps contributed to synaptic formation before birth. Notwithstanding the resolution of this question which demands future experiments, the predominant class of GABA receptors seemed to belong to $GABA_A$ category in view of the GABA response sensitivity to low concentrations of bicuculline.

Dendritic localisation of ρ1 and ρ2 mRNAs

A striking feature of the expression pattern of the ρ protein in the adult spinal cord is that dendritic processes and cell somata displayed strongly immunostained puncta similar to those observed in the retina using the same polyclonal antibody (Enz *et al.,* 1996). In their study Enz and co-workers (1996) suggested that this particular arrangement of the protein might correspond to local accumulation at synapses. This notion is of particular interest since we found that in the spinal cord as well as in other brain areas, the mRNAs for ρ1 and ρ2 were also localised to the dendrites, thus suggesting local protein synthesis through mRNA translation in response to neuronal activity (Steward, 1997; Kiebler and DesGrosseillers, 2000).

Another inhibitory receptor, the glycine receptor shows, on adult spinal motoneurons, somatodendritic localisation of its α1 and α2 subunit mRNAs while the β subunit mRNA is restricted to the cell body (Racca *et al.,* 1997). The analogy between $GABA_C$ and glycine receptors is interesting not only because both mRNAs are accumulated in distal dendrites and at dendritic branch points, but also because the corresponding proteins are accumulated in strong immunoreactive puncta distributed on the cell soma or dendrites which, for glycine receptors, have been shown to correspond to synaptic boutons (Kirsch *et al.,* 1996; Racca *et al.,* 1997). Moreover, a preliminary study showed co-expression of glycine and the $GABA_C$ receptors in the spinal cord (Wässle *et al.,* 1998). It would be interesting to find out conditions which might lead to translation of $GABA_C$ receptor mRNAs in a synaptic activity dependent manner since an analogous phenomenon has been thought to occur for glycine receptors (Racca *et al.,* 1997).

Discussion II:

role of the Na^+/K^+ATPase pump

The principal findings of the second part of the present study are:

- functional demonstration of the contribution by the sodium pump to network activity (spontaneous or evoked) when repeated firing is maintained for a few seconds (trains of DR stimuli, bursting activity);
- effectiveness of the pump block induced by strophanthidin and the absence of toxic effects due to long lasting spinal cord exposure to strophanthidin;
- observation and characterization of a new type of spontaneous activity (namely strophanthidin bursting), displayed by the spinal cord network in the absence of fast chloride mediated inhibition and of sodium pump activity.

Effectiveness of Na^+/K^+ ATPase inhibitors

The expression of α1 sodium pump isoforms with low ouabain affinity exclusively by a limited set of motoneurons (Mata *et al.,* 1991; Dolapchieva, 1998) plus the high ouabain affinity of all isoforms expressed by interneurons, suggested that 4 μM strophanthidin should be an effective blocker of the sodium pump. To validate our assumption, we measured the Na^+/K^+ ATPase activity with the standard method based on $^{86}Rb^+$ uptake (Longo *et al.,* 1991). Our preparations displayed a linear increase in the intracellular radioactive tracer accumulation (Bowen, 1992) during the first twelve min of $^{86}Rb^+$ incubation. As shown by Bowen (1992), a high concentration of ouabain severely reduced $^{86}Rb^+$ influx, leaving a small residual influx presumably due to $^{86}Rb^+$ permeation through membrane channels. Note that the IC_{50} value for ouabain of the rat α1 isoform is 50 μM at 37° C (Tao *et al.,* 1996). Our data on the sodium pump block did not disclose any relevant difference among 50 and 200 μM ouabain (20 min preincubation), and 4 μM strophanthidin (30 and 60 min preincubation). These responses therefore confirmed complete block of the electrogenic sodium pump in the spinal cord induced by strophanthidin or ouabain. This conclusion was important for our long-

lasting electrophysiological experiments because the electrogenic pump was fully inhibited after 30 min of 4 μM strophanthidin incubation, when the disinhibited rhythm was completely disorganised, as well as after 60 min when a new spontaneous activity pattern appeared.
Note that all our experiments were carried out at room temperature (about 22° C) because at higher temperature the increase in tissue metabolism (and O_2 demand) caused anoxia to the en bloc spinal cord (see also review by Kerkut and Bagust, 1995).
The consistently similar values of residual $^{86}Rb^+$ accumulation (normalised with respect to proteins content) and the reproducible linearity of this process suggest absence of cellular damage to the spinal cord induced by pump block. Moreover, the maintenance of stable spontaneous activity for many hours (more than 12) in the presence of strophanthidin, suggests that no gradual toxicity was building up within the spinal network after pump block. In a study on spinal axons Li and Stys (2001) observed cellular damage after sustained Na^+ pump block. However, in that report the pump inhibitor ouabain was administered in a high K^+ solution, a protocol that augmented tissue depolarization and maximize cell damage. These conditions were absent in our experiments.

Effects of strophanthidin on spinal reflexes

As previously described (Ballerini *et al.,* 1997), strophanthidin application *per se* did not induce any spontaneous activity in the spinal cord, only a modest VR depolarization, due to loss of the hyperpolarizing background pump current (Shen and Johnson, 1998; Li and Stys, 2001). The insignificant effects of the pump activity block on fibres impulse conduction, on reflex threshold values and on spinal reflexes evoked at low stimulus rate suggest that the role of the pump on synaptic transmission in the absence of intense spiking activity (at room temperature) was quite small. Under these conditions, ionic fluxes through neuronal membranes via resting conductances and/or occasional firing, were presumably relatively small so that other cellular mechanisms prevented relevant alterations in ionic gradients (Willis *et al.,* 1974).
To ascertain how sodium pump block might affect repetitive discharges in control solution, we applied trains of stimuli inducing strong depolarization and repetitive firing presumably associated with major influx of Na^+ and efflux of K^+, thus speeding up the pump rate or the other compensatory mechanisms (Fujioka *et al.,* 1998). In our experiments (3-60 pulses, 0.1-1.0 ms duration, 1.0-0.33 Hz, 2-10 xTh), electrogenic pump block induced significant variation in spinal cord evoked responses, namely a severe decrease in cumulative

depolarization amplitude, which grew monotonically at slow rate, and an increase in half decay time.

The decrease in amplitude of cumulative depolarization was also observed during application of depolarizing agents. For example, the excitatory agent NMDA mimicked the baseline depolarization induced by strophanthidin *per se* and also the reduction in cumulative depolarization evoked by stimulus trains. Thus, the amplitude decrease was due to network and motoneuron depolarization presumably consequent to a number of factors which included reduced driving force for excitatory synaptic responses and partial inactivation of spike mechanisms.

However, the effects of strophanthidin on responses summation and on depolarization recovery were not repeated by NMDA application, and appeared to be selectively caused by block of the electrogenic pump. Intracellular Na^+ accumulation during repetitive firing speeds up electrogenic pump activity and its hyperpolarizing current (Shen and Johnson, 1998), a process that might have slowed down the rate of growth of cumulative depolarization and, consequently, input summation. It seems likely that fast and long lasting linear summation of responses is normally prevented by the sodium pump to protect cells from excessive depolarization (Willis *et al.,* 1974; Davidoff and Hackman, 1980).

Once the train of stimuli in strophanthidin solution terminated, the decay time of VR polarization to baseline was largely increased. This effect showed the role of the sodium pump activity in the recovery phase after sustained depolarization: for several seconds the pump activity seemingly remained high in order to re-establish resting ionic gradients as observed with brain neurons (Thompson and Prince, 1986; Shen and Johnson, 1998).

It may be concluded that Na^+/K^+ ATPase activity normally limited network signal summation velocity, and speeded up recovery from persistent excitation. Thus, after the electrogenic pump block the network was partly depolarized at resting condition and lacked a braking mechanism during high frequency firing pattern from which it recovered slowly.

Long term strophanthidin application unmasked late bursting: comparison with disinhibited rhythm

The pattern of many spontaneous rhythms (Feller, 1999), and, in particular, of the neonatal rat spinal cord disinhibited rhythm, consists of bursting activity with high frequency firing maintained for several seconds (Bracci *et al.,* 1996a). Since such a condition seems likely to rely intensely on sodium pump activity, it should be disrupted by pharmacological pump

blockers.

The disinhibited rhythm (Bracci *et al.,* 1996a,b; Ballerini *et al.,* 1997) is, of course, unphysiological for the neonatal rat spinal cord, because it appears after blocking GABA and glycine mediated inhibition which develops during late embryonic life (at E18.5 and E20.5 respectively) to allow alternation between motoneuron pools (Nishimaru and Kudo, 2000). However, blocking fast, chloride-mediated inhibition largely simplifies the rhythmogenic network and enables preliminary studies of the processes which allow an excitatory network (with normal architecture) to develop and organize rhythmicity. This virtually purely excitatory network displays, like other spinal preparations without inhibition (see Sernagor *et al.,* 1995), a stable, robust, regular and organized rhythm made up of bursts of activity (Bracci *et al.,* 1996a,b). Disinhibited bursts comprise a rapid depolarization followed by a short plateau phase after which large, rhythmic oscillations develop (Bracci *et al.,* 1996a). While investigating the mechanisms responsible for rhythmicity, Ballerini *et al.* (1997) reported that the strophanthidin application during disinhibited rhythms induces VR baseline depolarization and increases network excitability, causing a very early, transient rhythm acceleration followed by pattern disruption.

In the present study one unexpected evolution of disinhibited activity, after about one hour of strophanthidin application, was the emergence of very slow, spontaneous bursting. This new pattern was defined "strophanthidin bursting" although no spontaneous activity was observed in the presence of strophanthidin alone during many hours (3-4 h) of application of this pump blocker. Strophanthidin bursting was generated only during sustained coapplication of strychnine, bicuculline and strophanthidin (1, 20 and 4 μM, respectively, to block glycine receptors, $GABA_A$ receptors and Na^+/K^+ ATPase) and it continued as long as drug coapplication was maintained. The new spontaneous activity was not regular (inter-burst interval and burst duration CV values were 50-70%). This is the reason why this pattern was designated bursting rather than rhythm.

When strophanthidin bursting was compared with disinhibited rhythm, it showed duration and inter-burst interval values one order of magnitude larger while both spontaneous activities were synchronous in all lumbar VRs. The strophanthidin bursts were characterised by a wave of depolarization (that remained above a pre-set noise threshold between 5 s and several min and did not evolve into a long plateau) and with superimposed slow oscillations that started at the onset of the event, increased their frequency and then decreased it during the decay phase. Within each oscillatory wave, high frequency firing was detected (from VRs) during the rising phase and peak of each oscillation. Because Na^+ channels of rat motoneurons have time

constants for recovery from inactivation (Lape and Nistri, 2001) faster than the oscillation period, it seems unlikely that the disappearance of firing during the descending phase of each oscillation was caused by temporary spike inactivation. It seems more likely that motoneurons were firing in response to rhythmic network inputs, a condition typical of a CPG.

The chick embryo spinal cord generates oscillatory episodes with a continuum of frequency decrease during each episode (O'Donovan, 1989; Tabak *et al.,* 2000). Likewise, the bursts of the disinhibited rhythm recorded from rat spinal motoneurons (Bracci *et al.,* 1996a) or interneurons (Ballerini and Galante 1998; Tscherter *et al.,* 2001) have an oscillatory structure with frequency decrease during each episode. On the other hand, the disinhibited rhythm induced in dissociated cultures of rat spinal cord does not usually show oscillatory activity within the burst (Streit *et al.,* 2001), suggesting the fundamental role of the network architecture for this aspect of pattern generation.

A further difference between strophanthidin bursting and disinhibited rhythm was the smaller amplitude of the former presumably due to the background depolarization which strophanthidin induced. Despite its decreased peak, bursts did not gradually decline over several hours of continuous recording. The stability of strophanthidin bursting suggests absence of metabolic disturbance to cells during sustained Na^+/K^+ pump inhibition.

One surprising feature of strophanthidin bursting was the time lag (almost 1 h) required to express it despite the fact that this drug, in a few min, depolarized VRs, accelerated disinhibited rhythm and rapidly replaced it with asynchronous, brief discharges of irregular nature. This observation indicates that drug access to the network was rapid and effective (Ballerini *et al.,* 1997) and pump block complete (see our previous biochemical data). It is also interesting that there was a gradual transition from the disinhibited bursting mode to the strophanthidin mode with the intermediate stage of rapid discharges replacing the slow rhythm observed in strychnine and bicuculline. Once strophanthidin bursting was fully generated, we never detected the previous fast discharges in between bursts or contaminating a single burst episode. This observation suggests that the same neuronal network which generated disinhibited bursting was converted into strophanthidin bursting mode. While the identification and distribution of network elements remain a goal for future studies, it seems clear that the extent of network activity remained large as indicated by the large size and duration of bursts. Recent work on spinal interneurons has indicated a surprising "degree of flexibility of spinal interneuronal networks" and their "multifunctional character in mammals" (Jankowska, 2001). In the light of these considerations, it seems possible that the similar, comprehensive network of interneurons was responsible for either the disinhibited rhythm or

the strophanthidin bursting. Since disinhibited rhythms and fictive locomotion are likely to be generated by the same spinal network (Beato and Nistri, 1999; Ballerini et al., 1999; Tscherter et al., 2001), it seems plausible that strophanthidin bursting was an extreme mode of operation of the same network which had resumed its original characteristics of irregularity and synchronicity observed in embryonic life (Nishimaru and Kudo 2000).

Strophanthidin bursting: potential mechanisms underlying its delayed onset and its maintenance

What were the reasons for the late emergence of strophanthidin bursting? While the sodium transporter protein responds with increased expression to sustained, high intracellular sodium within a few minutes (Senatorov *et al.,* 2000), this could not account for our findings in view of the continuous presence of the pump blocker. However, the spinal network might have compensated for the absence of sodium pump activity by expressing other transporters, through a process with a delay longer than a few minutes. Only when compensatory mechanisms had reached a certain level of expression, network bursting could emerge. Future studies should aim at clarifying the identity of compensatory processes that enabled the spinal network to resume bursting. This is an interesting goal as it may shed light on the mechanisms which allow a network to recover from disruption of its rhythmicity. During this phase "prodromic" to strophanthidin bursting, lack of electrical silence suggests that the network was not fully inactivated by sustained depolarization.

The regular operation of the sodium pump is a major user of cellular ATP (Glynn, 1993). In brainstem respiratory nuclei the relation between sodium pump activity and intracellular ATP determines the degree of block of K_{ATP} channels (Haller *et al.,* 2001). Such channels have the important inhibitory function to terminate burst episodes, thus linking the metabolic condition of neurons to their intrinsic rhythmogenic properties. If we were to apply an analogous scheme to the rat spinal cord network, the present experiments might then indicate that full and persistent block of the sodium pump should have strongly reduced demands on intracellular ATP and should have ensured sustained block of K_{ATP} channels. This situation might partly explain why strophanthidin bursts were so long. Future work with selective antagonists of K_{ATP} channels should help to resolve this issue.

Despite full block of the sodium pump, spinal neurons must have pumped out their excessive Na^+ load to preserve their excitability. A possible candidate for the mechanism of Na^+ extrusion would be the electrogenic Na^+/Ca^{2+} exchanger (Fujioka *et al.,* 1998). It is useful to consider that operation of this process should lead to intracellular rise in Ca^{2+} and facilitation

of neurotransmitter release, a phenomenon elegantly demonstrated in model cells like chromaffin cells (Tang *et al.,* 2000). If a similar process occurred in the rat spinal cord, it should have stimulated glutamate release from network interneurons and contributed to burst generation. Our experiments have, in fact, demonstrated (with the use of glutamate receptor antagonists) that this endogenous amino acid was essential for strophanthidin bursting. Within this framework, an additional source of glutamate release might have been the reverse operation of the glutamate membrane carrier as it is known to take place when the sodium pump is inhibited (Li and Stys, 2001). It is tempting to speculate that the combination of mechanisms designed to re-establish ionic gradients would also enhance excitatory transmitter release and prompt the onset of bursting.

General properties of strophanthidin bursting

To study distribution and correlation of burst parameters, we recorded from two preparations for about 12 h of continuous strophanthidin bursting without any further experimental interference (no stimuli or other substances were applied during those experiments). We then measured the interburst interval, duration, pause, time to plateau, recovery time, and amplitude for 107 and 166 consecutive events and calculated their statistical values.

We observed high correlation between amplitude and duration (or between amplitude and recovery time; $r = 0.9$) for each event. The very strong correlation ($r > 0.95$) of burst duration with recovery time, interburst interval and pause, was simply due to the fact that one of the two parameters was the main component of the other (interburst interval comprised pause, and duration included recovery time).

The high correlation observed between preceding pause and duration (or preceding pause and amplitude; $r = 0.8$) was one of the main features of the present analysis: we interpreted it as due to dependence of network activity (expressed as burst size) on the preceding silent period. In fact, it is likely that, during the pause, the interneuron population gradually recovered the efficiency of their synaptic connections and their firing ability in preparation to generate the next event. The second main result was the absence of correlation ($r < 0.3$) between burst duration and pause after each event (or between amplitude and pause). It seems possible that, once generated, bursts terminated in view of some intrinsic mechanisms which turned off network activity without influencing subsequent responses (Tabak *et al.,* 2000).

The high correlations between preceding pause and burst size (amplitude and duration) were observed in cultured spinal cord slices (Tscherter *et al.,* 2001) and dissociated spinal neurons (Streit *et al.,* 2001). In chick embryo spinal cord a similar phenomenon suggested to

O'Donovan and Chub (1997; see also O'Donovan, 1999) that the occurrence of an episode should be a population phenomenon controlled by activity-dependent network depression, a notion incorporated in their descriptive model (Tabak *et al.,* 2000). Likewise, depression was attributed to synaptic fatigue, due to depletion of presynaptic transmitters store, also in the case of rat spinal cord preparations (Lev-Tov and Pinco 1992; Streit, 1993). Because strophanthidin bursting shared these properties, it seems plausible that synaptic fatigue played a role in terminating a burst. Note, however, that theory could not be readily applied to explain the disinhibited rhythm because it did not show any correlation between preceding pause and burst duration and bursts could be promptly elicited by electrical pulses.

Burst onset and termination

The burst onset and termination during the activity of the locomotor network of the lamprey has been attributed to the interplay between synaptic mechanisms and intrinsic conductances (Grillner *et al.,* 2001). In this case synaptic inhibition would hyperpolarize CPG neurons during the pause between bursts (and reactivate any depolarization-inactivated channels). Bursts would develop for the combined action of excitatory synaptic inputs and background excitation, would grow due to activation of Na^+ and Ca^{2+} channels and terminate for the hyperpolarizing action of Ca^{2+} dependent K^+ channels. Somewhat analogous, though not identical, considerations have been applied to the tadpole (Dale, 1995) and rat (Kiehn *et al.,* 2000) spinal cord. Conversely, the spontaneous rhythmic bursts of the chick embryo spinal cord are thought to originate from network-driven motoneurons which activate Renshaw cells which, in turn, depolarize a large number of spinal neurons owing to the excitatory nature of GABA and glycine-mediated transmission at this early stage of development (Wenner and O'Donovan, 2001).

Multi-site recordings from rat organotypic slice preparations during disinhibited bursting (Tscherter *et al.,* 2001) have suggested that bursting starts at a certain site when there is a critical number of intrinsically active neurons (usually in the ventral area) with efficient synaptic connections, and that bursting does not require pacemaker cells as it simply depends on network excitability. A wave of excitation then spreads rapidly, via recurrent excitation, to engulf virtually all cells in the ventral and central areas (dorsal horn neurons are much less involved in this phenomenon). During the pause between bursts, network activity becomes low and has minimal spatial propagation.

Our recording conditions did not allow us to identify the relative contribution of certain membrane or cellular mechanisms to burst initiation for strophanthidin or disinhibited

bursting. However, we can exclude some and consider others probable. With strychnine and bicuculline in the bathing solution, all main components of synaptic inhibition were blocked (Bracci *et al.,* 1996b and present data on $GABA_C$ receptors), ruling out a major role of synaptic inhibition during the burst pause. Furthermore, in the neonatal rat spinal cord Renshaw cell activity is inhibitory, not excitatory (Marchetti *et al.,* 2001). In our experimental conditions burst onset was therefore likely to be start due to synchronous firing of a certain number of spontaneously active cells which recruited most other neurons via recurrent excitation. This phenomenon might have occurred periodically and regularly during disinhibited bursting because the sodium pump operation routinely restored neuronal excitability after each burst. During strophanthidin bursting, network neurons were presumably more depolarized, even during the silent pause, and might have fired more irregularly, thus generating irregular bursting. This prediction will require direct testing with experiments based on multi-site recording during strophanthidin bursting.

Once the rapid depolarization of each burst developed, burst duration was strongly limited by the sodium pump whenever this process was fully efficient. In the presence of strophanthidin, however, bursting episodes were typically very long presumably because other factors became responsible for burst prolongation and its eventual termination. Thus, persistent excitation might have resulted from facilitated glutamate release and sustained block of K_{ATP} channels, as previously discussed. However, against a background of network excitation it is likely that synaptic fatigue appeared as indicated by the correlation between preceding pause and burst size as well as the results with electrical stimulation. The contribution by Ca^{2+} dependent K^+ channels to strophanthidin bursting is unknown although they play a minimal role in disinhibited bursting (Ballerini *et al.,* 1997). In our model (see Appendix) simulated bursting was produced with the use of only four variables, namely the network activity, the fraction of network neurons not affected by fatigue, the fraction of synapses unaffected by fatigue and the fraction of neurons inhibited as a consequence of Na^+ pump activity. The good correspondence between simulated and observed bursts suggests that these variables represented important constraints for bursting and supports our mechanicistic hypothesis. Furthermore, the model closely replicated intraburst oscillations although we still ignore the mechanisms underlying these waveforms.

Pharmacology of strophanthidin bursting

Since application of TTX completely inhibited this form of activity, either spontaneous or evoked by DR stimuli, it appears that strophanthidin bursting was generated by the

interneuronal network and recorded via motoneuron pools.

Although interneuronal activity transmitted to motoneurons is usually thought to require spike firing, it has been recently suggested that a stable motoneuron rhythm could originate from synchronized oscillations of motoneurons coupled via gap junctions (Tresch and Kiehn, 2000). To evaluate the gap junction contribution to the present experiments, we applied the gap junction blocker carbenexolone that did not apparently modify bursting, showing a minimal role for this communication process under the present conditions.

Although strophanthidin bursting was a robust activity, continuously recorded for more than 12 h without impairment, it was very readily disrupted by glutamate receptors blockers (CNQX or D-APV) or excitatory agents (5-HT or NMDA or high K^+).

Excitatory transmission in the spinal cord is mainly mediated by glutamate through NMDA and non-NMDA receptors (Headley and Grillner, 1990), seemingly colocalized at the same postsynaptic sites (Kullmann, 1994). During disinhibited activity, non-NMDA receptors are believed to be sufficient to drive the rhythm despite NMDA receptor block (Bracci *et al.*, 1996a), a finding which indicates the predominant role of AMPA/kainate receptors. During strophanthidin bursting, activation of both glutamate receptor classes was instead necessary as demonstrated by experiments with receptor antagonists, suggesting less efficient connectivity within the network in these experimental conditions.

In the neonatal rat spinal cord, high K^+, NMDA or 5-HT are well known excitatory agents to induce (alone or in combination) fictive locomotion (Cazalets *et al.*, 1992; Kjaerulff and Kiehn, 1996; Bracci *et al.*, 1998). These excitatory agents also decrease interburst interval and burst duration during disinhibited rhythm (Bracci *et al.*, 1996a,b; Bracci *et al.*, 1998).

During strophanthidin bursting, the same excitatory agents (NMDA, 5-HT or high K^+), at a concentration sufficient to induce detectable VR depolarization, evoked a single large burst followed by a silent, stable plateau phase. Drug washout induced a slow repolarization and subsequent recovery of spontaneous activity.

In conclusion, although intact glutamatergic transmission was necessary for strophanthidin bursting, this recurrent excitatory activity appeared in a borderline-functional state because increasing background activity induced a stable plateau depolarization.

Effects of DR stimulation during strophanthidin bursting or disinhibited rhythm

The stimulus threshold for observing VR responses was apparently unmodified by strychnine and bicuculline coapplication as demonstrated by the fact that a single 1xTh pulse induced a minimal response in control or a stereotypic burst when applied during the silent period of the

disinhibited rhythm (see also Bracci *et al.,* 1997). The same pulse given during the silent period of strophanthidin bursting induced a burst, the amplitude of which was also unrelated to stimulus intensity.

Like the responses during disinhibited rhythm (Bracci *et al.,* 1997), in strophanthidin bursting the burst latency after a DR stimulus was progressively reduced by increasing the stimulus intensity, without any consistent effects on burst duration or amplitude. However, an unexpected observation was the increase in intraburst oscillation frequency induced by increasing stimulus intensity. Presumably the stronger stimulus activated a larger number of afferent fibres which released a proportionally larger amount of excitatory transmitter to recruit more rapidly network elements which then oscillated at higher rate. The transient nature of this excitation probably allowed the network to recover spontaneously, unlike the observation with bath-applied excitatory agents. It is likely that more widespread, synchronous and synaptically efficient activation of the network by electrical stimuli accounted for the larger amplitude of evoked versus spontaneous bursts. During strophanthidin bursting, each electrically-induced burst was positively correlated in size with the preceding pause. Thus, the same mechanisms responsible to control spontaneous burst amplitude and duration operated also for DR-elicited bursts.

When we applied trains of stimuli at various frequencies, entrainment of strophanthidin bursts was difficult and limited to the low frequency range. In this sense, there were two opposing factors: at low frequencies (for example ≥1/45 s) spontaneous bursts occasionally re-emerged, while with faster frequencies there was a sustained baseline depolarization influencing individual burst duration. These observations with single or repeated strophanthidin bursts suggest that slowly incrementing synaptic fatigue was an important factor to terminate bursts. This suggestion has been put forward before to explain strychnine-induced bursts in organotypic cultures (Streit, 1993) or the spontaneous activity of the chick embryo spinal cord (Tabak *et al.,* 2000). In contrast, disinhibited rhythm can be entrained to frequencies near 1/5 s (Bracci *et al.,* 1997), suggesting that, in this case, synaptic fatigue was a much less prominent phenomenon.

We employed electrically-evoked bursts as tools to explore network excitability and fatigue onset further. In particular, when a single pulse was applied at the end of a strophanthidin burst, the evoked burst was short. When the same protocol was applied during disinhibited rhythm, the evoked burst was marginally shorter than the preceding spontaneous response (same depolarization area in both cases) and manifested a series of oscillations. However, when successive electrical pulses were applied, evoked bursts became smaller. This was not

just the result of network entrainment as the last burst was shorter than the immediately preceding one. We interpret this result as due to manifestation of synaptic fatigue which became an important factor only when the disinhibited network was repeatedly stimulated at close interval.

In conclusion, fatigue was not a major contributor to the termination of one disinhibited burst whereas it was a prominent feature in the case of a strophanthidin one. This notion was applied to our model in which two distinct forms of bursting were simulated on the basis of sodium pump activity or synaptic fatigue. Modelling (see Appendix) confirmed that assuming such an important difference between the two bursting activities generated distinct bursting patterns resembling either the disinhibited one or the strophanthidin one.

Appendix:

Network modelling

We assumed that the same network (made up by excitatory connections only because of pharmacological block of fast synaptic inhibition) was responsible for either type of bursting activity ("disinhibited" or "strophanthidin"). In fact, it seems advantageous to seek a unitary theory to account for both bursting modes intended as state variations taking place within the same network.

In order to be considered useful to simulate disinhibited as well as strophanthidin bursting, our model should produce highly oscillatory bursts with distinctive properties depending on the different pharmacological treatment and should also be able to generate characteristic bursts when the network excitability is suddenly raised to mimick afferent fibre stimulation. The large difference in intraburst frequency between strophanthidin and disinhibited bursts (Table 6) was mathematically accounted for by a change in the temporal characteristics of the network system, although identification of underlying cellular processes will need future experimental work. Additionally, we considered that duration of simulated bursts had to be related to the preceding silent interval as observed experimentally (Fig. 33; Tscherter *et al.,* 2001). Furthermore, we supposed that slow neuronal depression (perhaps due to gradual build-up of synaptic fatigue; Tabak *et al.,* 2000) was contributing to the end of a single strophanthidin burst rather than of a single disinhibited burst (see experiments with electrical DR stimuli; Fig. 36-39). Indeed, after each spontaneous disinhibited burst one state

characteristic of the network was its rapid recovery of excitability which we propose to be due to the Na^+ pump operation.

As a starting point we applied the model derived from bursting of the chick embryo spinal cord (Tabak *et al.,* 2000) to our data. However, unless an extra variable was added, that model was unable to simulate disinhibited rhythms because it represented a topological difference. Our own model relied on two ordinary differential equations to display various dynamic network behaviours.

The system is represented by equations I and II:

$$\tau_a \dot{a} = \alpha(n \cdot (1-s) \cdot d \cdot a) - a = \frac{1}{\left(1 + e^{\frac{-(n \cdot (1-s) \cdot d \cdot a - \vartheta)}{k_a}}\right)} - a \qquad \text{eq. I}$$

$$\tau_d \dot{d} = \delta(a) - d = \frac{1}{\left(1 + e^{\frac{(\alpha - \vartheta_d)}{k_d}}\right)} - d \qquad \text{eq. II}$$

Simulation: according to Tabak et al (2000), the model equations were implemented within XPPAUT (freely available software by G. B. Ermentrout, http://www.pitt.edu/~phase/), a general purpose interactive package for numerically solving and analyzing differential equations. XPPAUT includes a tool for calculation of bifurcation diagrams (AUTO). Simulations were performed using the Runge-Kutta integration method with a time step of 0.1 (dimensionless units). We checked that the results were unchanged when the time step was 0.01. Simulations were run on Linux PC.

The three state diagrams of Fig. 41 represent the average network activity (see similar representation by Tabak *et al.,* 2000) and were constructed with the following parameters on the assumption that there was a sigmoidal function relating network activity to network input (cfr. Wilson and Cowan, 1972; Tabak *et al.,* 2000): a, an index of network activity such as the fraction of neurons firing at a given time; d is the fraction of network neurons not affected by slow depression; τ_a and τ_d are their time constants; n is the fraction of synapses unaffected by slow depression; s is the fraction of neurons inhibited as a consequence of Na^+ pump activity; ϑ is the neuronal firing threshold (presumed to be constant) while k_a is the sigmoid function

slope. When applied to d, threshold and slope become ϑ_d and K_d.

The average neuronal activity expressed as a (at time t) generated a series of signals returning to the same cells as $n \cdot d \cdot a$, i.e. their neuronal input inclusive of some activity-dependent loss of synaptic activity. The number of firing cells then became $(1\text{-}s) \cdot n \cdot d \cdot a$. The value $n(1\text{-}s)$ represented the overall number of synapses and neurons available for network activity. The variables d, n and s could be described by sigmoidal functions (Tabak *et al.*, 2000).

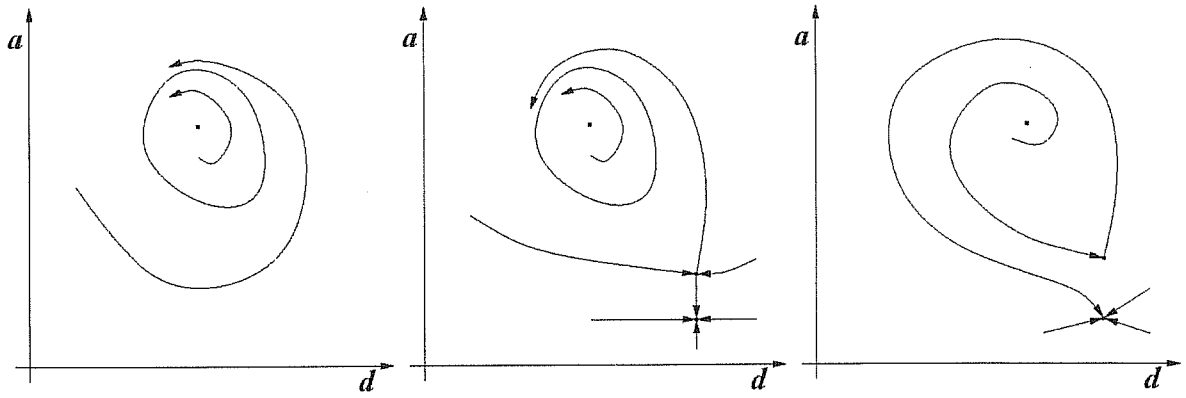

Fig. 40 The three state diagrams represent the average network activity.

The value $n(1\text{-}s)$, that represents the overall number of active elements in the network (available synapses and neurons), decreases from left to right, namely, from a stable oscillatory phase (left panel, high value) to bistability phase (middle) to silent period between bursts (right, low value).

If the system relied on a and d only, the solution depended on the value of the following parameters: τ_a, τ_d, $n(1\text{-}s)$, ϑ, ϑ_d, k_a, k_d. By plotting a versus d, we can show three basic network states when $n(1\text{-}s)$ decreased from left to right in Fig. 41.

In particular, in the left panel of Fig. 41, $n(1\text{-}s)$ was sufficiently large so that the system displayed a stable cycle, as indeed it should occur during a burst when the system follows the frequency of intraburst oscillations. The middle panel shows that, when $n(1\text{-}s)$ was getting smaller, there was a region of bistability in which the system could either continue oscillating or switch off. In the latter case it was possible to evoke a burst when the system was turned off as the stimulus made the network to return to the excited state. The right panel shows that, when $n(1\text{-}s)$ was very small, there was only one stable state corresponding to the pause observed between bursts. The system, therefore, shifted amongst these three states during both disinhibited and strophanthidin bursting, although the speed of transition in the case of strophanthidin bursting was considerably slower. The transition between the three states could

be described with differential equations for n and s, although for strophanthidin bursting the value of s became minimal.

It is worth noting that the Na^+ pump dynamics implied a time lag before pump activity could actually inhibit network discharges. If there was modest neuronal activity, there was only a small delay before the pump could repolarize neurons and regenerate their excitability. If there was intense neuronal firing, longer pump operation was necessary to reset the system to its ground state. In this framework we may therefore predict two distinct cases: disinhibited bursting with burst termination due to s, and strophanthidin bursting with burst termination due to n.

The equation describing n is eq. III:

$$\tau_n \frac{dn}{dt} = \frac{1}{\left(1 + e^{\frac{a-\vartheta_n}{k_n}}\right) - n} \qquad \text{eq. III}$$

While the equation for s is eq. IV:

$$\tau_s(a)\frac{ds}{dt} = \frac{m_s}{\left(1 + e^{\frac{-(a-\vartheta_s)}{k_s}}\right) - s} \qquad \text{eq. IV}$$

Note that m_s expresses the interneuron fraction reactivated (during the time unit) by membrane hyperpolarization due to maximal electrogenic ion transport (primarily Na^+ pump activity). The value of m_s was fixed at 1 for disinhibited bursting, and at 0.1 for strophanthidin bursting (we avoided setting it to zero because additional transport mechanisms might have partly compensated for lack of Na^+ pump activity).

The value $\tau_s(a)$ is given by eq. V:

$$\tau_s(a) = \frac{\tau_t}{\left(1 + e^{\frac{(\vartheta_t - a)}{k_t}}\right)} \qquad \text{eq. V}$$

The parameter $\tau_s(a)$, representing the time constant for the process to obtain s, is therefore crucial to explain the mechanism underlying the end of one disinhibited burst.

Fig. 41A, B, C compares the temporal changes in a, n and s values simulated during disinhibited (left) or strophanthidin (right) bursting while Table 10 shows the values assigned to the variables used for burst simulations.

Inspection of Fig. 41A-C (left column) indicates that in the case of disinhibited bursting, when a was elevated (during the oscillatory phase of a disinhibited burst), the value of $\tau_s(a)$ was large so that the peak value of s (i.e. inhibition of a substantial fraction of neurons) was rather slowly reached. When s reached a value critical to suppress bursting (corresponding to the large value of m_s, not shown), a became quite small and the burst terminated. Fig. 42 A reveals that the present model could generate spontaneous regular discharges similar to recorded disinhibited bursts, although simulated bursts lacked the short plateau phase with elevated firing just before the oscillatory phase. Fig. 42 B shows that, at the end of a spontaneous disinhibited burst, a single electrical stimulus (simulated to mimick the experimental protocol shown in Fig. 39 A) elicited a burst shorter but otherwise similar to the previous one (as observed experimentally in Fig. 39 A) because at this time point the value of $\tau_s(a)$ had become sufficiently small (see Fig. 41C). However, a further stimulus (see Fig. 42 B) induced an even shorter burst (compare it with experimental data in Fig. 39 B). The reason for the ability of the network to produce bursts with repeated stimuli lies in the relatively small and slow variation in n value during a single disinhibited burst (Fig. 41B, left). With closely repeated bursts induced by electrical pulses, n (despite its slow change) could reach a value significant to reduce network activity (see Fig. 39 for experimental data and Fig. 42 B for simulated ones).

In the case of strophanthidin bursting (Fig. 41A-C, right column; note time scale slower than in left column), m_s was small (0.1) because of Na^+ pump inhibition. Thus, the variable responsible for burst termination became n (Fig. 41B, right), as the number of active synapses fell below a certain value. The slow recovery of n influenced the time necessary to reset the network for subsequent bursting and presumably played a role in the observed correlation between pause and burst size (see Fig. 33). Note also that simulated data for strophanthidin bursting (Fig. 41C) show that stimulation shortly after the burst end could evoke a small burst only. In practice, the end of one strophanthidin burst was apparently determined by the number of excitatory synapses remaining active. Note that the present model cannot simulate

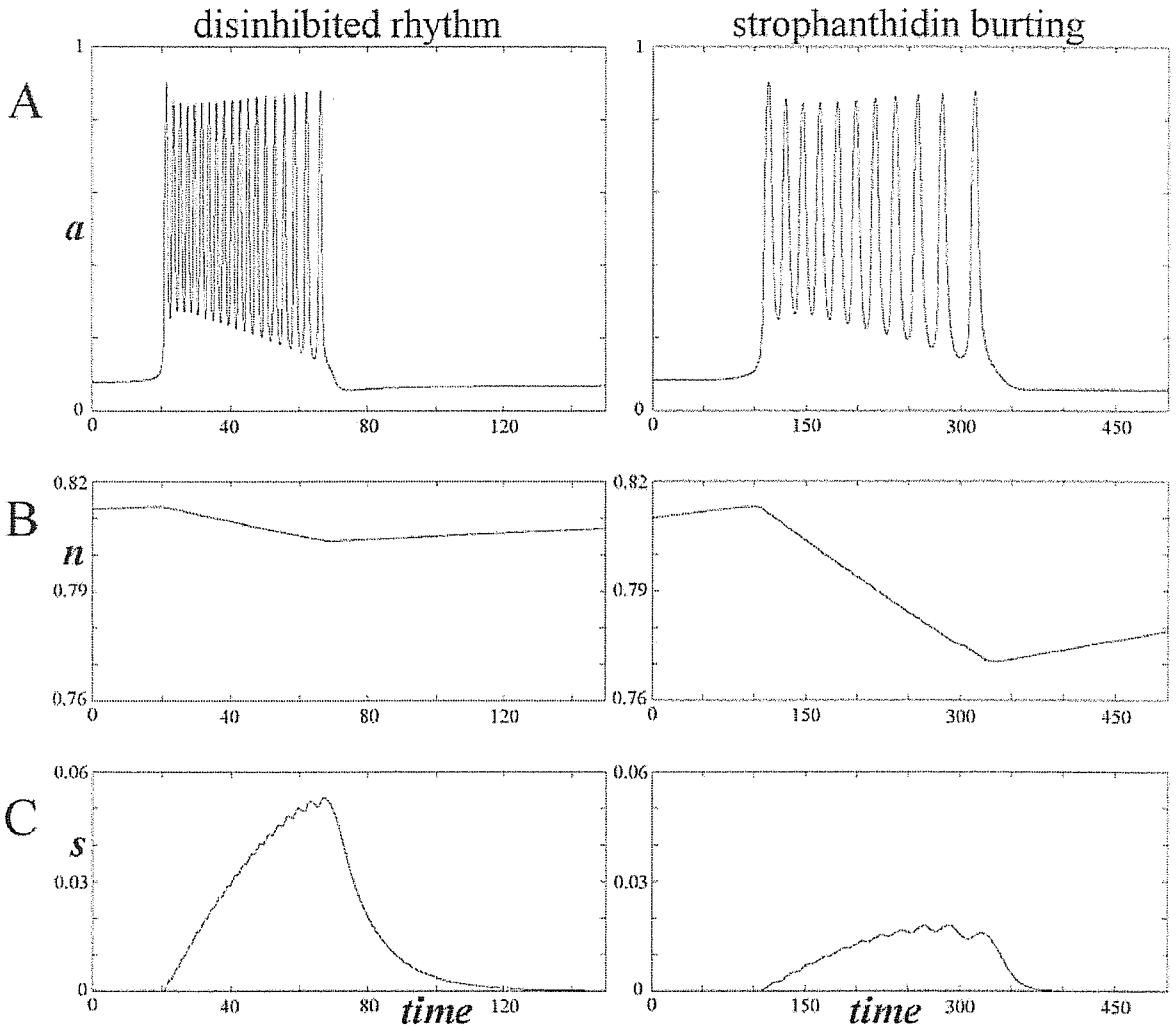

Fig. 41 Comparison between disinhibited (left graphs) and strophanthidin (right graphs) bursts generated by our network modelling.

a, is an index of network activity, ***n*** is the fraction of synapses unaffected by slow depression; ***s*** is the fraction of neurons inhibited as a consequence of Na^+ pump activity.

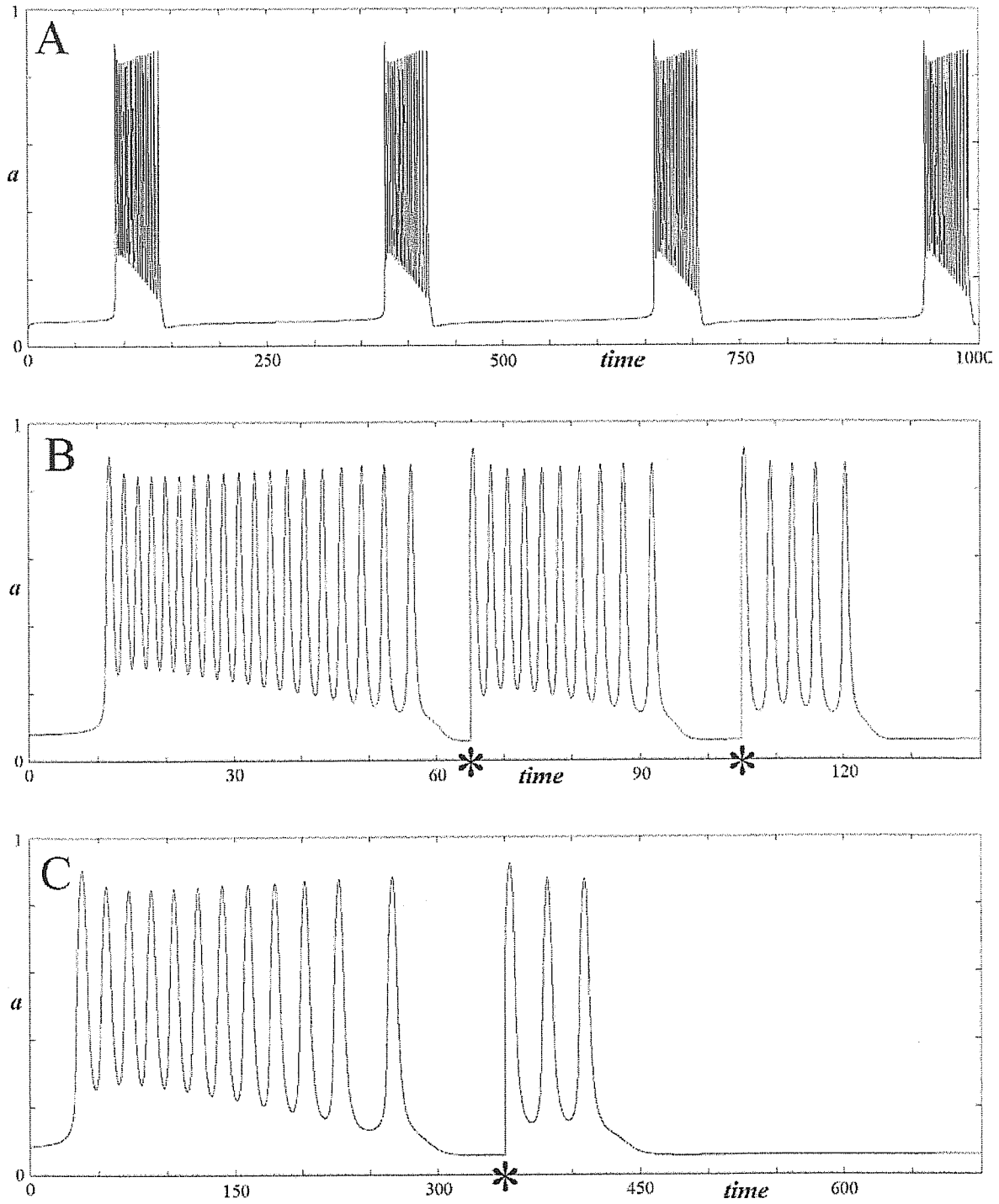

Fig. 42 Comparison between responses induced by DR stimuli (stars) applied during disinhibited (B) or strophanthidin (C) bursts generated by our network modelling. A represents a series of regular, disinhibited bursts. ***a***, is an index of network activity; time units (abscissa) are arbitrary. DR stimulation is simulated by suddenly moving ***a*** to 0.6.

the irregularity of strophanthidin bursting because it was based on a system of ordinary differential equations which, by definition, is deterministic. It is possible to add a stochastic variable to this model to describe the high variability of strophanthidin bursting. Nevertheless, as this approach would simply bring a further variable into the model and would not improve its ability to describe burst evolution and termination, it was not further pursued.

Finally, it should be considered that the network output was measured via motoneuron discharges (via VRs) and thus our readout was an indirect index of the interneuronal activity responsible for bursting (Bracci *et al.,* 1996a; present data with glutamate receptor blockers or TTX). This condition inevitably distorts the real behaviour of interneurons, but it has the experimental advantage of showing the integrative properties of the network at its final output stage and of demonstrating the signal sent to peripheral targets. Simulated behaviour depicted in Figs. 41 A and 42 reflects interneuronal activity (not their average membrane potential changes which remain unknown even experimentally) which may not be identical in time course to the changes in VR polarization level integrating the average membrane potential of motoneurons and their axons.

Table 10 Constant values used for burst simulations

	disinhibited bursting	**strophanthidin bursting**
τ_a	0.25	2
ϑ	0.18	0.18
k_a	0.05	0.05
τ_d	0.5	4
ϑ_d	0.5	0.5
k_d	0.2	0.2
ϑ_s	0.3	0.3
k_s	0.01	0.01
m_s	1	0.1
τ_n	4000	4000
ϑ_n	0.14	0.14
k_n	0.02	0.02
τ_t	500	500
ϑ_t	0.25	0.25
k_t	0.05	0.05

All values are dimensionless.

Conclusions

In this purely excitatory network we have identified and described the contribution by transmitter receptors and membrane transporter to the genesis of network rhythmicity. On the one hand we have demonstrated that when $GABA_A$ and glycine receptors are blocked the role of $GABA_C$ receptor in controller bursting is comparatively small, while the $GABA_B$ one is nil.

Since in the neonatal spinal cord $GABA_C$ receptors were found to be present and developmentally regulated, it seems likely that $GABA_C$ receptors were predominantly extrasynaptic and played a role in the network development rather than in network transmission. The role of the sodium pump appeared to be fundamental in controlling the duration and regularity of bursting.
However, after sustained block of the sodium pump, a novel type of bursting appeared, characterized by long episodes at irregular frequency.

Our theoretical model proposed that disinhibited rhythm was mainly limited by the electrogenic activity of Na^+/K^+ ATPase, while slow strophanthidin bursting was due to slowly developing synaptic fatigue.

This data should be interesting to future studies aimed at characterizing the mechanisms of operation of excitatory networks in the nervous system.

References

Abbate G. (2001) Analisi fattoriale applicata a una rete neurale. Degree thesis on Mathematics at the University of West Piemonte "Amedeo Avogadro" (sede di Alessandria)

Akinci M.K. and Schofield P.R. (1999) Widespread expression of GABA(A) receptor subunits in peripheral tissues. *Neurosci. Res.* **35**, 145-153

Albrecht B.E., Breitenbach U., Stuhmer T., Harvey R.J. and Darlison M.G. (1997) In situ hybridization and reverse transcription--polymerase chain reaction studies on the expression of the $GABA_C$ receptor rho1- and rho2-subunit genes in avian and rat brain. *Eur. J. Neurosci.* **9**, 2414-2422.

Allan R.D., Curtis D.R., Headley P.M., Johnston G.A.R., Lodge D. and Twitchin B. (1980) The synthesis and activity of *cis*- and *trans*-2-(aminomethyl) cyclopropanecarboxylic acid as conformationally restricted analogues of GABA. *J.Neurochem.* **34**, 652-654

Ballerini L., Bracci E. and Nistri A. (1997) Pharmacological block of the electrogenic sodium pump disrupt rhythmic bursting induced by strychnine and bicuculline in the neonatal rat spinal cord. *J. Neuriphysiol.* **77**, 17-23

Barbieri M. and Nistri A. (2001) Depression of windup of spinal neurons in the neonatal rat spinal cord in vitro by an NK3 tachykinin receptor antagonist. *J. Neuriphysiol.* **85**, 1502-1511

Beato M., Bracci E. and Nistri A. (1997) Contribution of NMDA and non-NMDA glutamate receptors to locomotor pattern generation in the neonatal rat spinal cord. *Proc. Roy. Soc. London B.* **264**, 877-884

Beato M. and Nistri A. (1999) Interaction between disinhibited bursting and fictive locomotor patterns in the rat isolated spinal cord. *J.Neurophysiol.* **82**, 2029-2038

Belley M., Sullivan R., Reeves A., Evans J., O'Neill G. and Ng G.Y. (1999) Synthesis of the nanomolar photoaffinity $GABA_B$ receptor ligand CGP 71872 reveals diversity in the tissue distribution of $GABA_B$ receptor forms. *Bioorg. Med. Chem.* **7**, 2697-2704

Barnard E.A., Skolnick P., Olsen R.W., Mohler H., Sieghart W., Biggio G., Braestrup C., Bateson A.N. and Langer S.Z. (1998) International union of pharmacology. XV. Subtype of γ-aminobutyric $acid_A$ receptor: classification on the basis of subunit structure and receptor function. *Pharmacol. Rev.* **50**, 291-313

Bormann J. (2000) The 'ABC' of GABA receptors. *Trends Pharmacol. Sci.* **21**, 16-19

Boue-Grabot E., Roudbaraki M., Bascles L., Tramu G., Bloch B. and Garret M. (1998) Expression of GABA receptor rho subunits in rat brain. *J. Neurochem.* **70**, 899-907

Bowen J.W. (1992) Regulation of Na^+-K^+-ATPase expression in cultured renal cells by incubation in hypertonic medium. *Am. J. Physiol. (Cell Physiol. 31)* **262**, C845-C853

Bracci E., Ballerini L. and Nistri A. (1996a) Spontaneous rhythmic bursts induced by pharmacological block of inhibition in lumbar motoneurons of the neonatal rat spinal cord. *J.Neurophysiol.* **75**, 640-647

Bracci E., Ballerini L. and Nistri A. (1996b) Localization of rhythmogenic networks responsible for spontaneous bursts induced by strychnine and bicuculline in the rat isolated spinal cord. *J.Neurosci.* **16**, 7063-7076

Bracci E., Beato M. and Nistri A. (1997) Afferent inputs modulate the activity of a rhythmic burst generator in the rat disinhibited spinal cord in vitro. *J. Neurophysiol.* 77, 3157-3167

Bracci E., Beato M. and Nistri A. (1998) Extracellular K^+ induces locomotor-like patterns in the rat spinal cord in vitro: comparison with NMDA or 5-HT induced activity. *J. Neurophysiol.* **79**, 2643-2652

Bradford M.M. (1976) A rapid and sensitive method for the quantitation of microgram quantities of protein utilizing the principle of protein-dye binding. *Anal. Biochem.* **72**, 248-254

Catsicas M., Bonness V., Becker D. and Mobbs P. (1998) Spontaneous Ca^{2+} transients and their transmission in the developing chick retina. *Curr. Biol.* **8**, 283-286

Cazalets J.R., Sqalli-Houssaini Y. and Clarac F. (1992) Activation of the central pattern generators for locomotion by serotonin and excitatory amino acids in neonatal rat. *J. Physiol.* **455**, 187-204

Cazalets J.R., Bertrand S., Sqalli-Houssaini Y. and Clarac F. (1998) GABAergic control of spinal locomotor networks in the neonatal rat. *Ann. N.Y. Acad. Sci.* **860**, 168-180

Chebib M., Mewett K.N. and Johnston G.A. (1998) $GABA_C$ receptor antagonists differentiate between human ρ1 and ρ2 receptors expressed in *Xenopus* oocytes. *Eur. J. Pharmacol.* **357**, 227-234

Chub N. and O'Donovan M.J. (1998) Blockade and recovery of spontaneous rhythmic activity after application of neurotransmitter antagonists to spinal networks of the chick embryo. *J. Neurosci.* **18**, 294-306

Crair M.C. (1999) Neuronal activity during development: permissive or instructive? *Curr. Op. Neurobiol.* **9**, 88-93

Dale N. (1995) Experimentally derived model for the locomotor pattern generator in the Xenopus embryo. *J. Physiol.* **489**, 489-510

Davidoff R.A. and Hackman J.C. (1980) Hyperpolarization of frog primary afferent fibres caused by activation of a sodium pump. *J. Phisiol.* **302**, 297-309

Dolapchieva S.D. (1998) Expression of Na^+,K^+ ATPase α and β subunit isoforms in the motor neurons of the rat spinal cord. *Membr. Cell. Biol.* **12**, 355-361

Drew C.A., Johnston G.A.R. and Weatherby R.P. (1984) Bicuculline-insensitive GABA receptors: studies on the binding of (-)-baclofen to rat cerebellar membranes. *Neurosci. Lett.* **52**, 317-321

Enz R., Brandstatter J.H., Hartveit E., Wassle H. and Bormann J. (1995) Expression of GABA receptor rho 1 and rho 2 subunits in the retina and brain of the rat. *Eur. J. Neurosci.* **7**, 1495-1501

Enz R., Brandstatter J.H., Wassle H. and Bormann J. (1996) Immunocytochemical localization of the GABAc receptor rho subunits in the mammalian retina. *J. Neurosci.* **16**, 4479-4490

Evans R.H. (1978) The effects of amino acids and antagonists on the isolated hemisected spinal cord of the immature rat. *Br.J.Pharmac.* **62**, 171-176

Feller M.B., Wellis D.P., Stellwagen D., Werblin F.S. and Shatz C.J. (1996) Requirement for cholinergic synaptic transmission in the propagation of spontaneous retinal waves. *Science* **272**, 1182-1187

Feller M.B. (1999) Spontaneous correlated activity in developing neural circuits. *Neuron* **22**, 653-656

Fujioka Y., Matsuoka S., Ban T. and Noma A. (1998) Interaction of the Na^+-K^+ pump and the Na^+-Ca^{2+} exchange via $[Na^+]_i$ in a restricted space of guinea-pig ventricular cells. *J. Phisiol.* **509**, 457-470

Fykse E.M. and Fonnum F. (1996) Amino acid neurotransmission: dynamics of vesicular uptake. *Neurochem. Res.*, **21**:1053-1060

Glynn I.M. (1993) All hands to the sodium pump (Annual review prize lecture). *J.Phisiol.* **462**, 1-30

Graham B. and Redman S.J. (1994) A simulation of action potentials in synaptic boutons during presynaptic inhibition. *J.Neurophysiol.* **71**, 538-549

Grillner S. (1975) Locomotion in vertebrates: central mechanisms and reflex interaction. *Physiol. Rev.* **55**, 247-304

Hackman J.C., Auslander D., Grayson V. and Davidoff R.A. (1982) GABA "desensitization" of frog primary afferent fibers. *Brain Res.* **253**, 143-152

Haller M., Mironov S.L., Karschin and Richter D.W. (2001) Dynamic activation of K_{ATP} channels in rhythmically active neurons. *J. Physiol.* **537**, 69-81

Headley P.M. and Grillner S. (1990) Excitatory amino acids and synaptic transmission: the evidence for a physiological function. *TiPS* **11**, 205-211

Horisberger J.D., Lemas V., Kraehenbühl J.P. and Rossier B.C. (1991) Structure-function relationeship of Na,K-ATPase. *Ann. Rev. Physiol.* **53**,565-584

Jansen A., Hoepfner M., Herzig K.H., Riecken E.O. and Scherubl H. (2000) $GABA_C$ receptors in neuroendocrine gut cells: a new GABA-binding site in the gut. *Eur. J. Physiol.* **441**, 294-300

Jankowska E.J. (2001) Spinal interneuronal systems: identification, multifunctional character and reconfigurations in mammals. *J. Physiol.* **533**, 31- 40

Johnson S.W. Seutin V. and North R.A. (1992) Burst firing in dopamine neurons induced by N-methyl-d-aspartate: role of electrogenic sodium pump. *Science* **258**, 665-667

Johnston G.A.R. (1976) Physiologic pharmacology of GABA and its antagonists in the vertebrate nervous system. In *GABA in nervous system function* (eds. Roberts E., Chase T.N., and Tower D. B.) pp 395-411 Raven Press, New York

Kemp J.A., Marshall G.R. and Woodruff G.N. (1986) Quantitative evaluation of the potencies of GABA-receptor agonists and antagonists using the rat hippocampal slice preparation. *Br.J.Pharmac.* **87**, 677-684

Kerkut G.A. and Bagust J. (1995) The isolated mammalian spinal cord. *Prog. Neurobiol.* **46**, 1-48

Kiebler M.A. and DesGroseillers L. (2000) Molecular insights into mRNA transport and local translation in the mammalian nervous system. *Neuron* **25**, 19-28

Kiehn O. and Kjaerulff O. (1998) Distribution of central pattern generators for rhythmic motor outputs in the spinal cord of limbed vertebrates. *Ann. N.Y. Acad. Sci.* **860**, 110-129

Kiehn O., Kjaerulff O., Tresch M.C. and Harris-Warrick R.M. (2000) Contributions of intrinsic motor neuron properties to the production of rhythmic motor output in the mammalian spinal cord. *Brain Res. Bull.* **53**, 649-659

Kirsch J., Meyer G. and Betz H. (1996) Synaptic targeting of ionotropic neurotransmitter receptors. *Mol. Cell. Neurosci.* **8**, 93-98

Kjaerulff O. and Kiehn O. (1996) Distribution of networks generating and coordinating locomotor activity in the neonatal rat spinal cord in vitro: a lesion study. *J. Neurosci.* **16**, 5777-5794

Kullmann D.M. (1994) Amplitude fluctuations of dual-component EPSCs in hippocampal pyramidal cells: implications for long-term potentiation. *Neuron* **12**, 1111-1120

Lape R. and Nistri A. (2001) Characteristics of fast Na^+ current of hypoglossal motoneurons in a rat brainstem slice preparation. *Eur. J. Neurosci.* **13**, 763-772

Latham P.E., Richmond B.J., Nelson P.G. and Nirenberg S. (2000a) Intrinsic dynamics in neuronal networks. I. Theory. *J. Neurophysiol.* **83**,808-827

Latham P.E., Richmond B.J., Nirenberg S. and Nelson P.G. (2000b) Intrinsic dynamics in neuronal networks. II. Experiment. *J. Neurophysiol.* **83**,828-835

Li S. and Stys P.K. (2001) Na^+-K^+ ATPase inhibition and depolarization induce glutamate release via reverse Na^+-dependent transport in spinal cord white matter. *Neurosci.* **107**, 675-683

Long S.K., Evans R.H. and Krijzer F. (1989) Effects of depressant amino acids and antagonists on an *in vitro* spinal cord preparation from the adult rat. *Neuropharmacol.* **28**, 683-688

Longo N., Griffin L.D. and Elsas L.J. (1991) A simple method for evaluation of Rb^+ transport and Na^+-K^+ pump stoichiometry in adherent cells. *Am. J. Physiol.* **260**, C1341-1346

Marchetti C., Donato R., Pepeu G. and Nistri A. (2001) Can GABA and glycine inhibit neonatal motoneurons. *Soc. Neurosci. Meet. 2001*, poster n. 490.1

Mata M., Siegel G.J., Hieber V., Beaty M.W. and Fink D.J. (1991) Differential distribution of (Na,K)-ATPase α isoform mRNAs in the peripheral nervous sysstem. *Brain. Res.* **546**, 47-54

Milner L.D. and Landmesser L.T. (1999) Cholinergic and GABAergic inputs drive patterned spontaneous motoneuron activity before target contact. *J.Neurosci.* **19**, 3007-3022

Murata Y., Woodward R.M., Miledi R. and Overman L. (1996) The first selective antagonist for a $GABA_C$ receptor. *Bioorganic & Medicinal Chemistry Letters* **6**, 2073-2076

Nishimaru H. and Kudo N. (2000) Formation of the central pattern generator for locomotion in the rat and mouse. *Brain Res. Bull.* 53, 661-669

Nistri A. and Constanti A. (1979) Pharmacological characterization of different types of GABA and glutamate receptors in vertebrates and invertebrates. *Prog.Neurobiol.* **13**, 117-235

O'Donovan M.J. and Chub N. (1997) Populatio behavior and self-organization in the genesis of spontaneous rhythmic activity by developing spinal network. *Semin Cell Dev. Biol.* **8**, 21-28

O'Donovan M.J. (1999) The origin of spontaneous activity in developing network of the vertebrate nervous system. *Curr. Opin. Neurobiol.* **9**, 94-104

Ogurusu T., Taira H. and Shingai R. (1995) Identification of $GABA_A$ receptor subunits in rat retina: cloning of the rat $GABA_A$ receptor rho 2-subunit cDNA. *J. Neurochem.* **65**, 964-968

Ogurusu T., Eguchi G. and Shingai R. (1997) Localization of gamma-aminobutyric acid (GABA) receptor rho 3 subunit in rat retina. *Neurorep.* **8**, 925-927

Ogurusu T., Yanagi K., Watanabe M., Fukaya M. and Shingai R. (1999) Localization of GABA receptor rho 2 and rho 3 subunits in rat brain and functional expression of homooligomeric rho 3 receptors and heterooligomeric rho 2 rho 3 receptors. *Recept. & Chann.* **6**, 463-475

Or E., Goldshleger R. and Karlish S.J. (1996) An effect of voltage on binding of Na^+ at the cytoplasmic surface of the Na^+-K^+ pump. *J. Biol. Chem.***271**, 2470-2477

Overton E. (1902) Beirträge zur allgemeinen Muskel- und Nervenphysiologie. II. Ueber die Unentbehrlichkeit von Natrium- (oder Lithium-) Ionen für den Contractionsact des Muskels. *Pflügers Archiv.***92**, 346-386

Penn A.A., Riquelme P.A., Feller M.B. and Shatz C.J. (1998) Competition in retinogeniculate patterning driven by spontaneous activity. *Science* **279**, 2108-2112

Polenzani L., Woodward R.M. and Miledi R. (1991) Expression of mammalian g-aminobutyric acid receptors with distinct pharmacology in *Xenopus* oocytes. *Proc. Natl. Acad. Sci. USA* **88**, 4318-4322

Racca C., Gardiol A. and Triller A. (1997) Dendritic and postsynaptic localizations of glycine receptor alpha subunit mRNAs. *J. Neurosci.* **17**, 1691-1700

Ragozzino D., Woodward R.M., Murata Y., Eusebi F., Overman L. E. and Miledi R. (1996) Design and *in vitro* pharmacology of a selective γ-aminobutyric $acid_C$ receptor antagonist. *Molecular Pharmacology* **50**, 1024-1030

Robinson H.P., Kawahara M., Jimbo Y., Torimitsu K., Kuroda Y. and Kawana A. (1993) Periodic synchronized bursting and intracellular calcium transients elicited by low magnesium in cultured cortical neurons. *J. Neurophysiol.* **70**, 1606-1616

Sernagor E., Chub N., Ritter A. and O'Donovan M.J. (1995) Pharmacological characterization of the rhythmic synaptic drive onto lumbosacral motoneurons in the chick embryo spinal cord. *J. Neurosci.* **15**, 7452-7464

Shen K.Z. and Johnson S.W. (1998) Sodium pump evokes high density pump current in rat midbrain dopamine neurons. *J. Phisiol.* **512**, 449-457

Sivilotti L. and Nistri A. (1991) GABA receptor mechanisms in the central nervous system. *Prog.Neurobiol.* **36**, 35-92

Solioz M. and Vulpe C. (1996) CPx-type ATPases: a class of P-type ATPases that pump heavy metals. *Trends Biocheml. Sci.* **21**, 237-241

Steward O. (1997) mRNA localization in neurons: a multipurpose mechanism? *Neuron* **18**, 9-12

Strata F. and Cherubini E. (1994) Transient expression of a novel type of GABA response in rat CA3 hippocampal neurones during development. *J. Physiol.* **480**, 493-503

Streit J. (1993) Regular oscillations of synaptic activity in spinal networks in vitro. *J. Neurophysiol.* **70**,871-878

Streit J., Tscherter A., Heuschkel M.O. and Renaud P. (2001) The generation of rhythmic activity in dissociated cultures of rat spinal cord. *Eur. J. Neurosci.* **14**, 191-202

Stuart G.J. and Redman S.J. (1992) The role of $GABA_A$ and $GABA_B$ receptors in presynaptic inhibition of I_a EPSPs in cat spinal motoneurones. *J.Physiol.* **447**, 675-692

Sweet J. E., Wikholm R.P., Blanks R.H.I., Sweet A.L. and Conley L.C. (1986) Motoneurons of the rat sciatic nerve. *Exp. Neurol.* **B93**, 227-252

Tabak J., Senn W., O'Donovan M.J. and Rinzel J. (2000) Modeling of spontaneous activity in developing spinal cord using activity-dependent depression in an excitatory network. *J. Neurosci.* **20**, 3041-3056

Tang Y.M., Travis E.R., Wightman R.M. and Schneider A.S. (2000) Sodium-calcium exchange affects local calcium signal decay and the rate of exocytotic secretion in single chromaffin cells. *J. Neurochem.* **74**, 702-710

Tao Q.-F., Hollenberg N.K., Price D.A. and Graves S.W. (1996) Sodium pump isoform specificity for the Digitalis-Like Factor isolated from human peritoneal dialysate. *Hypertension* **29**, 815-821

Thompson S.M. and Prince D.A. (1986) Activation of electrogenic sodium pump in hippocampal CA1 neurons following glutamate-induced depolarization. *J. Neurophysiol.* **56**, 507-522

Tongiorgi E. Righi M. and Cattaneo A. (1997) Activity-dependent dendritic targeting of BDNF and TrkB mRNAs in hippocampal neurons. *J. Neurosci.* **17**, 9492-9505

Tongiorgi E., Righi M. and Cattaneo A. (1998) A non-radioactive in situ hybridization method that does not require RNAse-free conditions. *J. Neurosci. Meth.* **85**, 129-139

Toudstrup-Jensen M., Hauge M. and Vilsen B. (2001) Mutation effect on conformational change of the dephospho-and phospho-forms of Na^+,K^+-ATPase. *Biochemistry* **40**, 5521-5532

Tresch M.C. and Kiehn O. (2000) Motor coordination without action potentials in the mammalian spinal cord. *Nature Neurosci.* **3**, 593- 599

Tscherter A., Heuschkel M.O., Renaud P. and Steit J. (2001) Spatiotemporal characterization of rhythmic activity in rat spinal cord slice cultures. *Eur. J. Neurosci.* **14**, 179-90

Wässle H., Koulen P., Enz. R. and Bormann., J. (1998) Immunocytochemical localization of $GABA_C$ receptors in the rat spinal cord. *Soc. Neurosci. Abst.* **24**, 2038

Wegelius K., Pasternack M., Hiltunen J.O., Rivera C., Kaila K., Saarma M. and Reeben M. (1998) Distribution of GABA receptor rho subunit transcripts in the rat brain. *Eur. J.Neurosci.* **10**, 350-357

Weliky M. and Katz L.C. (1997) Disruption of orientation tuning in visual cortex by artificially correlated neuronal activity. *Nature* **386**, 680-685

Wenner P and O'Donovan M.J. (2001) Mechanisms that initiate spontaneous network activity in the developing chick spinal cord. *J. Neurophysiol.* **86**, 1481-1498

Willis J.A., Gaubatz G.L. and Carpenter D.O. (1974) The role of the electrogenic sodium pump in modulation of pacemaker discharge in *Aplysia* neurons. *J. Cell. Phisiol.* **84**, 463-472

Wong W.T., Sanes J.R. and Wong RO. (1998) Developmentally regulated spontaneous activity in the embryonic chick retina. *J. Neurosci.* **18**, 8839-8852

Wong R.O. (1999) Retinal waves and visual system development. *Annu. Rev. Neurosci.* **22**, 29-47

Zhang D., Pan Z.H., Zhang X., Brideau A.D. and Lipton S.A. (1995) Cloning of a gamma-aminobutyric acid type C receptor subunit in rat retina with a methionine residue critical for picrotoxinin channel block. *Proc. Natl. Acad. Sci. USA* **92**, 11756-11760

Zhang P., Toyoshima C., Yonekura K, Green N.M. and Stokes D.L. (1998) Structure of the calcium pump from sarcoplasmic reticulum at 8-Å resolution. *Nature* **392**, 835-839

Acknowledgements

The Thesis is finished, thanks be to God! But before I write "the end" I have to say thanks to a lot of people for these four years of beautiful work; first of all

to Professor Andrea Nistri (a supervisor who tried also to teach me English),

to Professor Laura Ballerini (the best researcher in our lab and also a good friend),

to Dr. Enrico Tongiorgi and his team (in particular to Mara Armellin).

I collaborated with a couple of friends, a real couple: Stefano Bianchini (a mathematical genius and a very particular person) and Gilda Abbate (his, on average, patient wife)! I cannot forget Mario Barbieri (my set-up mate for a couple of years) who taught me how to adjust a set-up in all weather conditions. I prepared the rubidium experiments with Dr. Andres Muro (ICGEB, Trieste, Italy) and I am very grateful to Dr. Steward Lipton (Burnham Institute, La Jolla, California, USA) for supplying the ρ1 and ρ2 cDNAs and Prof. H. Wässle (Max-Planck-Institute for Brain Research, Frankfurt, Germany) for his kind gift of rho 63 polyclonal anti $GABA_C$ antibodies.

I have not listed all of the friends that I met and attended to in these four years (including my wife, but she is mentioned in the first page), however, I remember them with great pleasure and hope to maintain contact.

- The end -